REVIEWS OF MODERN PHYSICS VOLUME 45, NUMBER 1 JANUARY 1973

The Eigenchannel Method and Related Theories for Nuclear Reactions

R. F. BARRETT,* L. C. BIEDENHARN,† MICHAEL DANOS,‡ P. P. DELSANTO,§ W. GREINER, and H. G. WAHSWEILER

Institut für Theoret. Physik der Universität Frankfurt/Main, Frankfurt/Main, Germany

The theory of the treatment of particle hole states in the continuum is reviewed with emphasis on the eigenchannel method. The results of actual calculations are compared with experimental data. Some aspects of the experiments are rather well reproduced by the calculations. However, in certain other aspects a qualitative disagreement exists between theory and experiment, pointing to an essential inadequacy of the underlying nuclear model.

CONTENTS

I. Introduction 44
II. Descriptive Survey of Nuclear Reaction Theories 45
III. Theoretical Part 49
A. One-Particle One-Hole Nuclear States 49
B. Limitations of the $1p$–$1h$ Nuclear Model 49
C. The Eigenchannel Procedure in Detail 51
D. The Coupled Channel Method and the Random Phase Approximation 56
E. Particle–Particle Reaction Cross Sections 58
F. Calculation of the Photonuclear Cross Sections 60
G. Nuclear Structure Information 61
H. Related Numerical Treatments of the Shell Model in the Continuum 63
I. Sources of Inaccuracies of the Eigenchannel Method and Their Treatment 64
IV. Applications of the Reaction Theories 67
A. The Giant Dipole Resonance in ^{12}C, Experiment and Bound-State Calculations 68
B. The Giant Dipole Resonance of ^{12}C in a Continuum $1p$–$1h$ Calculation 71
C. Results for Other Multipole Excitations in ^{12}C 74
D. Photonucleon Branching Ratios and Angular Distributions in ^{12}C 78
E. Reaction Cross Sections of ^{12}C 81
F. The Giant Dipole Resonance in ^{16}O, Experiment and Bound-State Calculations 84
G. The Giant Dipole Resonance of ^{16}O in a Continuum $1p$–$1h$ Calculation 88
H. Photonucleon Branching Ratios and Angular Distributions in ^{16}O 94
I. Reaction Cross Sections of ^{16}O 95
J. The Giant Dipole Resonance in ^{40}Ca, Experiment and Bound-State Calculations 97
K. The Giant Dipole Resonance of ^{40}Ca in a Continuum $1p$–$1h$ Calculation 100
L. Photonucleon Angular Distributions in ^{40}Ca 103
M. Reaction Cross Sections of ^{40}Ca 104
V. Conclusions and Outlook 104
Acknowledgements 105
References 106

I. INTRODUCTION

This review article has two aims. The major aim is to describe in a rather detailed manner the eigenchannel method for treating nuclear continuum states and to indicate the practicality of the method for actually performing calculations. The second aim is to discuss the understanding of nuclear physics achieved by extending the nuclear structure calculations from the treatment of bound states to the treatment of continuum states. In other words, the first aim concerns mathematical methodology, the second aim concerns nuclear physics.

The need to combine these two aims into a single article is rather compelling. Besides being the *raison d'être* for the development of the method, the nature of the nuclear structure determines the mathematical complexity which the method has to be able to handle, and, on the other hand, a knowledge of the mathematical limitations of the method is required to judge the relevance of the obtained results to the interpretation of actual experimental data.

The present time seems to be an auspicious moment to undertake this task. Namely, after a rather active period during the later part of the sixties, a somewhat gloomy mood seems to have descended because of the rather disappointing quality of the obtained results. We hope to show that, in fact, the mathematical problems of treating one-particle continua have largely been overcome and, that the problems now indeed are those of nuclear physics.

The over-all organization of this article is such that it begins with the most mathematical parts and proceeds to the physical parts. So, we begin in Sec. II by describing briefly, in a general way, the mathematical problems encountered in extending the shell model to continuum states and show where the eigenchannel method lies; i.e., what are its mathematical similarities and differences compared with the other methods. This description contains some historical notes. The detailed description of the theory is given in Sec. III. In Secs. II.A and II.B the physical models which underly most of the continuum calculations which actually have been carried out are discussed.

The rest of this section contains the precise formulation of the eigenchannel, the coupled channel, and the RPA methods. It includes a discussion of the particular problems encountered when applying the eigenchannel method and the resolution of these problems.

Section IV is devoted to the review of actual calculations performed with both the eigenchannel and the

* Department of Physics, Duke University, Durham, North Carolina 27706.
† School of Physics, University of Melbourne, Vic., Australia.
‡ National Bureau of Standards, Washington, D.C. 20234.
§ Institut für Theoret. Physik der Universität Frankfurt/M. and Department of Physics, University of Puerto Rico, Mayaguez, Puerto Rico.

coupled channel methods. The results of these calculations are compared both with experiment and with bound-state calculations. Certain characteristic agreements and disagreements exist between experiment and calculations. In particular, not all gross features of the experiment are reproduced by the calculations. This is the surprising and disappointing feature, mentioned above, to emerge from all continuum calculations performed up-to-date.

A brief discussion of the present state of the field, and some speculations about future developments, are the topic of the concluding Sec. V.

II. DESCRIPTIVE SURVEY OF NUCLEAR REACTION THEORIES

We will delimit nuclear reaction theory as the following–Nuclear structure physics, we assume, is concerned with the interaction of nonstrange baryons, where, by assumption, the interactions are to be discussed *without explicit reference to meson or baryon resonances*. Hence all energies are necessarily nonrelativistic, and the interactions are typified by some general (but *a priori* unspecified) heuristic potentials. [We would like to mention that there is no assurance whatsoever that this schematization is not a gross distortion for certain important aspects of nuclear physics. For example, the momentum distribution and the electromagnetic moments in the deuteron appear to require contributions from mesons and baryonic resonances (cf. Kerman and Kisslinger, 1969).]

We shall explicitly assume that all three-body channels are closed. Our notation is that of Wigner as reviewed, for example, by Lane and Thomas (1958) or by Biedenharn *et al.* (1963). We define an alternative, denoted α, as a pair of bound nuclear states (possibly excited); a channel, denoted c, consists of an alternative α having relative kinetic energy corresponding to wave vector k_c; the channel spin, s, is the coupled spin angular momenta of the alternative α. A bound channel is one whose relative kinetic energy is negative; an open channel, positive. The channel radius r_c, is the relative coordinate of the pair comprising alternative α; similarly, the angular momentum l_c is the relative orbital angular momentum of the alternative α.

Let us turn now to nuclear reaction theory proper. The basic problem is to determine—from a specified Hamiltonian—the $N\times N$ scattering matrix $S^{J\pi}$ (where N denotes the number of open channels) at each energy E, angular momentum J, and parity π. There is a formal problem which precedes this: namely, to discuss, for a general class of admissible Hamiltonians, the properties of $S^{J\pi}$ abstractly. This is the content of (nuclear reaction) S-matrix theory. A complete (formal) answer can be given for (nonrelativistic) one-channel (potential) scattering, and has been discussed in exemplary fashion in the monograph of Regge and de Alfaro (1965). It is outside the scope of the present work to discuss this problem, but the formal answer for $1=0$ spinless nucleons interacting with a potential having a finite (cutoff) range is instructive. The S-matrix is then the ratio $S_0=f_0(k)/f_0(-k)$, where $f_0(k)$ is an entire function of k with a *finite* number of zeros [=bound states] on the imaginary axis in the upper half k plane and an *infinity* of zeroes (resonances) in the lower half k-plane.

For the practical problem—i.e., to determine $S^{J\pi}$ given H—there are a plethora of possible approaches. It was the very great merit of Bloch's (1957) work[1] to demonstrate that *all* approaches to nuclear reaction theory were variants of the same basic idea: i.e., to separate H into two parts; $H=H_0+H'$, and to develop a formal answer for S in terms of the spectrum of H_0. This is of course an idea long familiar from perturbation theory. Let us sketch now the way in which all reaction theories fit into this pattern. The most important class of theories, from our viewpoint, are those that impose boundary conditions in each channel and at a finite radius, a_c. In the *interior region* ($r_c<a_c$) we have a Hermitian Hamiltonian, and since the space is finite, the spectrum is discrete (the eigenvalues are complex if the boundary conditions are complex). In other words, *theories which postulate boundary conditions at finite channel radii are basically theories which discretize the continuum.* (Physicists should be aware of the long history of this idea: spherical Hertzian waves were analyzed in this fashion by Sommerfeld before the turn of the century.)

Using Bloch's idea it is easy to demonstrate this point, in a heuristic fashion, to be sure. Define the Bloch operator by

$$\mathfrak{L}(a,b)=\sum_c |c\rangle(\hbar^2/2m_c)\delta(r_c-a_c)(d/dr) -[(b_c-1)/r]\langle c| \quad (2.1)$$

where $|c\rangle$ are the surface channel ket vectors (a function of all variables *except* the channel radius r_c), and m_c is the reduced mass of the alternative in channel c.

The Hamiltonian may be written then in terms of H_0 and H' as

$$\begin{aligned} H&=H_0+H' \\ H_0&=H+\mathfrak{L}(a,b) \\ H'&=-\mathfrak{L}(a,b). \end{aligned} \quad (2.2)$$

The Hamiltonian H_0 has a discrete, denumerably infinite spectrum which allows a resolution of the identity in terms of eigenvectors $\{|\lambda\rangle\}$ and the dual space $\{\langle\tilde{\lambda}|\}$. The scattering problem is then solved,

[1] This point of view was especially emphasized, and extended, by Lane and Thomas (1958) and later Lane and Robson (1966, 1967). A subsequent paper by Robson and Robson (1969) showed that the Lippmann-Schwinger equation also falls into this formation.

formally, by the integral operator

$$(H-E)\psi=0,$$

$$\psi=(H+\mathfrak{L}-E)^{-1}\mathfrak{L}\psi. \tag{2.3}$$

Since the spectrum is discrete the operator $(H+\mathfrak{L}-E)^{-1}$ can be expanded as an (infinite) sum.

The outgoing wave boundary condition $\mathfrak{L}_{\text{out}}$—as discussed by Sommerfeld—plays a particularly important role in this development (see, e.g., Kapur and Peierls, 1938). One can see this from observing that $\mathfrak{L}_{\text{out}}\psi$ *contains only ingoing waves*. Since the ingoing waves are the "input data" in nuclear reactions, this shows that $\psi=(H+\mathfrak{L}_{\text{out}}-E)^{-1}\mathfrak{L}_{\text{out}}\psi$ is indeed a *solution* to the scattering problem (and not an integral equation for the solution). All other choices for $\mathfrak{L}(a, b)$ may now be expressed in terms of the $\mathfrak{L}_{\text{out}}$ solution.

Let the operator $(H+\mathfrak{L}_{\text{out}}-E)^{-1}$ be called G_0, and the operator $[H+\mathfrak{L}(a, b)-E]^{-1}$ be called G. Then we have

$$G_0=\{1+G[\mathfrak{L}(a, b)-\mathfrak{L}_{\text{out}}]\}^{-1}G. \tag{2.4}$$

If we define the eigenfunctions of the internal region by

$$(H-E_\lambda)\mid\lambda\rangle=0,$$

$$\mathfrak{L}(a, b)\mid\lambda\rangle=0, \tag{2.5}$$

then we may express G as the series

$$G=\sum_\lambda \mid\tilde{\lambda}\rangle\langle\lambda\mid/(E_\lambda-E). \tag{2.6}$$

This series is essentially Wigner's R-matrix; in fact, taking matrix elements at the channel surface (that is, using $\mid\psi_{\text{surface}}^{(c)}\rangle=(\hbar^2a_c/2m_c)^{1/2}[\delta(r_c-a_c)/r_c^2]\mid c\rangle$ one finds

$$\langle\psi_{\text{surface}}^{(c)}\mid G\mid\psi_{\text{surface}}^{(c')}\rangle\equiv R_{cc'}=\sum_\lambda[\gamma_{\lambda c}\gamma_{\lambda c'}/(E_\lambda-E)],$$

$$\gamma_{\lambda c'}\equiv\langle\lambda\mid(\hbar^2a_c/2m_c)^{1/2}\gamma_c^{-2}\delta(r_c-a_c)\mid c\rangle. \tag{2.7}$$

This elegant derivation for the class of boundary condition theories is taken from the papers of Lane and Robson (1966, 1967). These boundary condition theories all suffer from an obvious defect: They involve an *ad hoc* radius in every channel and moreover an arbitrary (boundary condition) parameter, b_c, for each channel. The resultant S-matrix is, however, completely independent—in principle—of these parameters $\{a_c, b_c\}$—although in fact the convergence and utility of the series depends markedly on these parameters, and if the series is truncated (as is necessary in practice) the dependence on $\{a, b\}$ is very strong. Criticisms of these theories (which for brevity we call R-matrix theories) all stem from this source, for, it is pointed out, a given Hamiltonian should lead to results dependent only upon intrinsically defined quantities and not upon superfluous auxiliary parameters (Rosenfeld, 1967, 1968).

It is useful at this point to recall that the boundary condition theories were formal elaborations of more accessible physical ideas. The original work of Breit and Wigner was patterned after the (weak coupling) model of atomic line widths. This was admittedly a very insecure foundation, yet the results were spectacularly successful. In 1947 Wigner accepted Fermi's challenge to give a sound proof, and successively developed, in three papers, what is now the R-matrix theory. The key physical idea, however, is in the *first* paper and has more or less disappeared in the subsequent generalizations. The idea is very simple: A resonance means that the nuclear system is, near the resonance energy, describable *approximately* by a state vector whose dependence on energy *approximately factorizes* $\psi(\{r_i\}, E)\cong f(E)\varphi(\{r_i\})$. Green's theorem (equivalently flux conservation) extends this zeroth order result to the next order, giving the Breit–Wigner resonance shape.

Wigner's physical idea makes quite obvious the involved discussion of Mahaux and Weidenmüller (1965) on the *strict* (mathematical) applicability of the one-level resonance formula. Clearly if a single state is to give truly zero error at an energy E in the continuum, then that state must completely dominate the wave function in any energy strip ΔE which includes E no matter how small ΔE is; in other words, it must be a bound state in the continuum (Mahaux–Weidenmüller's result). But this is patently an absurd result, for such a state is then orthogonal to the continuum (zero width)! One *cannot* then dispense with the approximate nature of Wigner's original idea. It follows that the analysis of experimental data in terms of (observed) resonance structures on limited energy intervals using the R-matrix approach is certainly valid (but only to some pre-assigned error). The question as to how to handle *large* energy intervals, or Rosenfeld's theoretical question as to the unique scattering solution for a given fixed Hamiltonian constitute, however, genuine criticisms of R-matrix theory.

Feshbach's (1958, 60, 62; Feshbach, *et al.*, 1967) approach to this was to eliminate channel radii completely and develop a formal scattering theory based on the distinction between open and closed channels.[2] Introduce the two projection operators P and Q defined by $P+Q=1$, $PQ=QP=0$, where P projects onto the open channels; Q projects onto the closed channels. The closed channels allow an expansion in terms of (discrete) eigenstates of QHQ; resonances arise through the coupling of these states to the open channel continuum by H–QHQ. We shall not discuss in any detail the several criticisms of such a formulation (Lane and Robson, 1966, 1967).

Suffice it to say that the original formulation (Feshbach, 1958) was incomplete for the construction of the

[2] A more general concept, that of partitioning the scattering matrix and the channel elimination procedure, had been introduced earlier by Teichman and Wigner (1952). Thomas (1955) applied this method to split the incident vs reaction channels and define a complex (optical) potential [cf. also Sec. X, of Lane and Thomas (1958)].

projection operators P and Q (since the definition of open vs closed channels is asymptotic, the projection operators are not unique); a special difficulty concerns the antisymmetrization requirement which, for the Feshbach approach, requires careful treatment [constructive procedures are discussed by Feshbach (1962), Kerman (1965), Friedman and Feshbach (1968)]. It is worth mentioning that not all resonances arise from this mechanism (closed channels)—the one-channel formal result given earlier provides a clear counter example.[3]

Feshbach's approach has the great merit that it leads very naturally to Weisskopf's (1961) concept (cf. Bloch, 1966) of a "nuclear state hierarchy" and has led to many further developments which are especially significant in discussing isobaric analog resonances. A very different line of development led to the currently important nuclear reaction theory problem of extending the shell model into the continuum. The shell model is, of course, by now the accepted foundation for all nuclear structure calculations despite the fact that this model is still heuristic and phenomenological. The success of this idea of single-particle excited states in the continuum of the (finite depth) shell model (optical) potential in accounting for the observed giant-resonance structure in low energy neutron scattering (optical model; "Mount Barschall") led Weisskopf in 1960 to propose that the model be taken more seriously and extended to include, in addition, particle–hole excitations. This is the basis of the hierarchy of nuclear states: $1p$, $2p$–$1h$, $3p$–$2h$, $\cdots$ in which the members of the hierarchy connect only to adjacent members of the hierarchy (via residual two body interactions) and the continuum couples essentially only to the first member of the hierarchy. The members of the hierarchy are given picturesque names; i.e.

$2p$–$1h$ "doorway" states (Feshbach), "dangerous states," (Migdal, cf. Bloch, 1966)
$3p$–$2h$ "hallway" states (MacDonald)

These concepts have been very successful in the understanding of isobaric analog resonances (where the isospin quantum number justifies in large part the hierarchy concept); nevertheless, it should be noted that the original starting point, the giant-resonance structure, for these concepts was based on a clear misinterpretation: the giant-resonant structure has nothing to do with single-particle resonances per se—it is the result of phase shifts *falling* (*not* rising) through 90° which, by the Wigner theorem, necessarily give very broad resonancelike maxima. (This important clarification is due to McVoy (1965). One possible extension of the shell model into the continuum can be sketched[4] in the following way):

(a) The nuclear Hamiltonian is taken to be: $H=H_0+V$, where H_0 is a sum of single-particle operators

$$H_0=\sum_{i=1}^{A} h_0(i)=\sum_{i=1}^{A}[t(i)+v(i)],$$

(one-body kinetic and potential energies), and

$$V=\sum_{i<j}^{A} v(i,j)-\sum_{i=j}^{A} v(i),$$

i.e., the true two-body interaction minus the (model) one-body potential. The one-body Hamiltonian, $h_0(i)$, is defined to have both a continuum and a discrete spectrum (the one-body potential being based on the observed nuclear charge distribution).

(b) The Hamiltonian H is diagonalized in a Hilbert space defined by the eigenfunctions of H_0, *truncated so that at most only one nucleon is a scattering eigenstate of* $h_0(i)$. (The mixing of the continuum states, the open channels, by the residual interaction presents particular difficulties and must be handled carefully.)

(c) The essential physical idea in this approach is similar to that of Feshbach: the particle–hole hierarchy comprises in zeroth approximation a set of bound states (=closed channels); the one-nucleon continuum (=open channels) overlaps the bound state spectrum; the two systems mix through the residual two-body interactions.

This extension of the shell model into the continuum is a very natural and reasonable development blending, as it does, the ideas developed by Feshbach with the microscopic shell-model approach. A very complete, and accessible, account of this model has been given in a monograph by Mahaux and Weidenmüller (1969).

Let us note only that the structure of the underlying calculational model [item (c) above] is precisely that developed originally by Dirac (1927) and by Rice (1933) and Fano (1935, 1961), and very extensively treated since then [cf. Bloch (1966), Mahaux and Weidenmüller (1969), Bardsley and Mandl (1968).] In the current terminology, the model considers as the zeroth approximation a "*B*ound *S*tate *E*mbedded in the *C*ontinuum"; the coupling between the discrete (bound) state and the continuous part of the spectrum discontinuously perturbs this spectral resolution, producing a sharp resonance. [Even this cursory description should convince the reader that mathematically this model for resonances as BSEC is not trivial. It seems to have been overlooked, however, that there does exist a mathematically precise treatment of Dirac's model justifying, by and large, the heuristic approach [cf. Friedrichs (1948), Brenig and Haag (1959)]. The restriction in the Mahaux–Weidenmüller approach to one nucleon in the continuum is rather severe (no such restriction is required in the R-matrix approach for energies below the two-particle

[3] It was originally held that this distinction between resonance mechanisms was an advantage, but this view was based on a misinterpretation of the giant-resonance phenomena (see below).

[4] This sketch is based on the Mahaux–Weidenmüller (1969) monograph.

threshold, i.e., before the appearance of *open* three-body channels. In principle, the nuclear problem in the inside region can be solved exactly by truncating the Hilbert space at an arbitrarily high energy). To a certain extent this restriction can be eliminated; Dietrich (1966) in his Trieste lecture has indicated a procedure for this. (This lecture is also a very fine survey of the shell model in the continuum.)

Let us now turn to the eigenchannel approach. This method is a development of the R-matrix theory and requires the use of a separation into internal and external regions. The two general properties of the S-matrix, unitarity (conservation of flux) and symmetry (time-reversal invariance of H) are exploited in the external region to write the external solutions in diagonal form. (The details are given below.) The physical significance of this eigenbasis is that an incident (ingoing) eigensolution scatters into the same eigensolution, that is, all components of the many channel wave function suffer the same phase shift. [It is a natural question at this point to ask for the form of the R-matrix theory expressed directly in terms of these eigenphases and eigenvectors; this inverse problem has been solved by Willard and Biedenharn (1958) and Biedenharn, *et al.*, (1963).]

The eigenchannel method, developed by Danos and Greiner, has a somewhat different motivation. It is characteristic of the R-matrix approach that the Bloch operator is singular; it follows that the expansion of the physical wave function in terms of the R-matrix basis functions, $|\lambda\rangle$, is not uniformly convergent at the boundary of the internal region. To put it differently, the wave function is continuous through the boundary but has a discontinuous derivative. The existence of such a discontinuity adversely affects the rate of convergence of the R-matrix expansion, and is, in fact, a weakness of the R-matrix approach.[5] Many ways to improve matters come to mind: one may use two separated boundaries [cf. Tobocman and Nagarajan (1967), Garside and Tobocman (1968), Robson (1968)] or, as a more general version of the same idea, one may smooth the Bloch operator into a volume operator [which leads to a three region version (Phillips, *et al.*, 1960) of the R-matrix approach: interior-transition surface-exterior]. Danos and Greiner (1966, 1967) have suggested a technique which leads to an optimally smooth joining onto the exterior solutions: this is *to use the eigenvectors and eigenphases of the open channels themselves as the boundary conditions at the surface of the interior region.* We shall discuss this method in detail in Sec. III.B below; for the moment, let us note only that the eigenchannel method in effect develops an exact solution to the scattering problem, valid at each energy for which the eigenchannel boundary conditions are applied and calculated. In this sense, the eigenchannel method is not so much a development of R-matrix theory as a practical procedure to treat a many-body nuclear Hamiltonian. It is thus a method rather similar in viewpoint to another practical procedure, the coupled-channels approach, which will be examined in detail in Sec. III.C.

Let us conclude this descriptive survey by mentioning a very different approach, which we shall call the "Sturmian function" approach, following Rotenberg (1962) who so named it when he revived the method (for both nuclear and atomic problems, especially three-body breakup.) This is a variant on the separation of H into two parts, H_0 plus perturbation, but this time (H_0-E) is so chosen that it has *only a discrete* spectrum but is not so singular at infinity as to preclude expansion of scattering solutions of H in terms of the eigenfunctions.

It is clear from the foregoing survey that practically all approaches to scattering theory are attempts to surmount the intractibility of the continuum by using denumerable bases. (The harmonic oscillator basis of the nuclear shell model would itself provide such a basis, but this attempt founders on the fact that one would then have to expand scattering functions finite at infinity.) The Sturmian function basis, $S_{nl}(r)$, are the solutions of

$$\left(-\frac{\hbar^2}{2m}\frac{d^2}{dr^2}+\frac{\hbar l(l+1)}{r^2}+\mu_{nl}(E)V(r)\right)S_{nl}=ES_{nl}. \tag{2.8}$$

Here E is a *fixed* energy and the eigenvalues $\mu_{nl}(E)$ are implicit functions of the energy. The boundary conditions are taken to be $S_{nl}(0)=0$ and $S_{nl}(r)\sim e^{ikr}$ $(E>0)$ or $S_{nl}(r)\sim 0$ $(E<0)$.

The functions S_{nl} have been thoroughly investigated (Ince, 1927). As a first orientation take $V(r)$ to be everywhere attractive (or zero) so that the potential energy becomes increasingly negative as μ_{nl} increases. In order to keep the energy, E, fixed, the kinetic energy must increase. It follows (also in the general case) that the S_{nl} have an increasing number of nodes; there are denumerably many $\mu_{nl}(E)$, the 'spectrum' is discrete.

The Sturmian functions obey an orthonormality relation

$$\int_0^\infty r^2\,dr S_{nl}(r)V(r)S_{n'l'}(r)=\delta_{nl}{}^{n'l'},$$

which, it should be noted, is weighted by the potential $V(r)$. Except for regions in which the potential vanishes, the Sturmian functions are complete.

(The eigenvalues μ_{nl} are the precise analogs to the 'well-depth parameters' introduced by Blatt in the effective-range theory. It is a rather striking fact that every concept of the effective-range approach has afforded a useful generalization in scattering theory.)

We shall not discuss the Sturmian function approach

[5] Numerical studies of the practical significance of this difficulty have been given by Buttle (1967).

to scattering theory further. Critical evaluation of the method has been given by Rotenberg (1963); see also Gallagher and Wilets (1968). Independent of Rotenberg, the Sturmian function approach was also given by Herzenberg and Mandl (1963). The generalization to (nonrelativistic) many channel resonance theory has been given by Herzenberg, Kwok, and Mandl (1964). It is probably worth mentioning that the same basic idea as in the Sturmian function approach has been applied, independently, by Weinberg (1963, 1964) (who used the lowest Sturmian functions to construct a Hilbert–Schmidt kernel for the Lippmann–Schwinger equation) and by Feshbach (1958, 1960, 1962) and Feshbach, *et al.* (1967) (who constructed antisymmetric projection operators using Sturmian functions).

III. THEORETICAL PART

In this section we describe in greater detail the different reaction theories which have the aim of extending the shell model to include the one-particle continuum states. We shall be concerned mainly with those formulations which have been applied in actual numerical calculations. Almost all of these calculations have been performed only up to $1p$–$1h$ excitations, i.e., up to the lowest member of Weisskopf's nuclear state hierarchy. Therefore we begin by a short description of the $1p$–$1h$ excitations, before going on to the discussion of the $1p$–$1h$ continuum calculations.

A. One Particle–One Hole Nuclear States

The most prominent $1p$–$1h$ state in nuclei is the giant dipole resonance. It was explained very early as a collective excitation by the Goldhaber–Teller (1948) description in which incompressible proton and nuclear "fluids" vibrate in opposition [cf. Migdal (1945), Jensen and Jensen (1950), Steinwedel and Jensen (1950)]. This simple physical model fits very well the essential facts; further elaboration of the basic model has been given by Danos (1958, 1961), Danos and Greiner (1964), and others [Le Tourneux, 1965; Weber, *et al.*, 1966; Drechsel, *et al.*, 1967; Arenhövel and Greiner, 1969.] An alternative explanation in terms of the shell model was advanced by Wilkinson (1956) at the Amsterdam Conference. In this description the giant dipole state is the result of $1p$–$1h$, 1^- states obtained by promoting a closed shell nucleon into the next higher shell. (Recall that photon–nucleus interaction is described by a one-body operator, and thus can excite only $1p$–$1h$ states.) The equivalence of this shell-model explanation (for a purely harmonic oscillator potential) to the collective picture has been shown by Wild (1955) and Brink (1957). The concentration of the greater part of the electric photoabsorption on a single mode can be interpreted in terms of the single particle spectrum; however, the observed frequency of absorption is appreciably greater than the average single particle excitation (especially in heavy elements). This shift is interpreted in terms of the residual two-particle interactions; namely, the $1p$–$1h$ states are coupled by the residual interactions in a very characteristic way: most of the dipole strength is concentrated on a single state, a "coherent" combination of the $1p$–$1h$ states, which is shifted in energy appreciably from its unperturbed (shell-model) energy. (This is a misuse of the word "coherent"; it means here that all components enter with the same sign.) These features of the coherent dipole state were elucidated schematically by the work of Fallieros and of Brown (c.f., Brown, 1966). It is found that this dipole state exhausts an appreciable fraction of the dipole sum rule.

The $1p$–$1h$ model has in the meantime undergone considerable development and refinement. We shall describe the work and give references to it below at appropriate points. We refer here only to a recent review by Spicer (1969) [cf. also Firk (1970)]. Still, it must be emphasized that the limitations imposed upon the nuclear model by the restriction to $1p$–$1h$ states are rather severe. They will be discussed in some detail below in Sec. III.I. At any rate one can hope to describe by the $1p$–$1h$ model only the simplest nuclei, and even there one can at best hope to describe the gross features of the experimental data. Therefore we shall restrict our discussion to the nuclei ^{12}C, ^{16}O, and ^{40}Ca.

B. Limitations of the $1p$–$1h$ Nuclear Model

As has been pointed out, in the eigenchannel treatment as described in this paper at energies below the appearance of open two-particle channels the only error of principle is the improper treatment of the center-of-mass motion. However, in practice this error is overshadowed by the limitations resulting from the truncation of the Hilbert space. The $1p$–$1h$ description clearly represents an extremely primitive and restrictive nuclear model. We shall now discuss briefly the consequences of the simplifications, and describe certain attempts to improve the nuclear model. We shall follow the customary procedure and discuss separately the two related subjects; viz. the influence of the $2p$–$2h$ states, and the impurity of the ground state.

The number of $1p$–$1h$ configurations is in general much too small to even begin to allow a description of the fine structure observed in the cross sections. The next members of the nuclear hierarchy, viz., the $2p$–$2h$ states, can be excited from the $1p$–$1h$ states via the nuclear two-body force: either the particle or the hole of the $1p$–$1h$ state can undergo an inelastic scattering process with one of the other nucleons, lifting it above the Fermi level. This state is a genuine $2p$–$2h$ state; it does not arise in the RPA treatment. The two resulting particle–hole pairs can have a variety of angular momenta. For the giant resonance a particularly important case is that in which one of the pairs is coupled to 1^-, and the other to 2^+. As a next

step, any of the four members of the $2p$–$2h$ state can undergo an inelastic collision and generate a $3p$–$3h$ state. Again, each of these resulting particle–hole pairs can be coupled to any angular momentum so long as the three angular momenta can be coupled to the required total angular momentum, i.e., 1^- for the dipole state. (In a RPA state each of the particle–hole pairs is coupled to the angular momentum of the considered state, i.e., 1^- for the dipole state.) This way all the higher members of the nuclear hierarchy can be reached. Of these, the ones of particular importance, besides the $2p$–$2h$ states, are the $4p$–$4h$ states, since they are required for the description of the α emission, and the $5p$–$5h$ states, since they would be needed for the coupling of the giant resonance to the low-lying $4p$–$4h$ states (e.g., the O^+ state at 6.06 MeV in ^{16}O). However, no treatment of these effects is in sight.

The influences of the $2p$–$2h$ states can be grouped roughly into splitting (introduction of structure) and damping. We begin by considering the bound-state treatment. The $2p$–$2h$ states acquire a dipole moment only through mixing with the $1p$–$1h$ states (the photon interaction is described by a one-body operator). Since, in general, every state becomes a mixed state upon diagonalization of the Hamiltonian matrix, the number of resonances becomes equal to the total number of states and the dipole states may spread over a larger energy region. The number of $2p$–$2h$ configurations is very much larger than the number of $1p$–$1h$ configurations. Therefore one in practice will have to radically restrict the number of $2p$–$2h$ configurations which one wants to add to the Hilbert space. A very useful criterion by which to select the retained states can be taken from the collective model, where the most important states are those which arise from mixing the giant dipole oscillation with the collective surface vibrations. In a microscopic picture, the surface modes are given by linear combinations of $1p$–$1h$ positive parity $T=0$ states (for $T=0$ nuclei). One thus is led to the following models: collective dipole mode, collective surface mode (Weber, *et al.*, 1966; LeTourneux, 1965); microscopic dipole-collective surface (Drechesel, *et al.*, 1967); microscopic dipole-microscopic surface. Until now, the first two models have been quite successful; the last, being more fundamental, has not given as good results, mainly because of the difficulty of describing the low energy spectra.

One may think that the only change between the bound-state structure and the case in which the $1p$–$1h$ states are continuum states is a widening of the sharp peaks into broader resonances. This would be true in an inverse case; i.e., where the quasibound states carry the strength, and the continuum states carry no strength. However, matters here are not as simple. As has been shown in detail by Fano (1935, 1961), a $2p$–$2h$ state that is in a $1p$–$1h$ continuum in general will lead only to a modulation of the cross section. Only under certain circumstances will this modulation have the shape of a resonance line.

Up to this time, only one nuclear physics calculation, that of Gillet, *et al.* (1967), has been published in which $2p$–$2h$ states were admixed to the $1p$–$1h$ continuum. Inspired by the observation that a certain resonance (Suffert and Feldman, 1967) of the $^{14}N(d,\gamma_0)^{16}O$ reaction coincides with a pronounced dip in the $^{15}N(p,\gamma_0)^{16}O$ cross section, Gillet, *et al.* (1967) performed the following continuum calculation. They assumed that the peak in the (d,γ_0) cross section was due to a quasibound $(2p$–$2h)$ state. Thus they added bound $(2p$–$2h)$ configurations to the $(1p$–$1h)$ continuum configurations. Only those coherent $(2p$–$2h)$ configurations were taken into account which, as a result of the residual force, coincide energetically with the giant-resonance region. These $1p$–$1h$ configurations were obtained by combining two diagonalized $1p$–$1h$ states of different J^π, one having $T=0$, the other $T=1$. This is, in fact, a kind of microscopic description of the giant-resonance–(surface) phonon coupling. Figure 1 shows the result of this calculation. As a consequence of an interference effect between the $(1p$–$1h)$ structure and the $(2p$–$2h)$ state which lies in the minimum at 22.7 MeV there occurs a peak at 23 MeV which has roughly the experimentally observed width. Also, one sees that diverse shapes occur in the structure, and that the average cross section remains the same upon addition of the $2p$–$2h$ states; the strength is not shifted to other energies.

A detailed agreement between this schematic calculation and experiment is not to be expected. After all, many more $2p$–$2h$ states exist and, also, above 24 MeV the $3p$–$3h$ configurations should become important (Puttaswamy and Kohler, 1966). [The influence of $3p$–$3h$ configurations on the ^{16}O giant resonance has

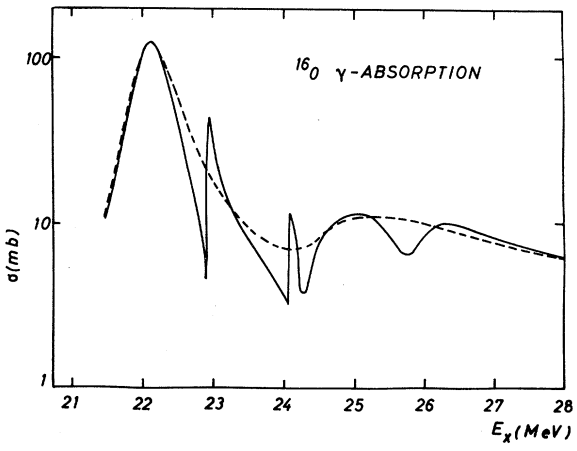

FIG. 1. Theoretical total photoabsorption cross section of ^{16}O obtained in a continuum treatment by Gillet, *et al.* (1967). The solid curve gives the result for inclusion of certain coherent quasibound $2p$–$2h$ states.

recently been investigated by Shakin and Wang (1971).] At any rate, the merit of this calculation lies in the fact that it illustrates the effect of the higher configurations on the cross section.

The damping mechanism is easy to understand in a time-dependent description. In general not only the considered $1p$–$1h$ channels are open, but, e.g., one or several α-particle channels as well. Thus, after having been excited by the absorption of a photon, the $1p$–$1h$ configuration excites a $2p$–$2h$ configuration, etc., until the, say, $5p$–$5h$ configuration, describing the α channel, has been reached. The emission of the α particle is reflected as an additional width on the original $1p$–$1h$ state, and no shifts of absorption strength or any other effect is expected to be associated with this process.

We now turn to the other implicit consequence of the restriction of the Hilbert space to $1p$–$1h$ excitations, viz. the assumption of a pure ground state. This assumption is, perhaps, even more restrictive than the one discussed above. Namely, as soon as the ground state has, say, a $2p$–$2h$ component, many more states are reached directly by the action of the one-body photon operator. This then not only leads to additional structure, but, more importantly, it also shifts absorption strength out of the giant-resonance region. In fact, this feature is responsible for the failure of all bound-state calculations in light nuclei to give the correct photon absorption cross section, and, at the same time, leads to the quasideuteron process. Nothing definitive is known at this time about possible further consequences of the ground state impurities.

C. The Eigenchannel Procedure in Detail

It is helpful in understanding the eigenchannel method to note that there are two distinct ideas, both of which are related to the concept of eigenchannels, involved in the method. This concept, as is well-known, derives directly from two general properties of the S matrix: unitarity (conservation of flux) and symmetry (time-reversal invariance of the Hamiltonian). That is, in symbols, $S^+=S^{-1}$ and $\tilde{S}=S$. These two relations together imply that S may be written in the form

$$S=Ve^{2i\Delta}V^{-1}, \tag{3.1}$$

where V is real and orthogonal, and Δ is real and diagonal. Both V and Δ (and hence S) are $N\times N$ matrices, where N is the number of open channels at energy E. The orthogonal matrix V may be considered as made up of N eigenchannel vectors $V^{(\nu)}$, where $\nu=1, 2, \cdots, N$ denotes the individual vectors. (Alternatively, one may parametrize V by a Cayley transform to introduce the mixing parameters, ϵ, but this is not particularly useful for the present paper.)

The advantage of this procedure is that it enables one to parametrize the S-matrix in terms of the minimal number of real parameters. Application to nuclear reactions of this parametrization has been given by Blatt and Biedenharn (1952); we will repeat the relevant parts of this in Secs. III.D and III.E.

The above definition of the eigenchannels as the set of numbers $V_c^{(\nu)}$ (eigenchannel vectors) is rather abstract. In order to obtain a better understanding of the physical significance of the eigenchannels, we construct them in configuration space; that is, we construct the corresponding Schrödinger wave functions. Consider, therefore, the most general wave function ψ in the asymptotic region; i.e., far from the scattering center (all $r_c>a_c$ with suitably chosen radii a_c)

$$\psi\sim\sum_c\left[A_cI_c(k_cr_c)+B_cO_c(k_cr_c)\right]\psi_c, \tag{3.2}$$

where ψ_c are the channel wave functions containing the hole wave function and the angular parts of the particle wave functions; I_c and O_c are the incoming and outgoing radial wave functions

$$\begin{aligned} I_c^*(k_cr_c)&=O_c(k_cr_c)\\ &=\{G_l(k_cr_c)+iF_l(k_cr_c)\}\exp(-i\sigma_{lc})\\ &\propto\exp\left[i(k_cr_c-\tfrac{1}{2}l\pi-\eta_c\log 2k_cr_c+\sigma_{lc}\right], \end{aligned}\tag{3.3}$$

where F_l and G_l are the regular and irregular solutions of the radial differential equation (i.e., Coulomb functions in the case of protons, and the spherical Bessel and Neumann functions multiplied by k_cr_c for neutrons). The Sommerfeld parameter η_c and the Coulomb phase shift σ_{lc} are given by

$$\eta_c=Ze^2/\hbar v_c \qquad \sigma_{lc}=\arg\Gamma(l+1+i\eta_c). \tag{3.3a}$$

Let us consider for simplicity neutrons only. Then the asymptotic form of (3.2) can be obtained with $I_c=\exp\left[-i(k_cr_c-1/2l\pi)\right]=O_c^*$. The amplitudes of the outgoing waves are defined via the S-matrix in terms of the amplitudes of the incoming waves by

$$B_c\equiv-\sum_{c'}S_{cc'}A_{c'}. \tag{3.4}$$

Let us also denote explicitly the equation for the eigenvalues of the S-matrix

$$SV^{(\nu)}=\epsilon^{(\nu)}V^{(\nu)}, \tag{3.5}$$

where the eigenvalues are of the form

$$\epsilon^{(\nu)}=\exp(2i\delta^{(\nu)}), \tag{3.5a}$$

with $\delta^{(\nu)}$ necessarily real, as they are the diagonal elements of the matrix Δ defined in Eq. (3.1). The $V^{(\nu)}$ are the eigenchannels.

Perform now the following "Gedanken experiment": assume that the incoming amplitudes A_c are identical with the components of an eigenchannel, e.g., $A_c=V_c^{(\nu)}$. It follows from Eqs. (3.4), (3.5), and (3.5a)

that $B_c = -\exp(2i\delta^{(\nu)})V_c^{(\nu)}$ and therefore, (3.2) becomes the representation of an eigenchannel in r space

$$\psi^{(\nu)} = \sum_c V_c^{(\nu)}[I_c - \exp(2i\delta^{(\nu)}O_c]\psi_c$$
$$\sim \sum_c V_c^{(\nu)} \exp(i\delta^{(\nu)}) \sin(k_c r_c - \tfrac{1}{2}l\pi + \delta^{(\nu)})\psi_c \quad (3.6)$$

for neutron channels. In the case of protons, (3.6) is only slightly more involved. We have thus obtained the important result that *an eigenchannel corresponds in r space to a standing Schrödinger wave consisting of a superposition of standing waves in all experimental channels with a common phase shift* $\delta^{(\nu)}$. (*Note that* $\delta^{(\nu)}$ *is independent of c.*)

This result will be the starting point for the practical calculation of eigenphases and eigenchannels. Namely, we construct those solutions of the Hamiltonian which have asymptotically precisely the form (3.6). The common phase shifts for which such solutions exist are then the eigenphases; the amplitudes with which the experimental channels are contained in $\psi^{(\nu)}$ are essentially the eigenchannel components $V_c^{(\nu)}$. If all the Schrödinger wave functions for the total energy E of the system have been constructed, that is, if the eigenphases $\delta^{(\nu)}(E)$ and eigenchannel components $V_c^{(\nu)}(E)$ are known, then the S-matrix is obtained according to (3.1) as

$$S_{cc'}(E) = \sum_\nu V_c^{(\nu)}(E) \exp[2i\delta^{(\nu)}(E)]V_{c'}^{(\nu)}(E). \quad (3.7)$$

This formula is exact and describes in principle all types of resonances with all possible shapes.[6]

The second distinct idea in the eigenchannel method is the use of the scattering eigenchannels to define "natural boundary conditions" for applying the R-matrix theory of nuclear reactions. The principle behind the method (we discuss the practical details below) is straightforward: in the usual R-matrix procedure, one generates solutions X_λ with energy E_λ of the complete Hamiltonian H obeying fixed boundary conditions (logarithmic derivatives) b_c at each channel radius a_c. The eigenchannel method poses an iteration loop: an *assumed* S-matrix at energy E yields the boundary conditions b_c at $r=a_c$ in all open channels; in general, no one of the E_λ is equal to E. The assumed S-matrix is then changed, and the loop repeated until for one E_λ we have $E=E_\lambda$. This, in effect, determines the S-matrix precisely at the energy E, and hence *the eigenchannel method represents an alternative (numerical) procedure to direct integration of the Hamiltonian.*

Our main interest lies in employing the eigenchannel method as a technique for treating the shell model in the continuum. For this we make the basic assumptions that:

(i) The nuclear Hamiltonian H is written as the sum of a one-particle operator $h(i)$ and a residual two-body interaction H'

$$H = H_0 + H', \quad (3.8a)$$

where

$$H_0 = \sum_{i=1}^{A} h(i) = \sum_{i=1}^{A} [t(i)+v(i)]. \quad (3.8b)$$

Here $t(i)$ is the kinetic energy operator of ith nucleon, and $v(i)$ is a suitable shell-model potential. [The $h(i)$ should be chosen as (localized) Hartree–Fock potentials.] Since the shell-model potential is a potential of finite depth, $h(i)$ has both a *discrete* and a *continuous* spectrum. The residual interaction H' in principle would have the form

$$H' = \sum_{i<j}^{A} V(i,j) - \sum_{i=1}^{A} v(i), \quad (3.8c)$$

where the $v(i,j)$ are the true two-body nucleon–nucleon residual interaction potentials. We shall, however, employ less general forms, namely, the schematic delta function interaction.

(ii) It is assumed that all potentials are zero beyond a separation distance a_c, (=channel radius) of any two fragments (except, of course, for the centrifugal and Coulomb potentials).

(iii) The problem of spurious states arising from the lack of translational invariance (common to all current treatments of the shell model in the continuum) is neglected. [It is known from bound-state calculations that the spurious (center of mass) states in mirror nuclei have $T=0$ and occur at an excitation energy of roughly 6–8 MeV. Since we are interested mainly in the $T=1$ states and in the energy region above ~15 MeV, no appreciable error arises here in our neglect of the spurious states.]

(iv) The calculations are to be carried out in a truncated Hilbert space. The actual calculations which we shall discuss in this article have considered only shell-model configurations of the $1p$–$1h$-type. One-nucleon scattering and exchange processes, as well as photo- and electronuclear reactions can be treated within this limitation of the basis space. As is usual, photon channels are introduced by a perturbation procedure.

Having sketched the basic ideas underlying the eigenchannel method let us now turn to the task of filling in the details. To do so we must specify the nuclear Hamiltonian on which the states of the internal region are to be based. As is customary in nuclear structure, we base this construction on the shell model. We shall see below that there are characteristic advantages in the eigenchannel procedure as contrasted to the shell model in the continuum based on Dirac's

[6] A more detailed discussion of the S-matrix, and especially of the R-matrix, expressed in terms of eigenphases and eigenchannels was given by Biedenharn, *et al.* (1963).

approach (cf. Mahaux and Weidenmüller, 1969) and to the coupled channels approach (discussed below).

The ground state of the closed shell A-nucleon system has quantum numbers $J^\pi=0^+$, and its wave function is taken to be a determinant of single-particle functions which should be calculated by means of the usual Hartree–Fock equations. It is assumed that the A particles occupy the lowest A levels of the self-consistent potential. The energy of the highest occupied single-particle level of the nuclear ground state defines the Fermi surface. The levels below the Fermi surface will be called unexcited states, while single-particle levels above the Fermi surface will be referred to as excited states.

The self-consistent Hartree–Fock equations for the wave functions of the unexcited states can be written in the form

$$[T_1+V_{\rm HF}]\phi_\alpha(r_1)=\epsilon_\alpha\phi_\alpha(r_1), \tag{3.9}$$

where ϵ_α is the single-particle energy, T_1 the kinetic energy operator, and $V_{\rm HF}$ the potential energy operator. The arguments of the functions denote the space, spin, and isospin coordinates of a particle. Explicitly we have

$$V_{\rm HF}\phi_\alpha(r_1)=V_0(r_1)\phi_\alpha(r_1) - \int dr_2 U(r_1,r_2)\phi_\alpha(r_2), \tag{3.10}$$

where

$$V_0(r_1)=\sum_{i=1}^{A}\int dr_2\phi_i^*(r_2)V(r_1,r_2)\phi_i(r_2), \tag{3.11}$$

$$U(r_1,r_2)=\sum_{i=1}^{A}\phi_i^*(r_2)V(r_1,r_2)\phi_i(r_1). \tag{3.12}$$

The quantity $V(r_1,r_2)$ is the effective two-body interaction. The states ϕ_i in Eqs. (3.11) and (3.12) are themselves eigenfunctions of Eq. (3.9) and the sums are taken over the A unexcited levels which are all occupied in the nuclear ground state. Suppose now that the Equations above have been solved self-consistently for the ϕ_α so that the potential $V_{\rm HF}$ may be evaluated. This potential can then be used to define other single-particle functions which are *not* necessarily restricted to be below the Fermi surface. In general, then we have

$$[T+V_{\rm HF}]\phi_\gamma(r)=\epsilon_\gamma\phi_\gamma(r). \tag{3.13}$$

The set of functions $\{\phi_\gamma\}$ includes the unexcited states determined from the Hartree–Fock equations and also the excited states which are solutions of Eq. (3.13) and represent bound or unbound single-particle levels not occupied in the nuclear ground state. All the wave functions for the unbound single-particle states are assumed to satisfy the same boundary conditions at the channel radii (this will be discussed in more detail); hence the extended group of functions ϕ_γ can be chosen to form an orthonormal set and we assume that this set is complete.

The quantum numbers labelling a single-particle state consist of the energy and angular momentum eigenvalues together with the isospin projection. For unexcited and excited states we write $\gamma\equiv(\epsilon_\gamma, l, j, m, \tau)$, respectively, where l is the orbital angular momentum, $j=l\pm1/2$ is the total angular momentum, and m is the z projection of j. The quantity τ is the z projection of isospin of a nucleon and is $+1/2$ for a proton and $-1/2$ for a neutron. Explicit forms for the wave functions are

$$\phi_\gamma(r)=\sum_{\lambda\mu}(f_{lj\tau}/r)(\epsilon_\gamma,r)\langle l\lambda s\mu\mid jm\rangle \times\{i^lY_l^\lambda(r)\}X_S^\mu X_t^\tau. \tag{3.14}$$

From Eq. (3.13) and the orthonormality of the single-particle functions, one obtains

$$\epsilon_\gamma\delta_{\gamma\gamma'}=\langle\gamma'\mid T\mid\gamma\rangle+\langle\gamma'\mid V_{\rm HF}\mid\gamma\rangle. \tag{3.15}$$

Using Eqs. (3.11) and (3.12) one may write this expression in the form

$$\epsilon_\gamma\delta_{\gamma\gamma'}=\langle\gamma'\mid T\mid\gamma\rangle + \sum_{\alpha=1}^{A}[\langle\gamma'\alpha\mid V\mid\gamma\alpha\rangle-\langle\gamma'\alpha\mid V\mid\alpha\gamma\rangle], \tag{3.16}$$

where

$$\langle i\mid T\mid j\rangle=\int dr\phi_i^*(r)T\phi_j(r), \tag{3.17}$$

$$\langle ij\mid V\mid kl\rangle=\int dr_1\,dr_2\phi_i^*(r_1)\phi_j^*(r_2) \times V(r_1,r_2)\phi_k(r_1)\phi_l(r_2). \tag{3.18}$$

(Note that the energy of the nuclear ground state is given by

$$E_0=\sum_{\alpha=1}^{A}[\langle\alpha\mid T\mid\alpha\rangle + \tfrac{1}{2}\sum_{\alpha'=1}^{A}\{\langle\alpha\alpha'\mid V\mid\alpha\alpha'\rangle-\langle\alpha\alpha'\mid V\mid\alpha'\alpha\rangle\}].) \tag{3.19}$$

The sums over α or α' in Eqs. (3.16) and (3.19) refer only to the unexcited states.

Our basic approximation for the dipole resonance states of the A-nucleon system is to represent them by linear combinations of particle–hole wave functions. This implies that each component of the approximate total wave function may be written as a determinant of single-particle functions in which one particle occupies an excited state above the Fermi surface, while all the other nucleons are in unexcited states. This clearly determines a hole state of the core nucleus with $(A-1)$ nucleons. (We are assuming, of course, that the excitation of a particle above the Fermi surface does not greatly alter the effective single-particle potential $V_{\rm HF}$, so that the particles in the core nucleus can still be regarded as occupying the unexcited basis states $\phi_{\alpha'}$.)

A hole state of the core nucleus with $(A-1)$ particles is defined in terms of the quantum numbers of the missing particle. It is customary at this point to

transcribe these equations into the language of second quantization, but this is of no particular usefulness for the eigenchannel method and will be omitted. (See, however, Sec. III.C.)

Consider now the problem of defining the shell-model (Hartree–Fock) basis functions in the continuum. It is essential, for computational reasons, to "discretize" the system, and there are almost as many prescriptions as there are authors. One may, for example, use the Weyl eigendifferentials, i.e., simply replace "strips" of the continuum by points, as has been done by Bloch and Gillet (1965; see also Gillet and Bloch, 1965).

In the eigenchannel approach, the continuum is made discrete by applying the natural boundary conditions at a radius of nuclear dimensions (the dimensions of the internal region of Wigner's R-matrix theory).

In order to carry out this step in detail, it is first necessary to recouple the Hartree–Fock functions (above) into the j–j form. Second, we shall now use explicitly the simplification of a contact (delta function) residual force (see Sec. IV.B). This yields the residual interaction energy matrix

$$V_{nc,n'c'}=(V_0/4\pi)(-)^{l+l'}[(2L+1)(2l+1)\times(2L'+1)(2l'+1)(2I+1)(2j+1)(2I'+1)(2j'+1)]^{1/2}\times\sum_{\Lambda}\sum_{S=0,1}(Ll00\mid\Lambda 0)(L'l'00\mid\Lambda 0)g_S^{\tau\tau'}(2S+1)\times\begin{Bmatrix}L&\frac{1}{2}&I\\ l&\frac{1}{2}&j\\ \Lambda&S&J\end{Bmatrix}\begin{Bmatrix}L'&\frac{1}{2}&I'\\ l'&\frac{1}{2}&j'\\ \Lambda&S&J\end{Bmatrix}\times\int_0^\infty u_{LI\tau}u_{nc}u_{L'I'\tau'}u_{n'c'}r^{-2}\,dr, \quad (3.20)$$

where U_{nc} and $U_{LI\tau}$ are the radial functions of the particles and holes respectively [these radial functions are defined similar to the $f_{lj\tau}(r)$ in Eq. (3.14)]. The exchange terms are

$$g_0^{\tau\tau'}=(2-\delta_{\tau\tau'})a_0-3\delta_{\tau\tau'}a_\sigma, \quad (3.20a)$$

$$g_1^{\tau\tau'}=-\delta_{\tau\tau'}a_0+(2+\delta_{\tau\tau'})a_\sigma. \quad (3.20b)$$

Here a_0 and a_σ are the strengths of the direct and spin-dependent parts of the residual forces. The last step is a truncation of the space of the Hartree–Fock basis functions.

We now recall that the correctly normalized νth eigenchannel wave function in the asymptotic region ($r>a$) is given by

$$\psi_{as}^{J\pi}=\sum_c v_c^{1/2}V_c^{J\pi,\nu}w_c^{\nu}(r)\psi_c, \quad (3.21)$$

where ψ_c is the channel function of channel c, $V_c^{\tau\pi,\nu}$ is the νth eigenchannel (column vector of the $S^{\tau\pi}$ matrix), v_c denotes the relative velocity of the particle in this channel, and

$$w_c^{\nu}(r)=\tfrac{1}{2}i\exp(-i\delta_{J\pi}^{(\nu)})I_c-\tfrac{1}{2}i\exp(i\delta_{J\pi}^{(\nu)})O_c. \quad (3.22)$$

The ingoing and outgoing radial functions I_c and O_c were defined in Eq. (3.3). From this equation follows that Eq. (3.22) can be rewritten in the form

$$w_c^{\nu}(r)=G_c(k_cr)\sin(\delta_{J\pi}^{(\nu)}-\sigma_c)+F_c(k_cr)\cos(\delta_{J\pi}^{(\nu)}-\sigma_c). \quad (3.22')$$

The radial parts in Eq. (3.22′) are real and the eigenchannel functions are standing waves in all experimental channels. They thus resemble a superposition of single-particle radial functions for a real potential. The wave numbers k_c can be obtained from

$$k_c=[2M_c(E-Q_c)/\hbar^2]^{1/2}, \quad (3.23)$$

where Q_c is the threshold energy in channel c for a given excitation energy E of the compound system.

Up to this point we have considered only the $1p$–$1h$ states. Almost all calculations have been done within this restricted basis. If one wants to enlarge the configuration space, one may simply add an arbitrary number of particle–hole or more particle–more hole states as long as they are bound states, i.e., if their wave functions are sufficiently small at the matching radius a_c. (The question of what constitutes "sufficiently small" will be discussed in Sec. III.I.) This would lead to an enlargement of the Hamiltonian matrix, i.e., one would have to add diagonal terms and potential energy matrix elements analogous to Eq. (3.20). The calculation of these matrix elements is the standard problem of bound-state nuclear physics. Certain problems of defining orthogonal functions in the interior arise if more than one particle simultaneously occupies states belonging to the continuum. This point has been discussed for the case of two particles by Danos and Greiner (1967) and Grauel (1971).

The eigenchannel procedure involves an *iteration loop*. With (trial) initial values of the boundary conditions at fixed energy E, specified by assuming a trial value, say δ, for the eigenphase the single-particle functions of the truncated basis can all be calculated. These functions determine the energy matrix

$$H_{nc,n'c'}=\delta_{nn'}\delta_{cc'}[\epsilon_{nc}+Q_c]+V_{nc,n'c'}. \quad (3.24)$$

This matrix is now diagonalized, and one determines the eigenvalues $E_\lambda(E,\delta)$ and the eigenvectors $A_\lambda(E,\delta)$, *both implicit functions of the (trial) boundary conditions.* One now compares the energies E_λ of the eigenvectors determined from diagonalizing the basis set in the internal region with the fixed energy E used in computing the boundary conditions, and closes the iteration loop by changing the assumed value for the eigenphase δ in Eq. (3.22a). The iteration is continued until the energy of one of the internal solutions of Eq. (3.24) agrees with the externally fixed energy E.

In other words, the eigenphases and eigenvectors are

obtained as solutions of the *transcendental consistency equation*

$$\Pi_\lambda[E_\lambda(E,\delta)-E]=0. \tag{3.25}$$

The amplitudes $V_c^{J\pi,\nu}$ can be determined by equating, in the asymptotic region at $r=a$, the form (3.21) of the nuclear wave function to that obtained by diagonalization of the nuclear Hamiltonian (3.24). The nuclear wave function obtained in the interior space by diagonalization will now be written as

$$|\psi^{J\pi,\nu}\rangle=\sum_{n,c} A_{nc}{}^{J\pi,\nu}\,|nc\rangle\rangle^{(\nu)}. \tag{3.26}$$

Here the $|nc\rangle\rangle$ denote the j–j coupled $1p$–$1h$ basis functions. Explicitly, we have

$$|nc\rangle\rangle=\sum_m (-)^{j-m}(jIM+m-m\,|\,JM)\,|\,IM+m\rangle^* \times|jm\rangle r_h^{-1}u_{LI\tau}(r_h)r^{-1}u_{nc}(r)\,|\,t_h\tau\rangle^*\,|\,t\tau\rangle. \tag{3.27}$$

The index ν on the particle–hole functions in Eq. (3.26) indicates that the particle states obey the boundary conditions of the νth eigenchannel.

Figure 2 gives an example of the behavior of E_λ as a function of the phase δ. We show a plot for the 1^- states in ^{12}C. Here E is equal to 25 MeV and at this energy six 1^- channels are open. It is obvious from the figure that there are six eigenphases.

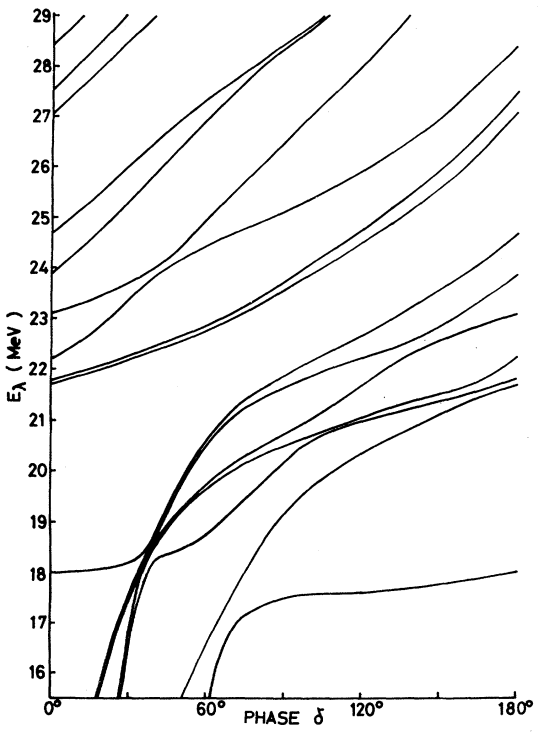

FIG. 2. Example of the behavior of the 1^- eigenvalues (E_λ) of the nuclear Hamiltonian of ^{12}C as a function of the common phase shift δ, which, together with the excitation energy, E, (in this case $E=25$ MeV) determines the boundary conditions for the particle states.

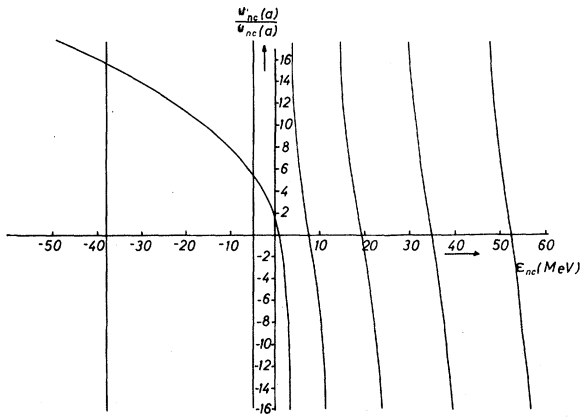

FIG. 3. Energy dependence of the logarithmic derivative of the $s_{1/2}$ radial state in a square well potential as specified in the text.

The "kinematics" of the plot (Fig. 2) is the following: Since the logarithmic derivative is a periodic function of δ with a period π, the topology of the plot is that of a cylinder. The eigenvalue curves are thus interlaced helices which do not cross as they "wind their way up." This is simply a consequence of Wigner's no-crossing theorem: At any fixed value of δ the problem is of the usual Sturm–Liouville type and thus, with an overwhelming probability, the eigenvalues of the Hamiltonian are nondegenerate. Therefore, a no-crossing theorem holds also for the eigenphases with the same kind of validity as for the eigenvalues of any Hamiltonian. The number of the eigenvalue lines equals the number of open channels, as can be seen by tracing each line "backwards." This is most transparent before switching on the residual interactions. Then each channel consists of a particle in the continuum together with an unperturbed residual nucleus in some discrete state. The unperturbed energy of such a system then consists of the fixed energy of the hole state plus the energy of the free particle, which can be read off a plot of the type of Fig. 3 as a function of the logarithmic derivative. Each open channel then disappears at a particular phase shift. Switching on the residual interaction shifts the energies somewhat and removes the level crossings.

Plots of the type shown in Fig. 2 may be used to locate the position of the bound states embedded in the continuum before the start of the phase iteration procedure. (See Barrett and Delsanto, 1971.) As intermediate structure in the cross section results from the BSEC, one thus knows *a priori* where this structure is likely to be found, and a considerable reduction of the required computational effort is achieved.

As an example of the energy dependence of the eigenphase, we consider the 1^- ^{16}O compound system (Fig. 4) assuming the parameters which are given in Sec. V.A. It is obvious from the figure that in realistic

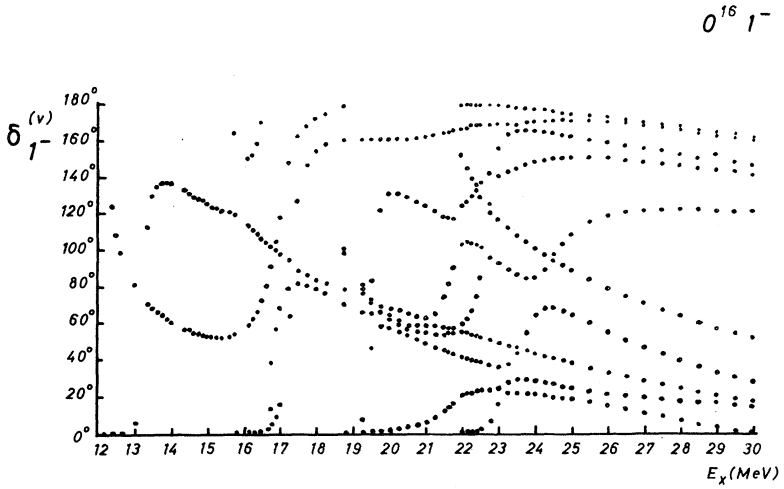

FIG. 4. Computed eigenphases $\delta^{(\nu)}$ of the 1^- O^{16} compound system versus excitation energy E. The parameter choice is that of Sec. 4.G. The computed points for the eigenphases have not been joined into curves since the behavior of the curves near crossing has not been determined to the required accuracy.

cases the situation may become rather complex. The "step width" used in the numerical computations is indicated in the plot.

We have not yet discussed the choice of the matching radius "a". The larger one chooses a, the larger the required numerical effort, both because the integration value increases and because the level density at positive energies increases. Thus, if one wants to truncate the Hilbert space at some higher energy, one has to enlarge the number of states. On the other hand, too small a matching radius leads to certain inaccuracies in the calculation. We shall discuss these points in Sec. III.I.

Another point concerns the difference between the dimensionality of the Hilbert space of the outside and inside regions. First notice that the normalizations of Eqs. (3.21) and (3.22) are different, because Eq. (3.26) contains open as well as closed channels and the particle radial functions are normalized to unity within $0\leq r\leq a$, while (3.21) contains only the open channels, and the radial parts are normalized to unit flux. To obtain continuity of the nuclear wave function at $r=a$, we replace [in Eq. (3.21)] in $V_c^{J\pi,\nu}$ by unnormalized coefficients $C_c^{J\pi,\nu}$. By equating the modified expression (3.21) with the expression (3.26) at $r=a$, and integrating over all coordinates except r, we obtain the matching condition

$$v_c^{-1/2}C_c^{J\pi,\nu}w_c^{\nu}(a)=\sum_n A_{nc}^{J\pi,\nu}u_{nc}^{\nu}(a). \quad (3.28)$$

Finally, the amplitudes $V_c^{J\pi,\nu}$ of Eq. (3.21) are obtained by normalization to give

$$V_c^{J\pi,\nu}=C_c^{J\pi,\nu}/N_{J\pi,\nu},$$
$$N_{J\pi,\nu}^2=\sum_c (C_c^{J\pi,\nu})^2. \quad (3.29)$$

The error involved in this step is discussed in Sec. III.I.

D. The Coupled-Channel Method and the Random Phase Approximation

The Hartree–Fock approximation for the single-particle motion is also the basis for these two closely related approaches to nuclear scattering theory. Both approaches have the added advantage of providing a self-consistent treatment. As has been emphasized by Villars (1967), the average field that scatters the incident nucleon turns out to be (or is believed to be) the Hartree–Fock potential, which in turn is determined by the same nuclear (two-body) interactions that lead to the formation of the bound and resonant states.

It is most economical to begin with Eq. (3.14), and transcribe it into the language of second quantization. Denote the Hartree–Fock orbitals by

$$\phi_\gamma(r)\equiv\langle r\mid\gamma\rangle; \quad (3.30)$$

Fermion operators, a_γ^+ and a_γ, (satisfying the usual anticommutation relations) will be defined as those which create or destroy the states denoted by the index γ, which expressed more completely, denotes $nljm\tau$. The state obtained by filling the lowest A orbitals will be denoted by $\mid g\rangle\equiv\pi a_\alpha^+\mid 0\rangle$, which plays the role of the Hartree–Fock vacuum. It is at this point that the two approaches differ in a minor way: in the coupled-channels method (Buck and Hill, 1967; Marangoni and Saruis, 1967, 1969) the continuum is made discrete by imposing fixed boundary conditions at a "large" radius. The random phase approximation (RPA) procedure (Lemmer and Veneroni, 1968; Dietrich and Hara, 1968; Hahne and Dover, 1969) works directly with the continuum by letting the index γ (more precisely n) have both a discrete and continuous range.

Although it is standard to adapt the notation to

accord with the state $|\,g\rangle$ as the "vacuum," it proves simpler for the work to follow not to define a separate "hole" creation operator. [In angular momentum coupling, involving destruction operators (hole operators), a_γ it is necessary to adjoin the phase $(-)^{j-m}$ denoted by $(-)^\lambda$.]

The Hartree–Fock Hamiltonian, defined on the basis $\{\langle x\,|\,\gamma\rangle\}$, then takes the usual form

$$H=\sum_{ij}\langle i\,|\,T\,|\,j\rangle a_i^+a_j + \tfrac{1}{2}\sum_{ijkl}\langle ij\,|\,V\,|\,kl\rangle a_i^+a_j^+a_la_k. \quad (3.31)$$

[The matrix elements have been defined in Eqs. (3.17) and (3.18).] In this language a typical particle–hole excitation of the A-particle system can be represented in the form

$$|\,p,h\rangle\rangle\equiv|\,\alpha,\beta\rangle\equiv a_\alpha^+a_\beta\,|\,g\rangle. \quad (3.32)$$

Since this state in general does not have sharp angular momentum, it is useful to couple the two operators $[a_\alpha^+\times a_\beta]_J^M$. In a fully explicit, but tiresome, notation these particle–hole creation operators are given by

$$A^+[JM;\,(nlj\tau)_p(n'l'j'\tau')_h] \equiv\sum_{mm'}(-)^\alpha(jj'mm'\,|\,JM)a_{nljm\tau}^+a_{n'l'j'm'\tau'}. \quad (3.33)$$

For brevity this operator will be denoted by $A_{JM}^+(ph)$. Note that there are an infinity of these particle–hole operators and that n may have a continuum part.

The objective is now to construct an *approximate* eigenfunction of H in the space of these particle–hole operators. The most direct procedure would be to construct a general linear combination over this space, that is,

$$F_\lambda^+\equiv\sum f_{ph}{}^\lambda A_{JM}^+(p,h), \quad (3.34)$$

and to determine the variables, $f_{ph}{}^\lambda$, by requiring that the state vectors

$$|\,\lambda\rangle\equiv F_\lambda^+\,|\,g\rangle \quad (3.35)$$

be an approximate eigenfunction of H having energy E_λ. Since the operator H does not preserve the number of particle-hole pairs, one cannot require that $H\,|\,\lambda\rangle\rightarrow E_\lambda\,|\,\lambda\rangle$, but rather only the weaker condition resulting from projection onto the particle–hole space; explicitly

$$\langle g\,|\,A(JM;ph)HF_\lambda^+\,|\,g\rangle=E_\lambda\langle g\,|\,AF_\lambda^+\,|\,g\rangle. \quad (3.36)$$

This requirement leads to an infinite set of algebraic equations for the coefficients $f_{ph}{}^\lambda$. These equations are actually of almost no interest since the scattering problem does not directly concern states $|\,\lambda\rangle$, but rather deals with the asymptotic properties of the particle wave functions in configuration space.

Thus a change of representation is desirable; the most useful representation is a mixed one treating the particle states in coordinate space, but leaving the hole states in occupation number space. The appropriate changes are easily accomplished. The particle creation operator becomes

$$a_{ljm\tau}^+(r)\equiv\sum_n R_{nlj\tau}(r)a_{nljm\tau}^+; \quad (3.37)$$

the particle–hole creation operator accordingly becomes

$$A^+(JM;\,(nlj\tau)_p(n'l'j'\tau')_h)=\sum_{mm'}(-)^{j'-m'} \times(jj'mm'\,|\,JM)a_{ljm\tau}^+(r)a_{l'j'm'\tau'}(r). \quad (3.38)$$

Just as before we seek the most general linear combination over this $1p$–$1h$ space to define approximate eigenfunctions; the required form is now

$$F_\lambda^+\equiv\sum f_{ph}{}^\lambda(r)A_{JM}^+(ph). \quad (3.39)$$

This (compressed) notation is rather vague; to be fully explicit let us write this as

$$F^+(\lambda,JM)\equiv\sum_{lj;n'l'j'}\int r^2\,dr\,f\,[\lambda,J,\,(nlj\tau)_p(n'l'j'\tau')_h] \times A^+(JM;\,(nlj\tau)_p(n'l'j'\tau')_h). \quad (3.40)$$

This formidable appearing operator has a simple physical interpretation: the state vector $F_\lambda^+\,|\,g\rangle$ consists of a linear combination of all possible particle–hole systems having sharp J and M, and (as will be shown) the total energy E_λ. The function $f(\cdots)$, above, plays the role of a particle radial wave function for each allowed p–h system of the vector $|\,\lambda\rangle$. More accurately, it is the *projected* function $f(\cdots)$ which is the effective (particle) radial wave function, since the antisymmetry of the operator $\{\alpha_\gamma\}$ automatically projects out all components in F_λ^+ which are common to the ground state $|\,g\rangle$.

The projected function $\phi(\cdots)$ is then

$$\phi[\lambda,J,\,(rlj\tau)_p(n'l'j'\tau')_h]\equiv\int(r')^2\,dr'[\delta(r-r')/r^2] -\rho_{lj}(r,r')f[\lambda,J,\,(nlj\tau)_p(n'l'j'\tau')_h;r'], \quad (3.41)$$

where

$$\rho_{lj}(r,r')\equiv\sum_{n\,\epsilon\,\mathrm{occ}}R_{nlj}(r)R_{nlj}(r'). \quad (3.42)$$

It remains now to derive the integrodifferential equations satisfied by ϕ_λ. This is accomplished by projecting the energy eigenvalue equation onto the $1p$–$1h$ subspace, as indicated earlier. Using the operator $A[JM,\,(nlj\tau)_p,\,(n'l'j'\tau')_h]$, denoted by A, to accomplish this projection, we have the equation

$$\langle g\,|\,AHF_\lambda\,|\,g\rangle=E_\lambda\langle g\,|\,AF_\lambda\,|\,g\rangle. \quad (3.43)$$

The reduction of this equation is simple in principle, but tedious; this reduction uses the result

$$\langle g\,|\,a_{\alpha'}{}^+a_\alpha Ha_\alpha{}^+a_{\alpha'}\,|\,g\rangle =\epsilon_{\alpha'}{}^{\mathrm{occ}}\epsilon_{\alpha'}{}^{\mathrm{occ}}(1-\epsilon_\alpha{}^{\mathrm{occ}})(1-\epsilon_\alpha{}^{\mathrm{occ}}) \times\{\delta_\alpha{}^\alpha\delta_{\alpha'}{}^{\alpha'}[E(g)+E(\alpha')-E(\alpha)] +\langle\alpha\alpha'\,|\,V\,|\,[\![\alpha'\alpha]\!]\rangle\}. \quad (3.44)$$

The notation is

$$\langle\alpha\beta \mid V \mid [[\gamma\delta]]\rangle \equiv \langle\alpha\beta \mid V \mid \gamma\delta\rangle - \langle\alpha\beta \mid V \mid \delta\gamma\rangle$$

$$\epsilon_\alpha{}^{\text{occ}} \equiv 1 \quad \text{if } \alpha \in \text{occupied state}$$

$$\equiv 0 \quad \text{if not}$$

$$E(\alpha) \equiv \text{energy of HF orbital } \alpha$$

$$E(g) \equiv \tfrac{1}{2} \sum_{\alpha \in \text{occ}} [T(\alpha) + E(\alpha)].$$

Introducing this result into the eigenvalue equation, we find that—aside from the interaction matrix element $\langle\alpha\alpha' \mid V \mid [[\alpha'\alpha]]\rangle$—the delta functions are sufficient to yield a simple result

$$[E_\lambda - E(g) - E(\alpha') - H_{\text{HF}}] \times \phi[J, \lambda, (nlj\tau)_p, (n'l'j'\tau')_h] = W\phi, \quad (3.45)$$

where W is the interaction term given below. Here H_{HF} denotes the Hartree–Fock Hamiltonian, Eq. (3.31), in the coordinate representation.

The interaction term is rather complicated, largely as a result of the fact that the interaction matrix element has not been put in a form in which the angular momentum restrictions are explicit. This interaction term has the form

$$W = \sum (-)^{j-m+j'-m'} (jj'mm' \mid JM)(jj'mm' \mid JM) \times f(\lambda, J, (nlj\tau)_p, (n'l'j'\tau')_h) \times \langle nlj\tau \mid r\rangle\langle r \mid nlj\tau\rangle \times \epsilon_{\alpha'}{}^{\text{occ}} \epsilon_{\alpha'}{}^{\text{occ}} (1-\epsilon_\alpha{}^{\text{occ}})(1-\epsilon_\alpha{}^{\text{occ}}) \langle\alpha\alpha' \mid V \mid \alpha'\alpha\rangle \quad (3.46)$$

[the sum is over $(mm'n)$, $(rnljm)$, $(n'l'j'm')$]. The structure of this integrodifferential equation for ϕ_λ is clear: ϕ_λ obeys the Hartree–Fock differential operator appropriate to an orbital function with the effective energy $[E_\lambda - E(g) - E(\text{hole})]$, with, however, an interaction term W which is an integral operator. The radial function, f_λ, in this integral operator is projected [by $(1-\epsilon_\alpha{}^{\text{occ}})$] into ϕ_λ; similarly there is a second projection operator acting on the other (particle) variable α. The net result of the $(1p$–$1h)$ approach (the Tamm–Dancoff approximation) is to yield effectively one-particle equations; the desired channel wave functions must be obtained by integration, and from the asymptotic behavior the scattering properties are obtained for each channel. These technical considerations are standard, and can be discussed equally well in the eigenchannel procedure.

This (TDA) eigenvalue equation for the effective radial wave functions is very complicated; in practice no solution has yet been attempted without gross approximation. In the work of Buck and Hill (1967), who were among the first to derive and apply Eq. (3.45), the following approximations were made:

(a) The two-body interaction $V(i, j)$ was schematized by a contact (delta function) interaction;

(b) The exchange terms [the terms (indicated by the $[[\ ]]$) introduced by the Pauli principle in both V_{HF} and in W] were omitted[7]; and

(c) The (nonlocal) Hartree–Fock potential V_{HF} was approximated by a local interaction.

It is necessary to mention that in the derivation of Eq. (3.45) above, the orbitals were defined relative to a fixed origin. This has the effect of neglecting the center of mass restriction (spoils translational invariance) and introduces spurious states. As argued earlier, this limitation is not too serious for the $T=1$ states considered by Buck and Hill (as well as the work reported below). One other approximation used by Buck and Hill should be mentioned: the term V_{HF} was not only taken to be local, but also to be a complex (optical) potential. This heuristic approach was necessary in order to obtain widths of the proper (experimentally observed) size.

Let us sketch briefly the ideas behind the random phase approximation, which extends the $(1p$–$1h)$ treatment given above. The essential idea is that the operators F_λ, which, acting on $\mid g\rangle$, generated the approximate eigenstates $\mid \lambda\rangle$, are to be generalized to destroy, as well as create, particle–hole pairs

$$F_\lambda{}^+ \rightarrow \sum [f_{ph}{}^\lambda A_{JM}{}^+(ph) - g_{ph}{}^\lambda A_{JM}(ph)].$$

Correspondingly, the ground state $\mid g\rangle$ is generalized to the state $\mid \psi_0\rangle$ defined by

$$F_\lambda \mid \psi_0\rangle = 0.$$

The new ground state thus contains particle–hole states; expressed differently, $\mid \psi_0\rangle$ contains long-range correlations generated by the "backward going graphs." Lemmer and Veneroni (1968) have given an elegant derivation of the coupled integrodifferential equations (not, however, in the angular momentum representation) for f^λ and g^λ; we shall not go into this further, since these formidable equations have, to date, not been applied numerically.

One particularly nice feature of the work of Lemmer and Veneroni is that they discuss in detail the application of their equations to the schematic model of Brown, *et al.* (1966) and show how the continuum contributions effectively renormalize the particle–hole matrix elements between bound pairs.

E. Particle–Particle Reaction Cross Sections

In this section we give the expressions of angular distributions, partial, and total cross sections for particle–particle reactions in terms of the eigenphases

[7] For negative parity states in ^{16}O (the case considered by Buck and Hill (1967) only the occupied $1s_{1/2}$ level would contribute to the error in this approximation. This level lies at ~ -35 MeV, and, according to Buck and Hill, would cause no serious error. In fact, in Fig. 13(b) we show that the effect of approximation (b) consists mainly in an energy shift of the giant resonance. This has been verified in a simplified case in the calculations of Raynal, *et al.*, (1967). Approximations (a) and (b) were not made in the calculation.

and the eigenvectors of the S-matrix. We closely follow the treatment of Blatt and Biedenharn (1952). Let us first recapitulate the case of elastic scattering of a single spinless particle by a central force (potential scattering). There the particle cross section $d\sigma$ is

$$d\sigma = |f(\vartheta)|^2 \, d\Omega, \tag{3.47}$$

with the following scattering amplitude:

$$f(\vartheta) = i\pi^{1/2}\lambda \sum_{l=0}^{\infty} (2l+1)^{1/2} \times [1-\exp(2i\delta_l)] Y_{l0}(\vartheta). \tag{3.48}$$

Here δ_l are the scattering phases which here are simply the eigenphases of the one-dimensional S-matrices, one for each angular momentum l, and λ denotes the wavelength of the scattering particle. By applying the addition theorem for spherical harmonics, one obtains

$$d\sigma/d\Omega = \lambda^2 \sum_{L=0}^{\infty} B_L P_L(\cos\vartheta), \tag{3.49}$$

with

$$B_L = \sum_{l=0}^{\infty} \sum_{l'=|l-L|}^{l+L} (2l+1)(2l'+1)[(ll'00 \mid L0)]^2 \times \sin\delta_l \sin\delta_{l'} \cos(\delta_l - \delta_{l'}). \tag{3.50}$$

Then the integrated cross section is given by

$$\sigma_0 = 4\pi\lambda^2 B_0. \tag{3.51}$$

The cross sections can be readily calculated if the eigenphases (scattering phases) of the S matrices are known. In the general case of interacting channels, the cross section is given by an analogous expression which, besides the eigenphases, also contains the amplitudes $V_c^{(\nu)}$.

In deriving the cross-section formulas for the general case, we need a wave function in which the N orthogonal eigenchannel functions, (3.21) and (3.26), respectively, have been superposed in such a way that they asymptotically represent an incoming plane wave plus outgoing spherical waves. For well-known reasons it is advantageous to do this in the channel spin representation. Thus we introduce the channel spin s by coupling the spin s_A of the scattering nucleon to the target spin I

$$\psi_I{}^{s\mu} = \sum_{\sigma} (-)^{1/2-\sigma} (I\, \tfrac{1}{2}\, \mu+\sigma\, \sigma \mid s\mu) \times \mid I\, \mu+\sigma\rangle^* \mid \tfrac{1}{2}\sigma\rangle. \tag{3.52}$$

The channel spin then can be coupled to the angular momentum l of the particle to give the spin J of the compound system (for sake of notational simplicity we will, in the following, drop the parity index π)

$$\mathcal{Y}_{Jls}{}^{M} = \sum_{\mu} (l\, s\, M-\mu\, \mu \mid JM) \psi_I{}^{s\mu} Y_{lM-\mu}(\Omega). \tag{3.53}$$

If the internal function of the $(A-1)$ system is denoted by ϕ_I, the basis functions (3.27) can be rewritten in the form

$$\mid nc\rangle\rangle = \sum_{s} k_{Islj}{}^{J} \mathcal{Y}_{Ils}{}^{M} \phi_I r^{-1} u_{nc}(r), \tag{3.54}$$

where

$$k_{\alpha slj}{}^{J} = (-)^{s+I+j+l}[(2j+1)(2s+1)]^{1/2} \times \begin{Bmatrix} s & I & \frac{1}{2} \\ j & l & J \end{Bmatrix}. \tag{3.54b}$$

The recoupling coefficients K fulfill the orthogonality relations

$$\sum_{s} K_{Islj}{}^{J} K_{Islj'}{}^{J} = \delta_{jj'}, \qquad \sum_{j} K_{Islj}{}^{J} K_{Is'lj}{}^{J} = \delta_{ss'}. \tag{3.55}$$

The different possible particle cross sections are defined by an experimental situation in which an incoming wave exists only in one experimental channel, and outgoing waves exist in all channels. The situation can be characterized by the quantum numbers $Is\mu$. Here μ is the projection of the channel spin s. Asymptotically, for large r, the properly normalized wave function which describes the process is given by

$$\psi = v_{c'}{}^{-1/2} \exp(ik_{c'}z)\psi_I{}^{s'\mu'*}\phi_{I'} + (i/k_{c'}) \sum_{Is\mu} v_c{}^{-1/2} \theta_{Is\mu,I's'\mu'}(\vartheta,\varphi) r^{-1} \times \exp(ik_c r)\psi_I{}^{s\mu}\phi_I. \tag{3.56}$$

By expanding the incident particle wave in terms of asymptotic eigenchannel functions (3.21), one obtains for the scattering amplitude

$$\theta_{Is\mu,I's'\mu'} = \sum_{J} \sum_{ll'} \sum_{m} i^{l'-l}\pi^{1/2}(2l'+1)^{1/2} \times (lsm\mu \mid Jm+\mu)(l's'0\mu' \mid J\mu') \times [\delta_{II'}\delta_{ss'}\delta_{ll'} - \dot{S}_{Isl,I's'l'}{}^{J}] Y_{lm}{}^{*}(\vartheta,\varphi), \tag{3.57}$$

where $\dot{S}^J$ denotes the S^J matrix in the channel spin representation

$$\dot{S}_{Isl,I's'l'}{}^{J} = \sum_{jj'} K_{I's'l'j'}{}^{J} S_{c'c}{}^{J} K_{Islj}{}^{J}, \tag{3.58}$$

and the dependence of $S_{cc'}{}^{J}$ on the eigenchannel parameters $\delta^{(\nu)}$ and $V^{J,\nu}$ can be seen from Eq. (3.7). The partial cross section for the reaction $I's' \rightarrow Is$ follows from

$$d\sigma_{Is,I's'}/d\Omega = [\lambda_{c'}{}^2/(2s'+1)] \times \sum_{\mu\mu'} \mid \theta_{Is\mu,I's'\mu'}(\vartheta,\varphi) \mid^2. \tag{3.59}$$

Using the proper statistical weights, one obtains, for a process where the channel spin is not observed,

$$d\sigma_{II'} = \sum_{ss'} [(2s'+1)/(2s_A'+1)(2I'+1)] d\sigma_{Is,I's'}. \tag{3.60}$$

Inserting Eqs. (3.7), (3.57), (3.58), and (3.59) in Eq. (3.60) and expanding the angular distribution in

terms of Legendre polynomials, one finally obtains

$$\frac{d\sigma_{II'}}{d\Omega}=\frac{\lambda\!\!\!^{-}_{c'}{}^2}{(2s_A'+1)(2I'+1)}\times\sum_{\Lambda=0}^{\Lambda_{\max}}\sum_{ss'}B_\Lambda(Is,I's')P_\Lambda(\cos\vartheta),\quad(3.61)$$

where $s_A'=\frac{1}{2}$ and

$$\sum_{ss'}B_\Lambda(Is,I's')=\sum_{J_1J_2}\sum_{\nu_1\nu_2}(2J_1+1)(2J_2+1)\times\sin\delta_{J_1}{}^{(\nu_1)}\sin\delta_{J_2}{}^{(\nu_2)}\cos(\delta_{J_1}{}^{(\nu_1)}-\delta_{J_2}{}^{(\nu_2)})\times T_\Lambda(I,J_1\nu_1,J_2\nu_2)T_\Lambda(I',J_1\nu_1,J_2\nu_2)\quad(3.62)$$

$$T_\Lambda(I,J_1\nu_1,J_2\nu_2)=(-)^{I-1/2}\sum_{l_1j_1}\sum_{l_2j_2}i^{\Lambda+l_1-l_2}\times[(2l_1+1)(2l_2+1)(2j_1+1)(2j_2+1)]^{1/2}\times(l_1l_200\mid\Lambda0)W(J_1J_2j_1j_2;\Lambda I)\times W(l_1l_2j_1j_2;\Lambda\tfrac{1}{2})V_{c_1}{}^{J_1\nu_1}V_{c_2}{}^{J_2\nu_2}.\quad(3.63)$$

The sums over ν_1 and ν_2 go independently over all eigenvectors of the S-matrix. Equation (3.61) gives the angular distribution for a process $I'L'\tau'\to IL\tau$, i.e., it gives the elastic scattering cross sections and the various particle–particle reaction cross sections.

By integrating Eq. (3.61) over the solid angle, one obtains

$$\sigma_{II'}=\sum_J\frac{\pi\lambda\!\!\!^{-}_{c'}{}^2(2J+1)}{(2s_A'+1)(2I'+1)}\times\sum_{lj}\sum_{l'j'}\mid\delta_{II'}\delta_{ll'}\delta_{jj'}-S_{cc'}{}^J\mid^2.\quad(3.64)$$

Summing over the final target states leads to the total cross section for the bombardment of an initial target state $I'L'\tau'$

$$\sigma_{I'}=\frac{4\pi\lambda\!\!\!^{-}_{c'}{}^2}{(2s_A'+1)(2I'+1)}\sum_{IL\tau}\sum_{ss'}B_0(Is,I's'),$$

$$=\frac{2\pi\lambda\!\!\!^{-}_{c'}{}^2}{(2s_A'+1)(2I'+1)}\sum_J(2J+1)\sum_{lj}[1-\mathrm{Re}\,S_{cc'}{}^J],$$

$$=\frac{2\pi\lambda\!\!\!^{-}_{c'}{}^2}{(2s_A'+1)(2I'+1)}\sum_J(2J+1)\times\sum_{lj}[1-\sum_\nu(V_c{}^{J\nu})^2\cos2\delta_J{}^{(\nu)}].\quad(3.65)$$

F. Calculation of the Photonuclear Cross Sections

As mentioned earlier, the photon channels can be treated by perturbation methods. Thus, photon emission and absorption processes are described as transitions between, say, the ground state of a nucleus and a particular eigenchannel state. A transition involving a linear combination of eigenchannel states, e.g., the process $^{16}\mathrm{O}(\gamma,P_1)^{15}\mathrm{N}$, is then described by a suitable superposition of the matrix elements for these eigenchannels. Thus, we want to compute

$$\sigma_\pm=(2\pi/\hbar)\rho_E(2\pi\hbar\omega e^2/c)\mid D\mid^2\quad(3.66)$$

for the absorption cross section. Here, the subscripts $\pm$ refer to the photon polarization and, specializing to electric dipole transitions,

$$D=(4\pi/3)^{1/2}\langle f\mid rY_{1\pm1}\mid i\rangle,\quad(3.67)$$

where the state $\mid f\rangle$ is, say, an eigenchannel state of the form (3.2). In Eqs. (3.66) and (3.67) the density of the final states ρ_E and the normalization of the final-state wave function $\mid f\rangle$ must be defined together in a consistent manner. We do this by using the eigendifferential method of Weyl. According to that method a continuum state is made normalizable to unity by integration over a finite but small energy interval ΔE. We shall denote such a state by $\mid\tilde f\rangle$. Then the density of states is simply

$$\rho_E=1/\Delta E.\quad(3.68)$$

As long as ΔE is very small the radial wave function is modified only at very large radii. Thus the modification of the wave function needed for convergence of the normalization integral is confined to extremely large r, say to $r>b$, so that all calculations for the matrix elements and the diverse matchings to be discussed can be performed with the nonmodified form of the wave function. In the asymptotic region, but before the Weyl modifications set in, the final-state wave function has the form

$$\mid\tilde f\rangle=\mid f\rangle=\tilde N^{-1}\sum_c v_c^{-1/2}V_cw_c(r)\tilde\psi_c\qquad r<b\quad(3.69)$$

which, differs from Eq. (3.21) only in having the normalization constant $\tilde N$.

For the Weyl function we introduce the notation

$$\tilde w_c(r)=W_c\int_E^{E+\Delta E}dE\,w_c(r).\quad(3.70)$$

Here the normalization constant W_c is chosen such that for the nonmodified region of the Weyl function there holds

$$\tilde w_c(r)=w_c(r)\quad\text{for}\quad r<b.\quad(3.71)$$

Then $\mid f\rangle$ goes over to $\mid\tilde f\rangle$ upon replacing w_c by $\tilde w_c$ in Eq. (3.69). The normalization condition for the wave function Eq. (3.69) thus becomes

$$\langle\tilde f\mid\tilde f\rangle=\tilde N^{-2}\sum_c v_c^{-1}(V_c)^2\langle\tilde w_c\mid\tilde w_c\rangle=1,\quad(3.72)$$

This completes the general formulation. We now go on to the details. We begin with Eq. (3.70). In the region $r\approx b$, the function $w_c(r)$ already has the completely asymptotic form $w_c(r)=\sin(k_cr+\delta-\frac{1}{2}l\pi)/r$. The addition of the logarithmic Coulomb phase in the case of charged particles is of no importance in the present context. We therefore can do the matching of Eq. (3.71) using this asymptotic form of $w_c(r)$. This then leads to the equation

$$W_c=M_{\mathrm{red}}/(\gamma\hbar^2k_c^2)=1/\Delta E.\quad(3.73)$$

Here M_{red} is the reduced mass, and we have used the abbreviation $\gamma=\Delta E\, M_{\text{red}}/(\hbar^2k^2)$. It has the physical meaning of defining the energy interval of the integration in Eq. (3.70) in terms of the momentum variable, i.e., if the limits of the integration are k_1 and k_2, then $k_2=k_1(1+\gamma)$. With Eq. (3.8) we have for the normalization of the Weyl functions

$$\langle\tilde{w}_c \mid \tilde{w}_c\rangle=(\pi k^2\hbar^2/2M_{\text{red}})(1/\Delta E). \tag{3.74}$$

Finally, we obtain for the over-all normalization constant

$$\tilde{N}^2=\tfrac{1}{2}\pi\hbar^2(1/\Delta E). \tag{3.75}$$

We now turn to the detailed form of the matrix element (3.67). Because of the normalization (3.71), the matrix element computed with the Weyl function $|\tilde{f}\rangle$ is the same as that computed with the unmodified function $|f\rangle$. Thus we can insert Eq. (3.69) into Eq. (3.67) or, more precisely, the equivalent inside solution Eq. (3.26) supplemented with the normalization constant $(\tilde{N}N_{J,\nu})^{-1}$. Here $N_{J\nu}$ accounts for the different normalization of the eigenchannel functions for $r<a$ and $r>a$ and is given by Eq. (3.29). This way we finally obtain for the total dipole absorption cross section

$$\sigma_{\pm}=4\pi^2(e^2/\hbar c)(\hbar\omega)\sum_{\nu}\mid D_\nu\mid^2, \tag{3.76}$$

where, using the wave function (3.26), the matrix element D_ν is given by

$$D_\nu=(4\pi/3)^{1/2}[\tfrac{1}{2}\pi\hbar\sum_c(C_c^{J\nu})^2]^{-1/2}\times\langle\bar{\psi}^{J\nu}\mid rY_{1\pm1}\mid i\rangle. \tag{3.77}$$

We now turn to some examples of partial cross sections. We begin with the differential cross section of a process leading to a final state specified by I. Writing $\psi_I{}^\nu$ for a wave function (3.26) in which the summation over I has been omitted, and introducing the notation

$$\psi_I=\sum_\nu D_\nu\psi_I{}^\nu, \tag{3.78}$$

we have for the differential cross section

$$d\sigma_I/d\Omega\propto\psi_I{}^*\psi_I=\sum_\Lambda\langle\psi_I\mid P_\Lambda\mid\psi_I\rangle P_\Lambda. \tag{3.79}$$

For the coefficients of the angular distribution we obtain

$$\begin{aligned}q\langle\psi_I\mid P_\Lambda\mid\psi_I\rangle&=\pi(e^2/\hbar c)(\hbar\omega)\\&\times\sum_s\sum_{lj\nu}\sum_{l'j'\nu'}\cos(\delta_{1^-}{}^{(\nu)}-\delta_{1^-}{}^{(\nu')})\\&\times V_c{}^{1^-\nu}D_\nu V_{c'}{}^{1^-\nu'}(-)^{(l+l')/2}[3(2\Lambda+1)(2j+1)\\&\times(2j'+1)(2l+1)(2l'+1)]^{1/2}(ll'00\mid\Lambda0)\\&\times\tfrac{1}{2}[1+(-)^\Lambda](\Lambda101\mid11)(2s+1)W(l's\Lambda1;1l)\\&\times W(Isjl;\tfrac{1}{2}1)W(l'sj'I;1\tfrac{1}{2}).\end{aligned} \tag{3.80}$$

The constant q converts the angular distribution (3.79) into an absolute cross section. The summation over the channel spin s can be performed explicitly. This way the product of three Racah coefficients in Eq. (3.80) reduces to a product of two Racah coefficients. Integrating over the solid angle we have, for the partial cross section,

$$\begin{aligned}\int(d\sigma/d\Omega)\,d\Omega&=4\pi q\langle\psi_I\mid P_0\mid\psi_I\rangle\\&=4\pi^2(e^2/\hbar c)(\hbar\omega)\\&\times\sum_{lj}\mid\sum_\nu\exp(i\delta_{1^-}{}^{(\nu)})V_c{}^{1^-\nu}D_\nu\mid^2.\end{aligned} \tag{3.81}$$

G. Nuclear Structure Information

The aim of any calculation of a reaction cross section is to provide access to the nuclear interior. The experiment can only give the integrated cross section and the angular distributions associated with a particular resonance. The extraction of nuclear information requires a theory. Therefore the computation of the observable cross sections is only the first step. The payoff comes when the theory yields nuclear information which is not accessible to direct observation. Quantities of this kind are, e.g., spectroscopic factors, configuration mixtures, correlations, etc. In the analysis of photonuclear reactions the customary quantities of interest are the configuration mixture and the isospin purity of the states. In bound-state calculations the configuration mixture is a well defined quantity, and the calculations are usually performed assuming isospin purity for the states. The problem of defining a quantity analogous to the configuration mixture when the continuum is included has been investigated by Barrett and Delsanto (1971). We shall follow closely their treatment. The question of the determination of the isospin purity in the continuum has been clarified in great detail by Robson (1965). We shall make only some brief remarks about this problem after discussing the configuration mixing.

In a bound-state calculation, a diagonalization of the shell-model Hamiltonian is performed on a basis of particle–hole configurations. After diagonalization, an eigenstate $|\nu\rangle$ of the Hamiltonian is represented by a mixture of the basis configurations $|cn\rangle$, i.e.,

$$|\nu\rangle=\sum_{c,n}X_{cn}{}^\nu\mid cn\rangle, \tag{3.82}$$

where $X_{cn}{}^\nu$ is the amplitude of the basis state $|cn\rangle$, c represents all quantum numbers except the radial quantum number, and thus characterizes a configuration and n is the radial quantum number. In general, the states $|\nu\rangle$ are non-degenerate; that is, no two energy eigenvalues, E_ν, coincide.

The contribution of a given configuration c to the state $|\nu\rangle$ can be regarded as $\sum_n X_{cn}{}^{\nu 2}$ where we have $\sum_c\sum_n X_{cn}{}^{\nu 2}=1$ due to the normalization of the wave function $|\nu\rangle$. The contribution of a configuration to different states can be meaningfully compared because the basis wave functions $|cn\rangle$ are the same for all states

$|\nu\rangle$. Consequently one can immediately compute the contribution of a certain configuration of a state $|\nu\rangle$ to any matrix element. Thus, for example, the dipole strength of the state $|\nu\rangle$ is proportional to the square of the dipole matrix element between the ground state $|i\rangle$ and the state $|\nu\rangle$; i.e., the dipole strength of $|\nu\rangle$

$$\propto |\langle\nu|D|i\rangle|^2 = |\sum_{cn} X_{cn}{}^{\nu *}\langle cn|D|i\rangle|^2, \quad (3.83)$$

where D is the dipole operator.

In the continuum two complications arise. First, for N open channels the states are N-fold degenerate. One therefore must first specify a classification scheme to "break" this degeneracy. Each of these so classified states will have a different configuration mixture. Since we are here interested in the photonuclear process, we specify the classification by asking for the configuration mixture of the dipole state.

The second problem is associated with the usual continuum problem of normalization, which here has been resolved by discretization. In the eigenchannel theory this leads to the specific difficulty that the basis states of the different eigenchannels are different as they obey different boundary conditions, and one must consider all eigenchannels together since, in general, they all contribute to the dipole state.

This difficulty can be resolved as follows: Consider the $1p$–$1h$ basis state wave functions [see Eq. (3.27)].

$$|n_a n_A; j_a j_A, JM\rangle\rangle = \sum_m (-)^{j_A-m}(j_a j_A M+m\ -m\,|\,JM) \times |(l_a S_a) j_a M+m\rangle^* |(l_A S_A) j_A m\rangle r_a{}^{-1} U_{n_A l_a j_a}(r_a) r_A{}^{-1} U_{n_A l_A j_A}(r_A) \times |\tau_a m_\tau{}^a\rangle^* |\tau_A m_\tau{}^A\rangle. \quad (3.84)$$

(Uppercase subscripts or superscripts refer to particles; lower-case subscripts or superscripts refer to holes. The kets containing τ characterize the charge of the nucleon, and n is the radial quantum number.)

A variation of the boundary conditions at the matching radius results in a different radial wave function for the particle, i.e., $r_A{}^{-1}U_{n_A l_A j_A}(r_A)$ is different for different eigenchannels. The angular part of the particle wave function, represented by $|(l_A s_A) j_A m\rangle$ in Eq. (3.84) is, however, unchanged. The basis state wave functions are orthogonal. The orthogonality between different branches of the same configuration, i.e., between states $|n_a n_A; j_a j_A; JM\rangle\rangle$ which differ only by the quantum number n_A arises from the fact that the radial wave function $U_{n_A l_A j_A}(r_A)$ is an eigenfunction of the radial Schrödinger equation solved in the inner region with the boundary conditions of the νth eigenchannel applied at the matching radius. The orthogonality between configurations; i.e., where any quantum number other than n_A differs, arises from the inherent orthogonality of the single-particle and single-hole angular wave functions $|(l_A S_A) j_A m\rangle$, $|(l_a S_a) j_a M+m\rangle^*$ and the single-hole radial wave functions. This orthogonality is independent of the boundary conditions applied at the matching radius.

If we simplify the nomenclature as before by letting c represent all quantum numbers except n_A, and letting n represent n_A, we have the $1p$–$1h$ basis wave function in the form $|cn^\nu\rangle$. The ν indicates the dependence of $|cn^\nu\rangle$ upon the boundary conditions of the νth eigenchannel. From the arguments of the last paragraph, we have

$$\langle c'n'^{\nu'}|cn^\nu\rangle = \delta_{cc'}\langle cn'^{\nu'}|cn^\nu\rangle. \quad (3.85)$$

The dipole cross section at a specific excitation energy is given in the eigenchannel theory by

$$\sigma = 4\pi^2(e^2/\hbar c)\hbar\omega \sum_\nu |D_\nu|^2, \quad (3.86)$$

where

$$D_\nu = (\tfrac{4}{3}\pi)^{1/2}[\tfrac{1}{2}\pi\hbar \sum_{c'} (C_{c'})^2]^{-1/2} \times \sum_{c,n} X_{cn}{}^*\langle cn^\nu|\tau_3 r Y_{1\pm1}|i\rangle. \quad (3.87)$$

The normalization of the basis wave functions to unity inside the matching radius is arbitrary. Hence a renormalization must be introduced to normalize the eigenvector of the S-matrix to unit flux. This is represented by the factor $\sum_{c'} (C_{c'})^2$ in Eq. (3.87).

Let us define a vector

$$|M_c{}^\nu\rangle = D_\nu \sum_n X_{cn}|cn^\nu\rangle. \quad (3.88)$$

Comparing Eq. (3.86) with Eq. (3.82) we could choose $\sum_n X_{cn}{}^2$ to be the percentage contribution of the configuration c to the eigenchannel $|\nu\rangle$, and

$$\sigma_c = 4\pi^2(e^2/\hbar c)\hbar\omega \sum_\nu \langle M_c{}^\nu|M_c{}^\nu\rangle \quad (3.89)$$

the total contribution of a configuration c to the cross section σ at a given energy. Then we have $\sigma = \sum_c \sigma_c$. For this to be a meaningful definition, we must show that $\sum_n |X_{cn}|^2$ is independent of the change of basis produced by the changing boundary conditions at the matching radius.

We have

$$|M_c{}^\nu\rangle/D_\nu = \sum_n X_{cn}|cn^\nu\rangle. \quad (3.90)$$

We change the basis $|cn^\nu\rangle$ to another complete set $|c'n'^{\nu'}\rangle$ describing the same space by changing the boundary conditions to those of the ν'th eigenchannel

$$|M_c{}^\nu\rangle/D_\nu = \sum_{c'n'n} X_{cn}\langle c'n'^{\nu'}|cn^\nu\rangle |c'n'^{\nu'}\rangle \quad (3.91)$$

$$= \sum_{n'} [\sum_n X_{cn}\langle cn'^{\nu'}|cn^\nu\rangle] |cn'^{\nu'}\rangle. \quad (3.92)$$

$X'_{cn'}$, the equivalent of x_{cn} on the new basis is thus given by

$$X'_{cn'} = \sum_n X_{cn}\langle cn'^{\nu'}|cn^\nu\rangle. \quad (3.93)$$

Similarly we have

$$\langle M_c{}^\nu|/D_\nu = \sum_{m,m'} X_{cm}{}^* \langle cm^\nu \mid cm'^{\nu'}\rangle \langle cm'^{\nu'}| \quad (3.94)$$

$$\sum_n |X_{cn}|^2 = \langle M_c{}^\nu \mid M_c{}^\nu\rangle / D_\nu{}^2$$

$$= \sum_{nn'}\sum_{mm'} X_{cn}X_{cm}{}^* \langle cm^\nu \mid cm'^{\nu'}\rangle \times \langle cn'^{\nu'} \mid cn^\nu\rangle \langle cm'^{\nu'} \mid cn'^{\nu'}\rangle$$

$$= \sum_{n'} [\sum_n X_{cn}\langle cn'^{\nu'} \mid cn^\nu\rangle] \times [\sum_m X_{cm}{}^* \langle cm^\nu \mid cn'^{\nu'}\rangle$$

$$= \sum_{n'} |X'_{cn'}|^2. \quad (3.95)$$

$\sum_n |X_{cn}|^2$ is thus independent of any change in the basis produced by the changing boundary conditions at the matching radius, and we are justified in using Eq. (3.89) to calculate the configuration mixing in the eigenchannel theory.

We now turn to the question of the isospin purity. As has been pointed out by Robson (1965) the main source of isospin impurities is the external mixing. [A corollary to that is that the nuclear bound states should have very pure isospin. This has been borne out by model calculations (Bohr, *et al.*, 1967; Mohan, *et al.*, 1971).] The central problem in turning this qualitative statement into a quantitative theorem lies in the impossibility of making an unambiguous separation of the space into an inside region and an outside region. This circumstance has no effect on the calculation of cross sections, etc., so long as the separation radius has been chosen *sufficiently large*, i.e., large enough to ensure that the wave function in the outside region has achieved its asymptotic form with *sufficient accuracy*. For example, except for computational difficulties, one could let the matching radius become very large, say, 50 times the nuclear radius. This option is not available if one wants to retain the physically very valuable Robson concept of external vs internal isospin mixing. In other words, the Robson classification changes the separation radius from an intermediate mathematical parameter into an important physical quantity. One now must make a deliberate compromise: too small a separation radius would include too much of the region in which the particles tunnel through their respective barriers (this difference of the barriers experienced by the protons and neutrons is the source of the external mixing).

In fact, taking all channel radii to be the same, the isospin impurity of the internal region in general increases monotonically with increasing separation radius before reaching its asymptotic value; i.e., it does not have a plateau. Therefore one must be guided by general arguments in choosing a particular value for the separation radius. In an eigenchannel calculation one is thus free to choose the separation radius to be equal to the matching radius in so far as one in general tries to use as small a matching radius as possible. Nevertheless, one has to remember the ambiguity of this choice.

As a result of this choice, one now can simply evaluate the expectation value of the operator T^2 for any eigenchannel state by integrating over the internal region. The same can be done for a linear combination of eigenchannel states, corresponding to different experimental conditions. For example, one may be interested in the linear combination which describes the dipole state, or that which describes the, say, proton scattering experiment. One must here remember that there will be cross terms between the different participating eigenchannels. This is a consequence of the fact that the Hamiltonian does not commute with T, since it contains the Coulomb potential, and that the boundary conditions are not T invariant, since they are different for protons and neutrons. In fact, this difference of the boundary conditions is precisely the mechanism by which the external mixing influences the internal nuclear wave function.

H. Related Numerical Treatments of the Shell Model in the Continuum

One of the first of these calculations was that of Lemmer and Shakin (1964), who treated the problem of elastic neutron scattering on ^{15}N. There are several reasons why this problem is of theoretical interest. First there is the simplification that one has to deal with only one type of particle, namely, neutrons, which reduces the number of $1p$–$1h$ configurations. Second, one populates only $T=1$ states, so it is reasonable to expect that there will be no complications from spurious center of mass states. Third, the lowest thresholds in ^{16}N are those for neutron emission and not α emission as in ^{16}O.

The treatment of Lemmer and Shakin was based on Feshbach's projection operator formalism (cf. Feshbach, 1958, 1960, 1962; Feshbach, *et al.*, 1965; Kerman, 1965; Friedman and Feshbach, 1968). This formalism, as also the formal theory of MacDonald (1964), has the advantage of displaying to a certain extent the structure of the S matrix and emphasizing the dynamical origin of the resonances (in terms of closed channels).

The projection operator P was defined to project onto the elastic channels described as combinations of standing wave eigenfunctions determined from potential scattering and ground-state target functions ($1p_{1/2}$-hole functions). Within this approximation, the antisymmetrization requirement, which is a source of difficulty in the Feshbach treatment, did not cause any complication.

The complementary projection operator Q was assumed to project onto channels belonging to excited target states ($1p_{3/2}$–hole states). Here, the single-particle functions were taken directly from the harmonic oscillator model. Thus, the inelastic channels were treated as closed channels. What is more important, however, is the simplifying assumption that

was made for the residual interaction, namely that it acts only between the inelastic-channel configurations and does not couple the elastic channels.

Due to the coupling between the scattering functions and the perturbed 1 particle–1($1p_{3/2}$-hole) configurations, relatively narrow resonances are produced in the elastic scattering in addition to the $d_{3/2}$ potential scattering resonance. The omission of any coupling between the open channels became necessary, because this coupling makes difficult the application of the formal theories of the shell model in the continuum and requires the introduction of some heuristic approximation scheme. A more reliable, numerically testable approximation scheme was suggested by Bloch and Gillet (1965). Their aim was to extend the diagonalization method used for discrete configurations to scattering problems. The formal theory of nuclear reactions which they applied is essentially Dirac's model, a method developed in more detail by Fano for atomic problems, and applied by Weidenmüller (cf. Mahaux and Weidenmüller, 1969), among others, to nuclear reactions. The basic idea is the introduction of two kinds of orthogonal subspaces depending on whether all nucleons are in bound states or whether one is in a continuum state, and the use of this basis for expanding the solution of the Schrödinger equation. Introducing the formal expansion into the Schrödinger equation, one obtains a system of coupled integral equations for the energy dependent expansion coefficients. It becomes essential to study the singularities of the energy-dependent coefficients, since they determine the asymptotic behavior of the wave functions, and therefore of the S-matrix.

Bloch and Gillet then eliminated the continuum problem by replacing the energy variable in the continuum by a discrete summation. This approximation forces the coupled integral equations into the form of systems of linear equations. This method has been used by Gillet, Melkanoff, and Raynal (1967) for a realistic calculation of the photo disintegration of ^{16}O within the $1p$–$1h$ approximation, and also for studying the effect of incorporating $2p$–$2h$ configurations. Raynal, Melkanoff, and Sawada (1968) have performed extensive test calculations for the example ^{16}O in which they compared the method with the coupled-channel procedure. They obtained excellent agreement when the number of integral equations was not too large. This gives confidence in both the iteration procedure used in the solution of the coupled equations and in the discretization of the continuous variable. Because of the existence of a narrow single-particle resonance in the $d_{3/2}$ channel, one has to use a small step width for the discretization in the vicinity of the $d_{3/2}$ resonances.

In this context one should also mention the work of Balashov, *et al.*, who treated the photoabsorption process in ^{16}O as well as the ^{15}N$(n, n')^{15}$N reaction. Their formalism is based on the Lippmann–Schwinger equation and the introduction of separable integral operators. Little is known about the accuracy of this method.

Numerical work on the ^{15}N$(n, n')^{15}$N reaction has been carried out by the Heidelberg group (Ebenhöh, *et al.*, 1967a, b). This work is based upon the formal investigations of the shell model in the continuum developed by Weidenmüller (1966a, b, 1967) and his collaborators (Dietrich and Weidenmüller, 1966; Hüfner, *et al.*, 1967; Mahaux and Weidenmüller, 1967). A comprehensive and very informative account of this theory has been given by Weidenmüller and Mahaux (1969) in their monograph.

The application to the elastic and inelastic scattering of neutrons on ^{15}N was carried out by Ebenhöh, *et al.* (1967a, b) and by Glöckle, *et al.* (1967). The residual force used was of zero range and had a Soper-type exchange mixture. A comparison between the resonance energies and the energy eigenvalues of a corresponding bound-state calculation shows that the energies of the two calculations differ by up to several 100 keV. This difference arises from several sources. First, the bound-state single-particle wave functions are not exactly the same. Second, the coupling between the bound states embedded in the continuum and the continuum itself introduces energy shifts. Finally, the interaction between the different open channels also leads to a shift. Thus, a bound-state calculation can give the resonance energies, at best, within a few hundred kiloelectronvolts. Beyond that, partial widths, in general, can be obtained also only with very poor accuracy from a bound-state calculation.

Buck and Hill (1967) reformulated the scattering problem in terms of a system of coupled integro-differential equations. (We have discussed the details of this method above.) They applied their method to a numerical calculation of the ^{16}O $T=1$, 1^- states. As the widths of the resonances they obtained were much too narrow, in order to remove this difficulty, they introduced in the (diagonal) Hartree–Fock potential a purely imaginary absorption potential. This had the desired effect of increasing the widths and lowering the peaks. The agreement between their best calculated curves cross sections and the experimental data can be viewed as satisfactory, although not outstanding.

I. Sources of Inaccuracies of the Eigenchannel and their Treatment

The eigenchannel method was derived in order to remove one of the basic difficulties inherent in the R-matrix theory, namely, the lack of uniform convergence of the nuclear wave function. The eigenchannel method certainly overcomes this difficulty; not only is the wave function smooth across the boundary of the interior region, but also the S-matrix itself reduces to a single term (if but one channel is open) or to only those eigenphases which are rapidly changing in the case of many channel scattering. (It is exceptional if just one eigenphase moves rapidly; if so, however, the eigenchannel method reduces to a single term.)

The relevant question is, however; what is the price for this advance? The major disadvantage of the method lies in the fact that *many* diagonalizations are required to achieve a self-consistent solution at any given energy. This is to be contrasted to the R-matrix approach, which achieves an approximation to the S-matrix involving but a *single* diagonalization at each energy. This is quite definitely a disadvantage for the eigenchannel approach.

Weidenmüller and Mahaux (1968) have recently discussed in a very detailed way the pros and cons of the R-matrix vs eigenchannel procedures. They drew special attention to the fact that in both the R-matrix and eigenchannel procedures, the use of (true) shell-model bound-state eigenfunctions (with the boundary condition $\psi \to 0$ at $r \to \infty$) and of shell-model eigenfunctions discretized by fixed boundary conditions leads to *nonorthogonality* and to redundant (cf. Danos and Greiner, 1967) state functions. In the R-matrix approach, these difficulties are not serious, in that one may avoid the problem by choosing negative values for the boundary parameters, b_c. In the eigenchannel approach, this option is unavailable since the boundary conditions are *not* arbitrary. [In fact, spurious structure in all the early eigenchannel calculations (Wahsweiler, *et al.*, 1966, 1968; Delsanto, *et al.*, 1967) was associated with this nonorthogonality.] A second important criticism is that, because of the energy dependence of the natural boundary conditions, the truncated Hilbert space has different properties at different energies. (This would not occur if, instead of truncating, the full Hilbert space were used. The point is that at different energies the functions have different radial dependence, and the net overlap with the true wave function may vary.) It was the conclusion of Weidenmüller and Mahaux, that these difficulties of the eigenchannel procedure *might* be serious, and *might* cause spurious energy dependence (spurious wiggles or spurious resonances). We shall discuss each of these difficulties in turn below, along with the other problems of a technical nature that arose during the calculations.

Let us consider first the question of the proper choice of the "matching radii," a_c, which determines the joining of the internal region onto the external, asymptotic region. These radii serve to discretize the continuum (open-channel) energy spectrum; clearly the level spacing decreases as the matching radius increases. On the other hand, the internal region must be large enough to validate the asymptotic joining condition; this latter requirement includes the condition that no channel coupling via the residual interactions occurs outside the internal region.

Since the hole wave functions are asymptotically proportional to $\exp\{-|k_c|r\}$, their decay between the nuclear and matching radii a_c can be easily estimated. Choosing $a_c = 12$ F, one obtains an amplitude ratio less than 0.002 for the least bound hole in ^{16}O. Thus the hole function can be normalized to unity inside the matching radius without any sizeable error and, moreover, the effect of the channel coupling will be negligible in the vicinity of the matching radius. The Hilbert space of functions over which we expand in the internal region is an implicit function of the matching radius, as was pointed out by Weidenmüller and Mahaux. This question has been answered numerically for the present calculations; and it has been found that in the case of four radial quantum states per channel an increase of 1 fm in the matching radii led to a change in the eigenphases of less than 0.3° (Rabie, 1970). The effect on the cross section is thus negligible.

The next question concerns the truncation of the Hilbert space for positive energy states. Using an exactly solvable two-channel model, one may estimate the convergence of the cross section with respect to the number of radial states (Delsanto, *et al.*, 1969). Asymptotically it was found that the error was proportional to ϵ_{nc}^{-2} in the limit of large radial quantum numbers. Thus the convergence for large quantum numbers is quite satisfactory. For small radial quantum numbers, however, the convergence is not very fast and even fluctuates. We have, however, found *no indication that spurious wiggles or spurious resonances result from this cause.* In the simplified two-channel model this truncation gave rise *only* to a resonance shift as can be seen from Fig. 5. We would like to emphasize that a similar effect (a resonance shift only) was seen in the R-matrix calculations of Buttle (1967). In our final calculations, we used six radial states per channel for ^{12}C, five for ^{16}O, and four for ^{40}Ca.

We turn now to the problem of the nonorthogonality of the single-particle basis states belonging to different boundary conditions—one of the main problems mentioned above. There are two different effects we may single out as resulting from the nonorthogonality. The first is the existence of cross terms in the energy expectation values—this will be discussed shortly; the second effect concerns the requirement that the scattering channel wave function be orthogonal to all occupied shell-model basis states of the same channel (recall that the shell model boundary conditions are: vanishing at $r = \infty$). Our way of solving this problem is closely related to the way in which the negative energy single-particle states are treated; let us then discuss the construction of radial single particle states in more detail.

Figure 3 shows the logarithmic derivative of a radial single-particle function versus energy. A given boundary condition (vertical axis) defines a horizontal line, whose intersections yield the eigenvalues of the single-particle energy ϵ_λ. In the region of negative energies the curve is (see figure) essentially a parabola, except for very narrow intervals in the vicinity of the shell-model bound-state energies. Radial eigenfunctions defined by a given boundary condition are, apart from states belonging to the above intervals, of the form

$$U_{nc}(r) \approx (2|k_c|)^{1/2} \exp\{|k_c|(r-a)\}; \quad (3.96)$$

i.e., they are practically zero over the whole nuclear

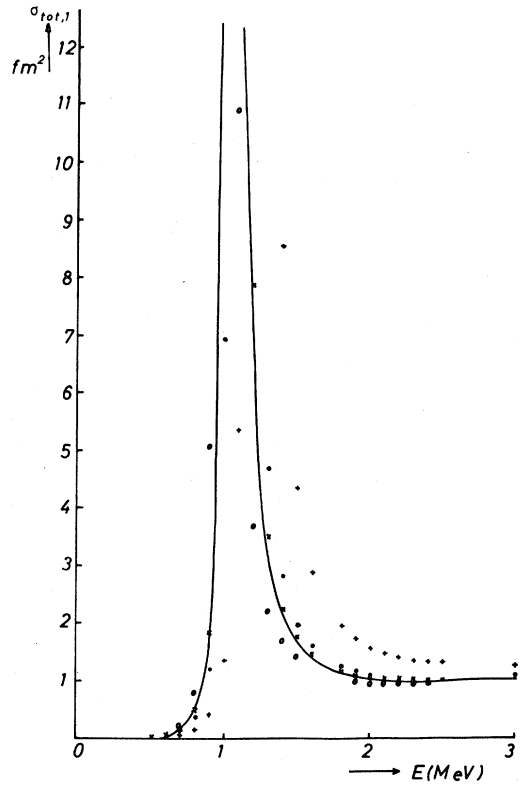

FIG. 5. E.C. results for a simple two-channel model compared to the exact solution (Delsanto, *et al.*, 1969) (full line). The E.C. calculations were performed with various numbers of radial states per channel; the different symbols represent +4, ●6, ×7, ○9 radial states. The channel coupling was relatively strong (typical matrix elements ~5 MeV).

volume, and finite only in a small range close to $r=a$. The behavior expressed in (3.96) gives rise to the parabola in Fig. 3 at negative energies, since $|k| \sim (|\epsilon|)^{1/2}$.

On the other hand, the radial hole functions under the integral in Eq. (3.20) represent bound shell-model states which are concentrated inside the nuclear volume and become extremely small at $r=a$ for reasonably large values of a. Thus, low-lying basis states in the expansion of the scattering functions

$$f_c^{J\nu} = \sum_n A_{nc}^{J\nu} U_{nc}^{(\nu)}(r) \qquad (3.97)$$

will practically not be admixed to the nuclear wave function, *except* if they "almost coincide" with a shell-model bound state.

The question which now must be answered is: which of the "almost coinciding" bound states of the basis set can be replaced by the bound shell-model states. This question is equivalent to the question of the orthogonality of the bound basis set states to the positive energy shell-model states. (If the orthogonality requirement is fulfilled, then the completeness of the retained set of states is guaranteed. This can be seen immediately when remembering that both sets, i.e. the shell model states and the basis states, form complete sets of states.) The orthogonality would be exact for $a\to\infty$. For finite a the overlap integral can be estimated in the following manner. The shell-model bound state falls off exponentially with a characteristic length $(|\epsilon|)^{1/2}$. The behavior of an "almost coinciding" bound basis state is similar except for small region around $r=a$ where it has a component which grows exponentially with the same characteristic length. The nonorthogonality thus has two contributions; first, the omission of the integral for $r>a$ (the basis set function is equal to zero in the outside region), and second, the overlap integral of the continuum function with the rising exponential for $r<a$. Both of these integrals are of the order $\psi(a)\Delta r \propto \exp(-a|\epsilon|^{1/2})\,|\epsilon|^{-1/2}$. This can be made arbitrarily small by choosing a sufficiently large value for a, or, given a value for a, replacing the expansion states by the shell-model states only for $\epsilon<E_{\min}$; i.e., by using the expansion states down to a cutoff energy $E_{\min}<0$. The first numerical calculations using the eigenchannel method (Wahsweiler, *et al.*, 1968; Delsanto, *et al.*, 1967) were partly in error because of an improper choice of the cutoff energy. The choice $E_{\min}=0$ was made for convenience, but this is not acceptable for a matching radius equal, or smaller than 12 F. This error led to a spurious structure ("wiggles") in the numerical results for ^{16}O in the region between 22 and 23 MeV. It was found in check calculations performed by Rabie (1970) that these erroneous results are eliminated when using a larger matching radius (increased from 12 to 17 F), or (in a separate calculation) when using a lower cutoff energy ($E_{\min}=-15$ MeV rather than $E_{\min}=0$) with $a=12$ F. No noticeable difference in the calculated results was observed when the minimum energy was increased from $E_{\min}=-15$ MeV to $E_{\min}=-12$ MeV. Figure 6 shows the results that were obtained with the increased matching radius. (For completeness, we should state that the increased radius decreased the energy spacing so that the number of radial states per channel was increased from 4 to 6 to compensate for this change.)

Let us turn now to the problem, also resulting from the nonorthogonality, of the cross terms in the energy matrices.

The energy expectation value will then contain cross terms of the type

$$\langle \det[\psi^1(1)\phi_2(2)\cdots\phi_A(A)\,|\,\sum_{i<j} V(i,j)\,| \times \det[\psi^{(2)}(1)\phi_1(2)\cdots\phi_{A-1}(A)]\rangle, \qquad (3.98)$$

where $\psi^{(1)}, \psi^{(2)}$ are the nonorthogonal functions, and the ϕ_i denote the hole states with ϕ_1 different from ϕ_A. *These states can be assumed to differ* in their ljt values. The expression (3.98) can be rewritten as follows:

$$\langle\psi^1(1)\phi_A(2)\,|\,V\,|\,[[\psi^2(1)\phi_1(2)]]\rangle + \langle\psi^{(1)}\,|\,\psi^{(2)}\rangle \times \sum_i \langle\phi_i(1)\phi_A(2)\,|\,V\,|\,[[\phi_i(1)\phi_1(2)]]\rangle. \qquad (3.99)$$

Here i runs from 2 to $(A-1)$, but can clearly be extended from 1 to A without altering the value of (3.99). Introducing the HF field (3.10) into the second term of (3.99) yields

$$\langle\psi^{(1)} \mid \psi^{(2)}\rangle\langle\phi_A \mid V_{\mathrm{HF}} \mid \phi_1\rangle. \qquad (3.100)$$

If V_{HF} is interpreted as a local spherical potential (closed-shell nuclei), this matrix element vanishes. Moreover, for the same reason, the shell-model part H_0 of the nuclear Hamiltonian can contribute no off-diagonal terms to the energy matrix.

Since the first term in (3.99) is the usual residual force matrix element expected from the conventional particle–hole formalism, the nuclear eigenvalue problem of the $1p$–$1h$ E.C. (eigenchannel) treatment resembles that of the conventional $1p$–$1h$ calculations, provided the shell-model potentials of the hole states are chosen in such a manner that they can be interpreted as local HF potentials.

A discussion of the numerical accuracy of the eigenchannel method would be incomplete without sketching the precise way in which the single particle eigenenergies are calculated. The eigenchannel method, as applied in the present numerical treatment, actually involves two distinct search procedures: (a) the search (iteration loop) for the eigenphases, and (b) the search procedure for determining radial states obeying given boundary conditions. This latter search requires much computer time and must be optimized or avoided if possible. In both procedures the code has been considerably improved over the original versions used in earlier calculations. To optimize the second search,

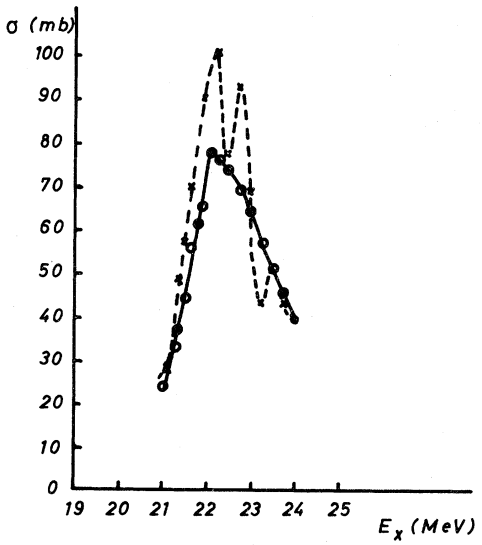

FIG. 6. Dependence of the E.C. photoabsorption cross section in ^{16}O on the matching radius, if $\epsilon_{\min}$ is put equal to zero; dashed curve: $a=12$ fm; solid curve: $a=17$ fm. (Note: F is used to denote Fermi in text.)

interpolation formulas for the ambiguous functions

$$\epsilon=\mathrm{funct}\ (b_c) \qquad (3.101)$$

were stored. These formulas, however, must be extremely accurate near bound states (above the Fermi surface), since there may occur large amplitudes $A_{nc}{}^{J\pi,\nu}$ of the nuclear eigenvector (3.26): thus, $A_{nc}{}^{J\pi,\nu}u_{nc}{}^{(\nu)}$ may become sizeable at the matching radius, because of the exponentially increasing part in $u_{nc}{}^{(\nu)}$. A slight error in ϵ_{nc} could affect (3.26) and via (3.21) the eigenvectors of the S-matrix. In the actual calculations, the error in ϵ_{nc} was below 2 keV for positive energies, and below 10 keV for negative energies (but considerably less close to bound states).

Before concluding, we wish to add that at the end of both search procedures a certain test of the accuracy of the calculation is provided by the explicit calculation of the scalar products

$$\Delta_{\nu\nu'}=\sum_c V_c{}^{J\pi,\nu}V_c{}^{J\pi,\nu'}. \qquad (3.102)$$

These should be zero for $\nu\neq\nu'$ because of the unitarity of the $S^{J\pi}$ matrix. In our calculations they were always less than 0.01, a quite satisfactory result. However, the formulae for the computation of the diverse cross sections in terms of the S-matrix are derived under the assumption that the S-matrix is indeed unitary; i.e., that the eigenchannels indeed form an orthogonal set. It is therefore advantageous to orthogonalize the eigenchannels so as not to introduce spurious, unnecessary inaccuracies. Naturally, the orthogonalized S-matrix is not more accurate than the original S-matrix; however, it is a proper S-matrix. The rationale thus is the same as that which one employs in renormalizing a wave function after admixing some configurations by a perturbation treatment, which, as is well known, does not preserve the normalization.

The procedure used to obtain an exactly unitary S-matrix was to introduce the K-matrix

$$S=(1+iK)^{-1}(1-iK), \qquad (3.103)$$

which, in terms of the eigenchannels, is given by

$$K_{cc'}{}^{J\pi}=-\sum_\nu V_c{}^{J\pi,\nu}\tan\delta_{J\pi}{}^{(\nu)}V_{c'}{}^{J\pi,\nu}. \qquad (3.104)$$

A diagonalization of this approximate $K^{\tau\pi}$ matrix leads to orthogonalized eigenphases $\delta_{\tau\pi}{}^{(\nu)}$ and eigenvectors $V_c{}^{\tau\pi,\nu}$.

IV. APPLICATIONS OF THE REACTION THEORIES

In this section we review briefly the experimental situation and the bound-state calculations, and discuss the available continuum calculations against this background. We concentrate mainly on the calculations using the eigenchannel and coupled-channel

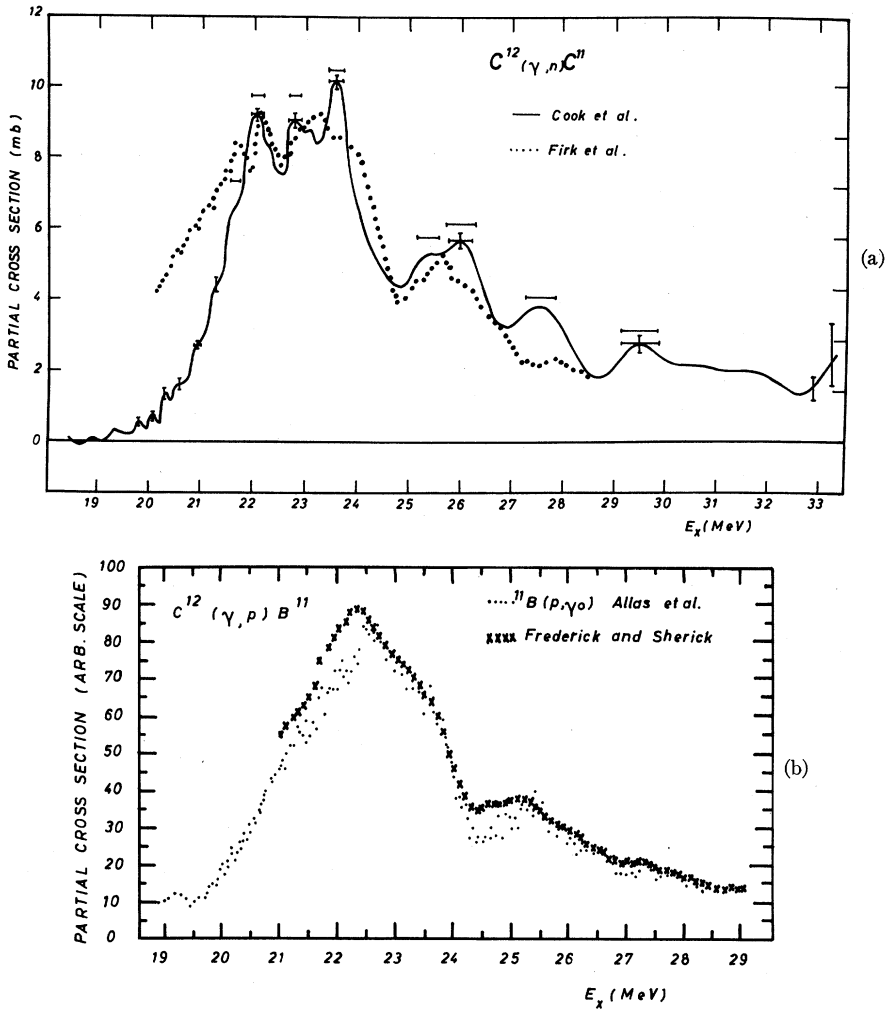

FIG. 7. (a) Comparison of the $^{12}C(\gamma, n)$ cross section of Cook, *et al.* (1966) with the photoneutron yield of Firk, *et al.* (1962). (b) Comparison of the $^{12}C(\gamma, p)$ cross section of Frederick and Sherick (1968) with the cross section obtained from the inverse ^{11}B (p, γ_0) reaction (Allas, *et al.*, 1964). The curves are matched together between 25.6 and 28.6 MeV.

methods. Some of the eigenchannel results have not been published previously.

A. Giant Dipole Resonance in ^{12}C; Experiment and Bound-State Calculations

The range of nuclear excitation, E_x, of interest in the excitation of 1^- states in ^{12}C runs from the proton threshold at 15.96 MeV up to 30 MeV. Since the (γ, pn) threshold is at 27.4 MeV, and the $(\gamma, 2n)$ threshold is at 31.8 MeV, there is some justification in restricting oneself to the treatment of one-nucleon reactions. Then the only threshold in the range 16 MeV$\leq E_x \leq$30 MeV is the neutron threshold at 18.72 MeV.

The major experimental information comes from photonuclear reactions (Firk, *et al.*, 1962; Danos and Fuller, 1965; Verbinsky and Courtney, 1965; Cook, *et al.*, 1966; Fultz, *et al.*, 1966; Lochstet and Stephens, 1966; Frederick and Sherik, 1968; Wu, *et al.*, 1968), $^{11}B(p, \gamma)^{12}C$ (Allas, *et al.*, 1964) and inelastic electron scattering experiments. (Dodge and Barber, 1962a; Goldmann and Spamer, 1970). Experiments on the total photodisintegration process have been performed by Shevchenko and Yuden (1965) and by Wyckoff, *et al.* (1965).

The experiments indicate two characteristic features, namely (i) a main peak centered at 22.8 MeV which seems to be composed of at least three components, and (ii) a substantial peak on the high energy side of the dipole resonance at 25.5 MeV which again shows indications of some substructure. To illustrate we show Figs. 7(a) and 7(b) (Cook, *et al.*, 1966 and Frederick and Sherik, 1968, respectively). The first figure shows the analysis of a (γ, n) bremsstrahlung yield curve, together with the relative (γ, n) yield found by Firk, *et al.*, (1962). The second figure shows a (γ, p) bremsstrahlung result together with the inverse $^{11}B(p, \gamma_0)$ cross section (cf. Allas, *et al.*, 1964).

The photoproton cross section looks smoother than the photoneutron cross section, in spite of the fact that the effective resolution of the (γ, p) experiment is 300

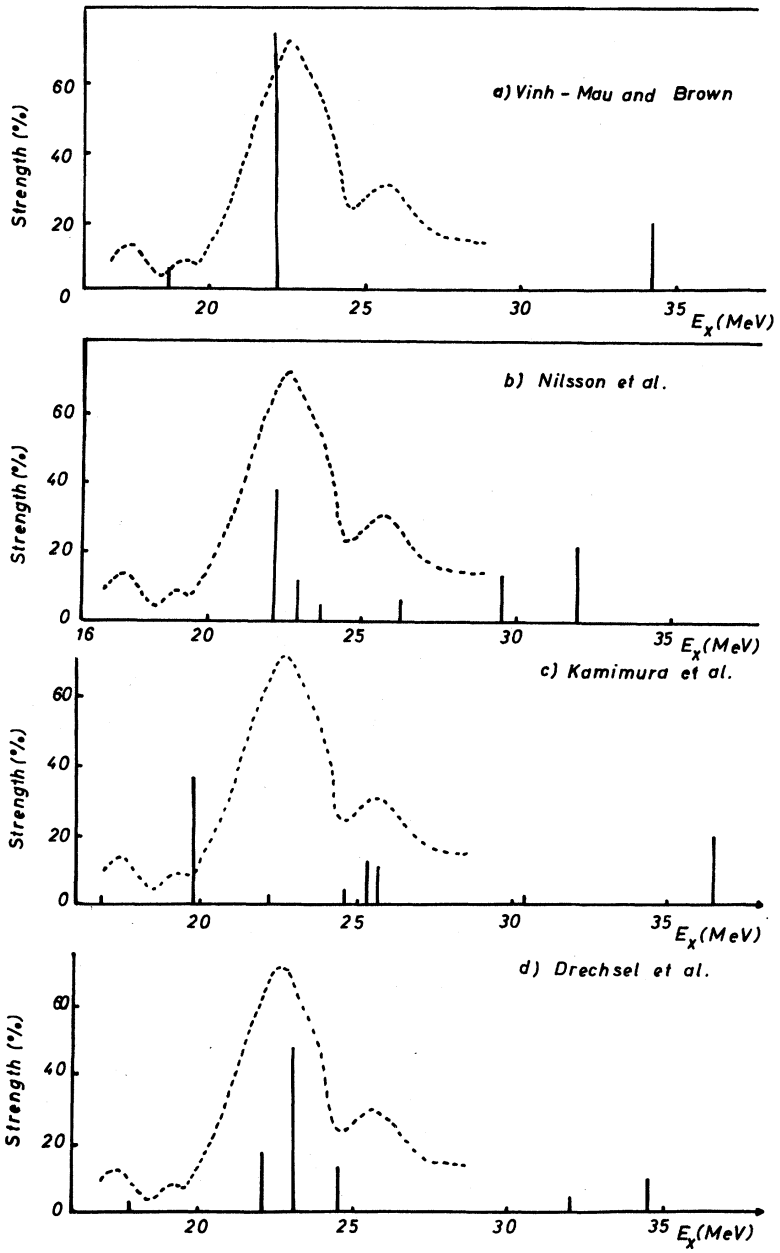

FIG. 8. Theoretical distributions of the dipole oscillator strengths in ^{12}C compared with the experimental results of Allas, *et al.* (1964). (a) Spherical $1p$–$1h$ basis (Vinh-Mau and Brown, 1962); (b) permanently deformed potential (Nilsson, *et al.*, 1972); (c) microscopic treatment of coupled dipole oscillations and quadrupole vibrations (Kamimura, *et al.*, 1967); (d) particle–hole dipole states are coupled to surface phonons (Drechsel, *et al.*, 1967).

keV i.e., finer than the spacing of the structure on top of the main (γ, n) peak in Fig. 7(a) (which is 800 keV). Also, the (γ, p) cross section has a peak at 22.5 MeV where there is a dip in the (γ, n) cross section.

The good agreement between the two experimental results depicted in Fig. 7(b) indicates that the contribution of nonground state protons in the (γ, p) result is less than 10% above 22.5 MeV, except from 24 to 25 MeV. On the other hand, the (γ, n) result of Firk, *et al.* [Fig. 7(a)] resembles closely the $\theta = 90°$ differential (γ, n_0) cross section found by Wu, *et al.* (1968). Thus the most characteristic differences in the shape of the photoneutron and photoproton cross sections are not due to nonground state transitions, but have already shown up in the ground-state transitions, and are normally interpreted in terms of isospin mixing (Hayward, 1964). The problem, however, is not yet solved. The photonuclear process also shows fine structure having 200 keV spacing on top of the 25 MeV peak and on the low energy side of the main resonance.

TABLE I. Comparison of $\int \sigma\, dE$ in several energy intervals with the predictions of various calculations.

Energy range (MeV)	Experiment[a] (%)	$1p$–$1h$ Bound-state description[b] (%)	Nilsson *et al.* (%)	Kamimura *et al.* (%)	Drechsel *et al.*[c] (%)
16–25	47	74	57	53	69
25–30	29	0	21	22	15
30–40	24	26	22	25	16

[a] We refer to Cook, *et al.* (1966).
[b] The results of Vinh-Mau and Brown (1962) and Gillet and Vinh-Mau (1964) agree up to +1%.
[c] Here we have replaced the limit 25 MeV by 24 MeV.

One particle–one hole shell-model calculations in a spherical basis were performed by Vinh-Mau and Brown (1962) for a contact force, and by Gillet and Vinh-Mau (1964) for a finite range force. Both results for the 1^- $T=1$ states of ^{12}C look similar, in spite of the difference in the residual force. This is due to the fact that the j–j coupled $1p$–$1h$ basis states remain rather pure after diagonalization. Only two levels are obtained which carry an essential part of the dipole strength [cf. Fig. 8(a)]. The level at about 23 MeV exhausts the dipole sum to 75%. This level explains the occurrence of the observed main giant-resonance peak. It consists of about 95% of a $(1d_{5/2}1p_{3/2}^{-1})$ configuration and is shifted with respect to the unperturbed energy by 5 MeV. This results mainly from the diagonal elements of the residual force.

The state at 34 MeV which carries 25% of the dipole strength contains the configuration $(1p_{1/2}1s_{1/2}^{-1})$ to about 95% and is shifted by 4 MeV. No experimental evidence for a sharply defined state at 34 MeV has been found (Reay, *et al.*, 1963).

A major insufficiency of the $1p$–$1h$ calculation is that it does not allow any explanation of the substantial peak observed at 25.5 MeV. Some dipole strength can be shifted to that energy region by employing a deformed single-particle potential and thus removing most of the degeneracy of the spherical model. Nilsson *et al.* (1962) performed a $1p$–$1h$ calculation for a static deformed oblate spheroid potential with the rather small nuclear deformation $\beta=-0.21$ [Fig. 8(b)]. Since $E1$ transitions to states corresponding to rotational bands with projection quantum number $K=0$ and $K=1$ are possible, many more transitions are involved than in the spherical case. The main giant-resonance peak splits into three levels at 22.2, 23.0, and 23.7 MeV.

A different approach has been taken by Kamimura, *et al.* (1967) who enlarged the spherical $1p$–$1h$ basis by adding certain $2p$–$2h$ configurations. The latter consist of a $(1p_{1/2}1p_{3/2}^{-1})^{2^+T=0}$ $1p$–$1h$ pair coupled to some other $1p$–$1h$ pairs having $T=1$. The $(1p_{1/2}1p_{3/2}^{-1})^{2+}$ configuration is considered as a sufficient description of the first excited state of ^{12}C. Thus one may consider this treatment as a microscopic approach to the problem of simultaneously excited dipole oscillations and quadrupole vibrations [Fig. 8(c)].

In a more phenomenological way this problem was treated by Drechsel, *et al.* (1967) [Fig. 8(d)]. They combined the $1p$–$1h$ doorway states with the collective quadrupole surface phonons, following closely the treatment of dipole excitations in the collective model where the nuclear surface is allowed to perform slow quadrupole oscillations (Danos and Greiner, 1964; Weber, *et al.*, 1966). This collective description was their guide for constructing the interaction Hamiltonian. The level spacing for the quadrupole oscillations was put equal to the excitation energy of the lowest 2^+ state in ^{12}C. The amplitude $\beta_0=[5\hbar/(2B_2\omega_2)]^{1/2}$ of the quadrupole oscillations was determined from the $B(E2)$ value to be $\beta_0=0.43$. Many-phonon excitations were allowed. From a comparison with Fig. 7 the results of Drechsel, *et al.* seem to explain the structure of the dipole giant-resonance somewhat better. However, their state at 24.5 MeV should be shifted to higher energies by 1 MeV. Nevertheless, the full structure seen in the (γ, n) experiment (Cook, *et al.*, 1966) cannot be explained by any of these more sophisticated calculations.

For a more quantitative comparison of the different approaches we have listed in Table 1 the contributions of three different energy intervals to the integrated cross section.

The Table shows again that only a sophisticated description of the nucleus leads to a fair amount of dipole strength in the 25.5 MeV region. In addition, the more detailed approaches give the correct mean energy of 22.8 MeV (Allas, *et al.*, 1964) for the energy range 16–28.8 MeV, while the mean energy of the pure $1p$–$1h$ description is 1 MeV too low (Kamimura, 1967).

Finally, we must mention that the computed integrated photon absorption cross section of the giant resonance exceeds the experimental value by about a factor of 2. This together with the experimental fact that a large fraction of the photon absorption strength lies at energies above 40 MeV indicates that a complete

description will have to include short-range correlations (Danos, 1968).

That is outside the scope of the present article.

B. The Giant Dipole Resonances of ^{12}C in a Continuum $1p$–$1h$ Calculation

For the ^{12}C nucleus, there exists a coupled-channels calculation by Marangoni and Saruis (1967), and eigenchannel calculations using different single-particle potential parameters performed by Delsanto and Wahsweiler (1970), Antony-Spies (1972), and Mshelia (1971). We begin by discussing the eigenchannel calculations.

As described in Sec. III, one should begin the calculation by obtaining a self-consistent nonlocal Hartree–Fock potential for the particles and holes. In practice, a local Saxon–Woods-type potential is always used instead. It is found that a single local potential does not allow one to reproduce the experimental single-particle energies, or, in other words, the experimental threshold energies. The use of such a potential thus is an unacceptable oversimplification, and one must compensate for this in some manner later. Thus, the potential is assumed to have the form

$$V(r)=V_c\rho(r)-V_{so}(\mathbf{l}\cdot\boldsymbol{\sigma})r^{-1}[d\rho(r)/dr], \quad (4.1)$$

with

$$\rho(r)=[1+\exp\{(r-R_0)/d\}]^{-1}. \quad (4.1a)$$

The parameters of Eq. (4.1a) used by Delsanto and Wahsweiler were chosen so as to agree with electron scattering data (cf. Elton, 1961). This leads to $R_0=2.3$ F and $d=0.45$ F. The above referred to oversimplification was here compensated for by allowing the parameters of Eq. (4.1) to depend on the symmetry; i.e., on l and j, of the state, but not on the velocity. The strength V_{so} of the spin–orbit force was taken from a fit (Buck and Hill, 1967) for the p- and d-shell neutron levels in ^{16}O. Then the depths V_c of the central potentials for the various single-particle states in ^{12}C were determined in such a way that the experimental neutron hole and particle energies (Gillet and Vinh-Mau, 1964) were reproduced. With respect to the $d_{3/2}$ state this means that the single-particle resonance occurs at 3.39 MeV. Its theoretical width turns out to be 1 MeV, which is fairly close to the experimental value (Willis, 1958). The various well depths and the fitted single-particle energies ϵ_b are listed in Table II.

TABLE II. Well parameters and single-particle energies in ^{12}C.

State	ϵ_b (MeV)	V_c (MeV)	V_{so} (MeV)
$1d_{3/2}$	3.39	94.64	5.3
$2s_{1/2}$	−1.86	88.83	...
$1d_{5/2}$	−1.10	87.07	5.3
$1p_{1/2}$	−4.95	68.13	9.6
$1p_{3/2}$	−18.72	74.82	9.6
$1s_{1/2}$	−35.	68.33	...

TABLE III. ^{12}C 1^-, $T=1$.

Brown (MeV)	%	Gillet E (MeV)	Continuum calc E (MeV)	Continuum calc Γ (MeV)	Experiment E (MeV)
18.7	6.5	17.7	17.7	0.9	18.1
22.2	75	21.9	22.2	2.1	22.8
23.9	0.5	24.2	24.5	4	25.5

For the protons, a Coulomb potential V_{Coul} of a homogeneously charged sphere of radius R_0 was added to the expression (4.1). For f waves, which contribute to the positive parity states of ^{12}C, the same values V_c were used as quoted for the p waves. The strength of the spin–orbit potential V_{so}, however, was chosen to be 5.3 MeV, i.e., the same as for the d waves. The relatively large V_c values for the d shell indicate that the values for R_0 and d used here are rather small from the point of view of a nuclear structure calculation.

The following configurations were taken into account for both protons and neutrons in calculating the 1^- states:

$$1^-: d_{5/2}p_{3/2}^{-1}; \quad d_{3/2}p_{3/2}^{-1}; \quad s_{1/2}p_{3/2}^{-1}.$$

As in the calculations of Vinh-Mau and Brown (1962), a zero-range force with Soper exchange mixture was used

$$V(1,2)=-V_0[0.865+0.135\,\boldsymbol{\sigma}_1\cdot\boldsymbol{\sigma}_2]\delta(r_1-r_2). \quad (4.2)$$

The strength V_0 was taken as $V_0=-500$ MeV F^3. This brings the main peak of the nuclear dipole absorption cross section to 22.2 MeV, i.e., close to the experimental value 22.8 MeV.

The strength V_0 used in the bound state calculations of Vinh-Mau and Brown is given by

$$V_0/4\pi b^3=8.50 \text{ MeV}, \quad (4.3)$$

where b denotes the range parameter of the ^{16}O harmonic oscillator model. From elastic electron scattering, one deduces (Elton, 1961) $b=1.76$ fm. This leads to $V_0=-582$ MeV fm^{-3}. In spite of this larger value, the position of the giant dipole resonance obtained coincides with the peak of the continuum calculation. This results from a smaller overlap in the diagonal elements of the residual force for the oscillator model.

Quite different Woods–Saxon potentials and a stronger residual force were used in the coupled-channel treatment of the photodisintegration of ^{12}C by Marangoni and Saruis (1969). Their results are in qualitative agreement with those discussed here.

A more recent eigenchannel calculation was performed for 1^- states by Mshelia (1971) who used the same single-particle potential parameters as Marangoni

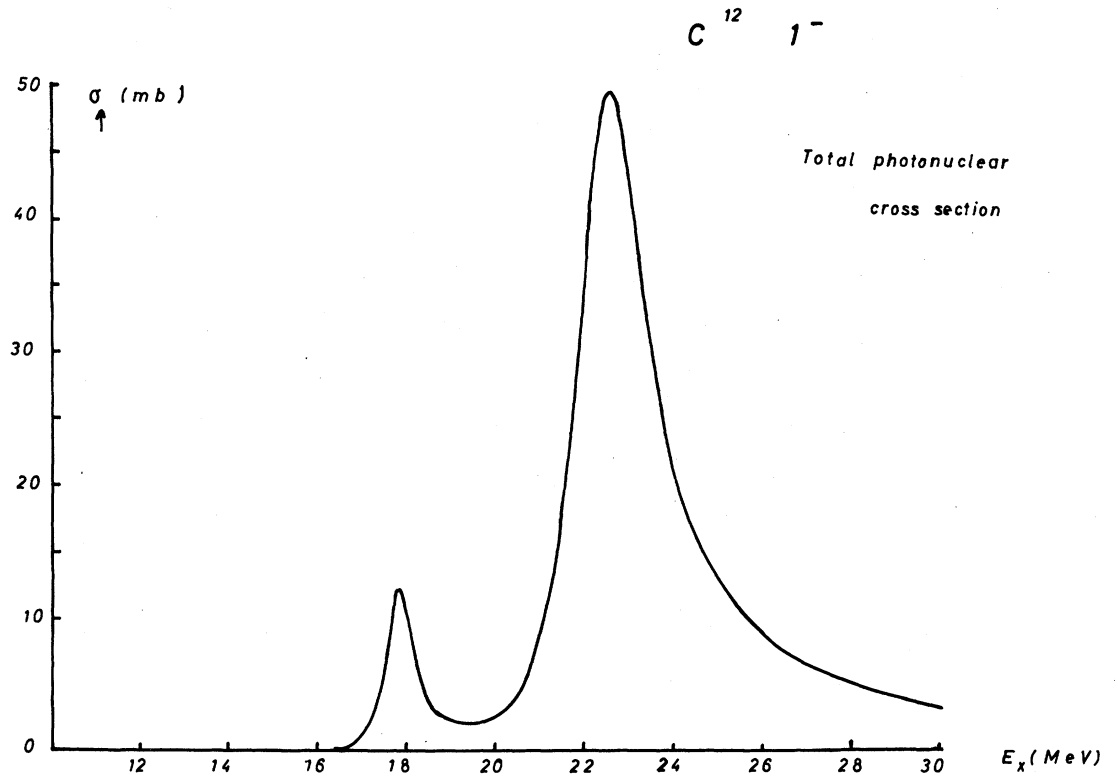

FIG. 9. The total theoretical 1^- photodisintegration cross section of ^{12}C from the $1p$–$1h$ continuum calculation described here (Delsanto and Wahsweiler, 1970).

and Saruis and included the $1s_{1/2}^{-1}1p_{1/2}$ configuration. His results are in excellent quantitative agreement with those of the coupled channels calculation.

Figure 9 exhibits the result of the $1p$–$1h$ continuum calculation for the total 1^- photo-absorption cross section of ^{12}C between 16 MeV and 30 MeV nuclear excitation performed by Delsanto and Wahsweiler (1970). The peak at 17.7 MeV lies below the neutron threshold (18.72 MeV). It is almost a pure s-wave resonance and might be identified (Donnelly, *et al.*, 1968) with the peak seen at 18.1 MeV in the inelastic electron scattering experiments of Goldenberg and Barber (1964). The theoretical total width of 0.9 MeV does not deviate too strongly from the experimental result. The theoretical width of 2.5 MeV for the main peak is too small by 1 MeV [see Figs. 7(a, b)]. This is due to the neglect of the coupling to more complicated configurations, and the neglect of the open α-particle channels. It also depends to some extent on the single-particle potential parameters and residual forces used.

The ratio of dipole strengths contained in the two peaks is about 10 in agreement with the $1p$–$1h$ result of Vinh-Mau and Brown (1962). In Table III the positions of the 1^- $T=1$ levels of the bound state and the continuum calculations are compared with the experimental result. We have included the 24.5 MeV state of the continuum calculation (see below) whose dipole strength is too weak to show up as a separate peak in Fig. 9.

The area under the γ-absorption cross section from 16 to 28.8 MeV in Fig. 9 is 159 MeV·mb. The experiment of Wyckoff, *et al.* (1965) yields about 110 MeV·mb, in good agreement with what is expected from Cook's (1966) (γ, n) data. The nonenhanced classical dipole sum rule gives 180 MeV·mb. The mean energy for this energy range is 23.1 MeV, i.e., larger than the value from the more sophisticated bound-state treatments of the ^{12}C compound system.

In Fig. 10, we show the contributions of the different configurations to the dipole state obtained from the calculation by Mshelia (1971) when the $1p_{1/2}1s_{1/2}^{-1}$ configuration was included. They were computed according to the prescription outlined in Sec. III.F, and thus represent the wave function of the compound nucleus, the nucleus inside the matching radius. Thus the contribution of both open and closed channels is represented. Note also that therefore the behavior of the wave function in the asymptotic region cannot be read off directly as it is modified by barrier penetration effects. For example, the $(\gamma, p)/(\gamma, n)$ ratio is not directly given by the ratio of the heights of the respective curves in Fig. 10. Information of this kind is con-

tained directly in the S-matrix, as discussed in Secs. III.D and III.E.

The first observation which is made from inspection of Fig. 10 is that it contains more structure, which is hidden when all the contributions which yield the total cross section are added up. This structure shows up both in the form of peaks, and in the form of non-Lorentzian shapes. Thus, for example, the $p_{3/2}^{-1}d_{3/2}$ proton configuration has a peak at 21 MeV and a peak which is 10 times smaller at about 23 MeV, while the shapes of the dominant $p_{3/2}^{-1}d_{5/2}$ configurations are different: the proton configuration has rather a Lorentzian shape, while the neutron configuration has a markedly non-Lorentzian shape. This immediately brings up the question of isospin purity, which here concerns the inside region. Recall however, that any separation into inside and outside regions is somewhat arbitrary. Statements of the isospin purity of continuum states therefore of necessity have only qualitative significance. Nevertheless, they can have very clear informative value. Having made this *caveat* we can proceed with the discussion.

The peak at 17.7 MeV is almost purely an s-wave resonance. It has very pure isospin despite the fact that it has a proton particle width of almost 1 MeV while it lies below the neutron threshold, a very surprising result. On the other hand, the $p_{3/2}^{-1}d_{3/2}$ configuration shows very strong isospin breaking in the region 19–24 MeV. This is evidently associated with the difference of independent particle continuum resonances of the $d_{3/2}$ protons and neutrons; i.e., the differences in the spectra of H_0. Thus the neutron resonance which in the unperturbed spectrum lies at 3.4 MeV above threshold appears shifted higher by only about 0.5 MeV. It appears to be able to "pull in" the corresponding proton configuration only very weakly; the resulting peak has only about 0.1 of the neutron peak height, a rather surprising result in view of the 17.7 MeV peak in the $s_{1/2}$-configuration. The converse holds for the peak at 21 MeV, which appears only in the proton configuration.

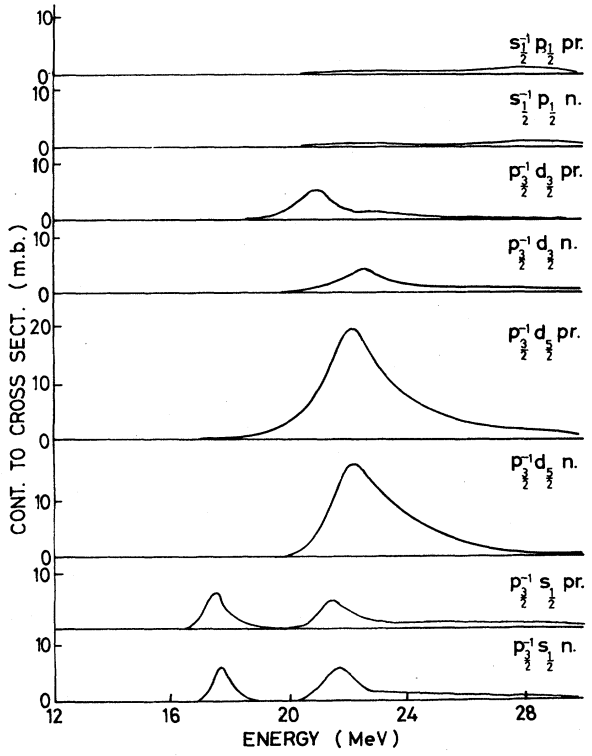

FIG. 10. Contributions of the different $1p$–$1h$ configurations to the dipole state in ^{12}C (Mshelia, 1971).

An investigation by Mshelia (1971) of the configuration mixing occurring when different single-particle potential parameters are used, and when the $1s_{1/2}^{-1}1p_{1/2}$ configuration is omitted reveals that the contribution of the $p_{3/2}^{-1}d_{3/2}$ configurations to the total cross section, particularly in the giant-resonance region, depends strongly on the particular parameters chosen. This effect is not as pronounced with the other configurations.

This seeming contradiction between the behavior of the $s_{1/2}$ and the $d_{3/2}$ configurations can be understood as follows: In this light nucleus, the isospin impurities undoubtedly arise from external mixing. In the eigenchannel formalism this manifests itself in different boundary conditions for protons and neutrons [the logarithmic derivative of w_c, Eq. (3.22a)], can be quite different for Coulomb functions and spherical Bessel functions for the same value of $\delta^{(\nu)}$. However, as long as the proton energy does not exceed the Coulomb barrier the influence of the boundary conditions is attenuated by the barrier penetrability factors. This is the case for the 17.7 MeV resonance. On the other hand, at 22 MeV both protons and neutrons are above the Coulomb and centrifugal barriers and differences in boundary conditions directly induce differences in the shapes of the radial wave functions. Consequently the matrix elements of the residual two-body force have a reduced value; i.e., the interaction between the protons and neutrons is reduced. Hence we find a difference between the 17.7 MeV region and the 22 MeV region.

The difference between the $p_{3/2}^{-1}d_{3/2}$ configurations and the other configurations is further emphasized by the fact that there exists no bound particle state for the $d_{3/2}$ configurations. The unperturbed configuration energies and the radial wave functions of all branches of these states depend strongly on the boundary conditions, and therefore differ for neutrons and protons. The other configurations have a bound particle state which implies that the configuration energy and the radial wave function of one of the important branches of all those states remains essentially independent of the eigenchannel boundary conditions. Isospin mixing is thus likely to be most pronounced in the $p_{3/2}^{-1}d_{3/2}$ configurations.

The $p_{3/2}^{-1}d_{5/2}$ configuration, the principal carrier of the dipole strength, has a pure isospin in the region of the peak. On the high-energy side, the isospin purity deteriorates, evidently because of the difference between the proton and neutron thresholds.

Finally, in the $p_{3/2}^{-1}s_{1/2}$ configurations there seems to be an indication of a broad peak at 24 MeV with a width of about 4 MeV for both protons and neutrons. Perhaps it contributes to the distortion of the shape of the giant-resonance peak in the $p_{3/2}^{-1}d_{5/2}$ configuration, and it may be also visible in the $p_{3/2}^{-1}d_{3/2}$ configuration. The $s_{1/2}^{-1}p_{1/2}$ configurations contribute weakly and only at higher excitation energies. Their strength is spread over several MeV and does not result in a sharp peak in the total cross section, as predicted by bound-state calculations.

Recalling now the bound-state calculations, one notices that essentially all their results carry over into the continuum calculations, even though the bound-state calculations were performed assuming exact isospin purity. However, differences do exist on the quantitative level. The most important difference concerns the purity of the states: The configuration mixing is more pronounced throughout. Thus, for example, in the bound-state calculation, the main giant-resonance peak contains 95% of the $p_{3/2}^{-1}d_{5/2}$ configuration, while this peak contains only about 75% of this configuration in the continuum calculation.

C. Results for Other Multipole Excitations in ^{12}C

Before we go into further details concerning the 1^- states of ^{12}C, [i.e., discussions of the various partial (γ, n) and (γ, p) cross sections and of the angular distributions] we prefer to report on the results of a calculation concerning the other angular momentum and parity states of ^{12}C. In contrast to the photon absorption process, these states are important in particle reactions, and also in the electroexcitation process.

In the calculations referred to (cf. Delsanto and Wahsweiler, 1970; Antony-Spies, *et al.*, 1970), the configurations involving the excitation of the deep $1s_{1/2}$ hole were not retained since its influence on the states in the considered energy range 16–30 MeV is likely to be negligible, as is the case for the 1^- states. For the additional negative parity states thus the following neutron and proton configurations were retained:

0^- $d_{3/2}p_{3/2}^{-1}$
2^- $d_{5/2}p_{3/2}^{-1}$, $d_{3/2}p_{3/2}^{-1}$, $s_{1/2}p_{3/2}^{-1}$
3^- $d_{5/2}p_{3/2}^{-1}$, $d_{3/2}p_{3/2}^{-1}$
4^- $d_{5/2}p_{3/2}^{-1}$.

The 0^- states are not excited in the lowest order in electron scattering.

In the $1p$–$1h$ space, the positive parity states involve "$2h\omega$" excitations. Thus sharp resonances can be associated only with the $1p_{1/2}1p_{3/2}^{-1}$ configuration. That means that the positive parity states mainly contribute a direct reaction background only. The following states were considered:

0^+ $p_{3/2}p_{3/2}^{-1}$
1^+ $p_{1/2}p_{3/2}^{-1}p_{3/2}p_{3/2}^{-1}f_{5/2}p_{3/2}^{-1}$
2^+ $p_{1/2}p_{3/2}^{-1}$; $f_{7/2}p_{3/2}^{-1}$; $p_{3/2}p_{3/2}^{-1}$; $f_{5/2}p_{3/2}^{-1}$.

The potential and force parameters used in this calculation are those given in the preceding section.

We now turn to the transverse form factors in which the same operators appear as in the transition matrix elements of the photonuclear process. The definition for the form factors used was essentially the same as that given by de Forest and Walecka (1966). Since the final target states are scattering states, the squares of the form factors acquire the dimension 1/MeV.

Extensive graphs of transverse and longitudinal form factors for inelastic electron scattering in ^{12}C as a function of momentum transfer and excitation energy are found in the paper by Antony-Spies (1972). Here, we restrict ourselves to a typical case, where the momentum of the ingoing electron is $k_i = 55.1$ MeV/c, and the scattering angle of the electron is $=141°$. This corresponds to the kinematical data from a recent Darmstadt experiment (Antony-Spies, *et al.*, 1970; Goldman and Spamer, 1970). Then the momentum transfer, corresponding to a nuclear excitation $E_x = 23$ MeV, amounts to $q = 82$ MeV/c.

The momentum transfer is related to the momenta of the incoming and outgoing electron by

$$q^2 = (k_i^2 + k_f^2 - 2k_i k_f \cos\theta). \tag{4.4}$$

Through the energy interval 16 MeV$\leq E_x \leq$30 MeV, q does not vary more than ± 7 percent. Since $E_x/(qc) < [J(J+1)]^{1/2}$, the longitudinal form factors of the electric transitions actually are larger than the corresponding transverse form factors (De Forest and Walecka, 1966). On the other hand, we are still close to the long wavelength limit, since $q/(hc) \lesssim 0.5$. Thus, in general, the longitudinal form factor shows an energy behavior similar to the transverse one. The only remarkable difference arises in the 1^- case, where the transverse form factor shows an additional bump at 24.5 MeV.

The various transverse form factors as functions of the excitation energy E_x are represented in Fig. 11. The

TABLE IV. ^{12}C 2^- $T=1$.

Brown (MeV)	(%)	Gillet (MeV)	Continuum calc (MeV)	Γ (MeV)	Experiment (MeV)
18.1	6	18.2	18.2	0.3	18.1[a]
19.2	72	19.4	19.4	0.3	19.1[a,b]
22.9	22	23.2	23.0	≈3	···

[a] Goldmann and Spamer, 1970.
[b] deForest, 1965.

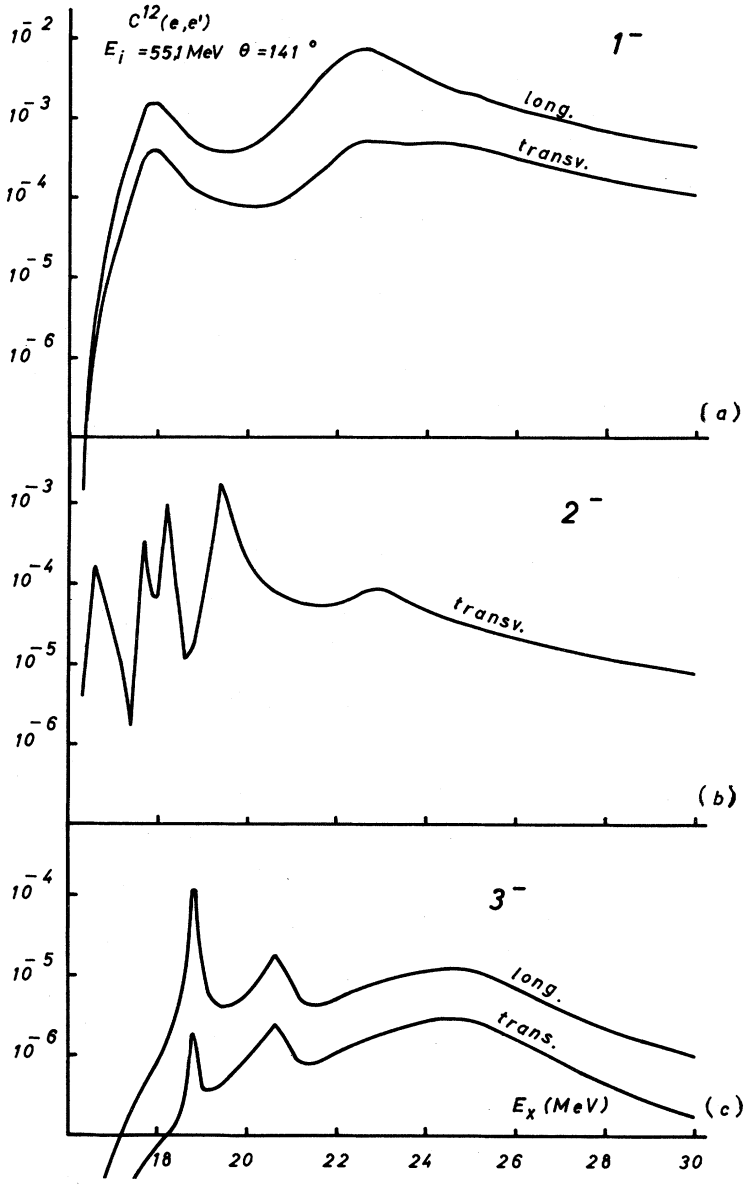

FIG. 11. Calculated squared form factors (in MeV^{-1}) for inelastic electron scattering on ^{12}C versus the nuclear excitation energy. The energy of the incoming electron is specified to be 55.1 MeV, and the scattering angle is 141°. Excitations of the following multipolarities are considered: (a) 1^-; (b) 2^-; (c) 3^-.

energy dependence is in the first place due to the nuclear wave function and is only slightly affected by the dependence of q [Eq. (4.4)] on the excitation energy E_x. From the curves of Fig. 11, one can, in principle, obtain the required information on the position of the nuclear levels, on the total particle escape widths, and on the relative multipole strengths of the different levels.

The shift of dipole strength from 22.6 to 24.5 MeV observed in Fig. 11 has been studied theoretically in a continuum model calculation by Friar (1966). At $q \approx 80$ MeV/c the upper level carried most of the strength. Experimental evidence for the increasing importance of the spin–flip mechanism at higher q comes from the measurements of Goldenberg and Barber (1964). A further increase of the momentum transfer, however, drastically reduces the height of the 24.5 MeV state in comparison to that of the 17.8 MeV state.

The most important 2^- resonance [Fig. 11(b)] is the one at 19.4 MeV. For very small q values, the contribution of the 2^- states to the (e, e') cross section is negligible. However, at $q \approx 100$ MeV/c it is already quite large and the 19.4 MeV state should be noticeable in the experiment. Indeed, for 65-MeV electrons, de Forest

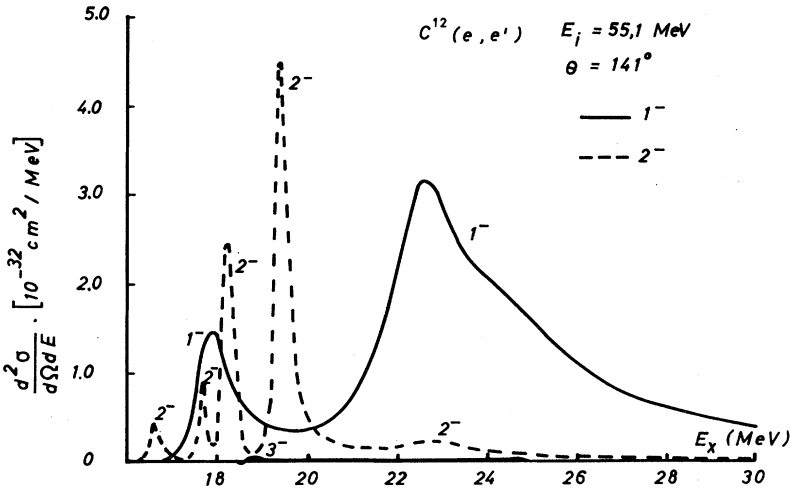

FIG. 12. Calculated differential cross section for inelastic electron scattering in ^{12}C for $E1$ and $M2$ transitions. The $E3$ cross section is too small to be seen on this scale. The parameters are the same as in Fig. 11.

(1965) has observed a strong state at 19.2 MeV which can be identified with the calculated "giant magnetic quadrupole state" (Crannel, *et al.*, 1967; Buret, *et al.*, 1968) obtained theoretically at 19.4 MeV.

In Table IV we compare the positions of the $2^- T=1$ levels for the range 16 MeV$\leq E_x \leq$30 MeV obtained by Vinh-Mau and Brown (1962), and by Gillet and Vinh-Mau (1964) as well as the continuum calculation and also quote the known experimental values.

In addition, the continuum calculation predicts $T=0$ states at 16.6 MeV ($\Gamma=0.3$ MeV) and 17.8 MeV ($\Gamma=0.2$ MeV). These are the two lowest $2^- T=0$ states. They are practically not shifted from the unperturbed $1p$–$1h$ energies 16.9, and 17.6 MeV, respectively. This is in accordance with the remark of Vinh-Mau and Brown (1968) that the particle–hole force is weak in the $T=0$ magnetic states because of approximate compensation of the direct and exchange matrix elements. The position of the third $2^- T=0$ state should be roughly 22 MeV.

The relative weakness of the $T=0$ magnetic quadrupole transition reflects the isobaric spin selection rules for these excitations (Warburton, 1966) at low momentum transfer. These selection rules are due to the approximate cancellation of the neutron and proton magnetic moments.

In Fig. 12 we present the differential cross section $d^2\sigma/d\Omega dE$ of the (e, e') reaction exciting 2^- states in ^{12}C. Next we turn to the 3^- states [Fig. 11(c)], for which $q\approx$80 MeV/c. For $q=120$ MeV/c and $E_x=20$ MeV, one expects from Weisskopf estimates only a 1% contribution to the (e, e') cross section (de Forest, 1965). At about $q=500$ MeV/c the importance of the $E3$ excitations, however, strongly exceeds that of the $E1$ excitations (Antony-Spies, 1972).

Figure 13(a) exhibits the total 3^- photoabsorption cross section. The level at 20.7 MeV is $T=0$. There seems to be no strong collectivity for these octupole states. The level positions are shown in Table V.

The total 2^+ photoabsorption cross section is depicted in Fig. 13(b). The sharp peak ($\Gamma=0.3$ MeV) at 17.2 MeV results from the bound $1p_{1/2}(1p_{3/2})^{-1}T=1$ nuclear state. The structureless increasing cross section above 18 MeV probably is too small to account for the $E2$ contribution expected from the measured (γ, p) angular distributions (Frederick and Sherik, 1968).

To conclude this section we present a survey of the various integrated transverse form factors (Fig. 14). Here the integration has been performed over E_x from 20 MeV to 26 MeV, keeping q constant. Some attention should be paid to the famous dip in the 1^- form factor for small momentum transfer, which is well known from the work of Lewis and Walecka (1964). It is remarkable, that in the continuum calculation this dip appears for fixed E_x, i.e., without the integration procedure. Its occurence depends on the influence of the spherical Bessel function $j_0(qr)$ contained in the transverse 1^- form factor.

Finally, we compare the sum of the various theoretical (e, e') cross sections with the experimental data of Goldman and Spamer, 1970) (Fig. 15). The gross structure of the giant dipole resonance, including the 25 MeV peak, and the 19.2 MeV 2^- state are nicely reproduced.

TABLE V. ^{12}C 3^-.

	Gillet		Continuum calc		Experiment
T	(MeV)	%	(MeV)	Γ (MeV)	(MeV)
1	18.5	40	18.8	0.25	18.6
0	19.6	···	20.7	0.8	···
1	23.5	60	24.7	≈4	···

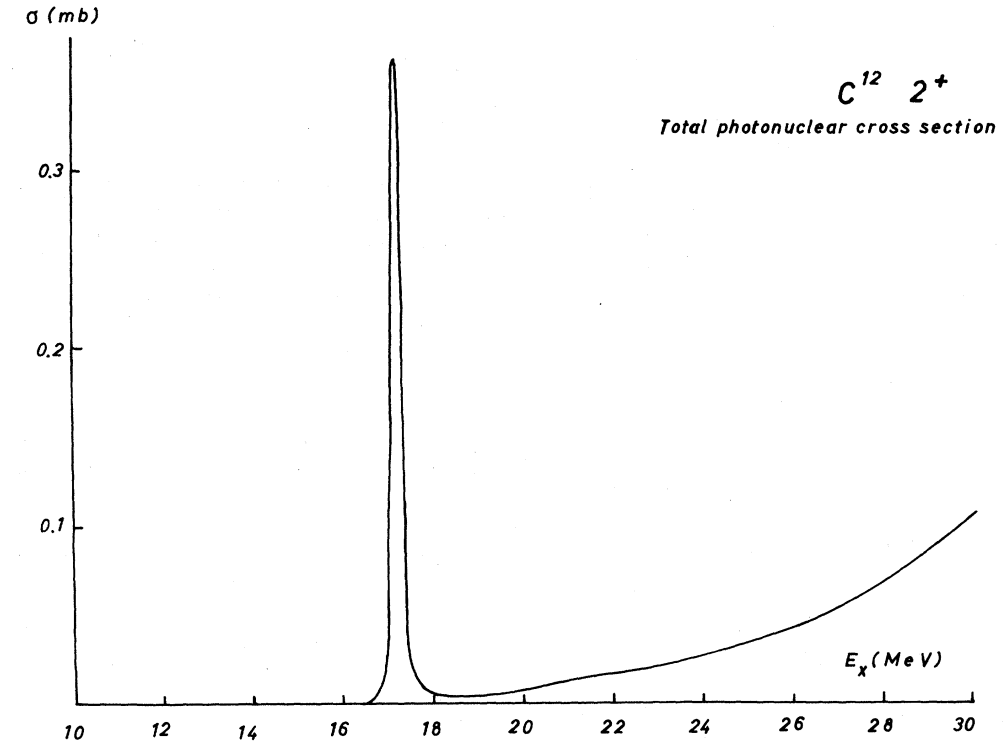

(b)

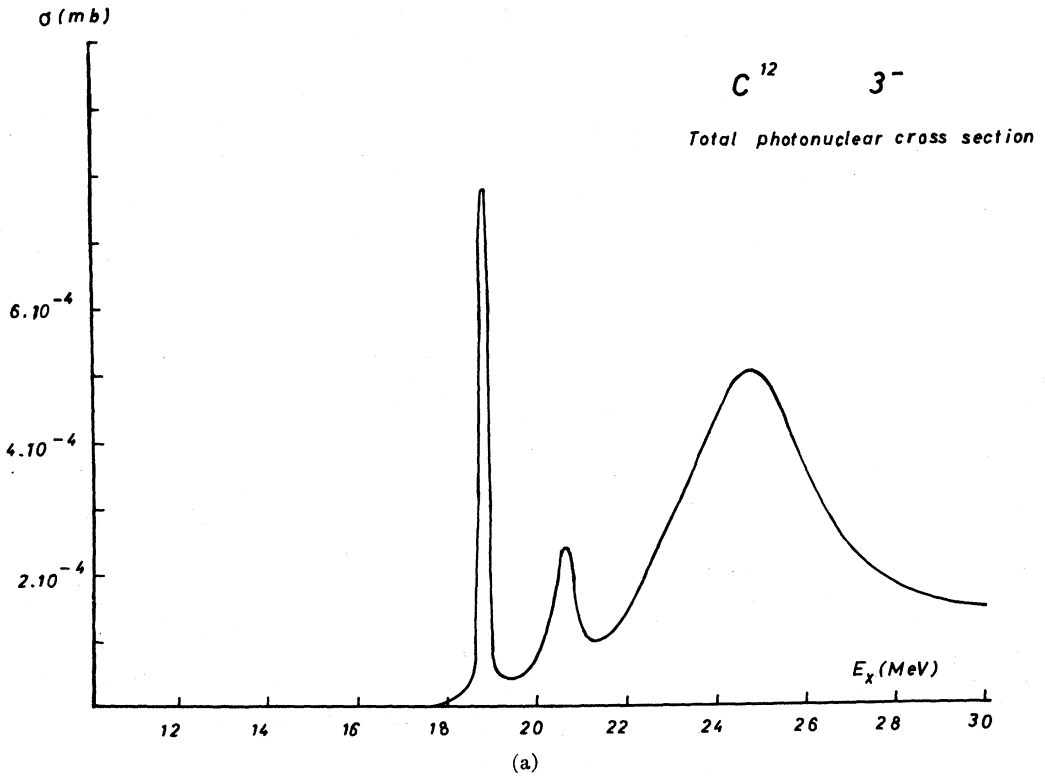

(a)

FIG. 13. (a) Predicted contribution of electric octupole transitions to the total photodisintegration cross section in ^{12}C. (b) The same for electric quadrupole excitations.

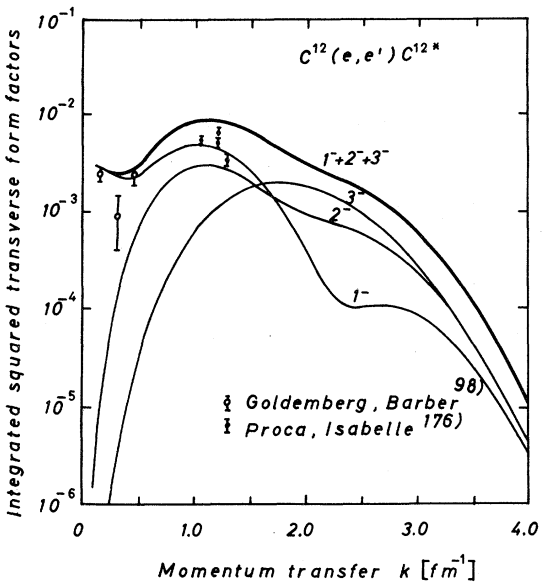

FIG. 14. Integrated [20–26 MeV] squared transverse form factors of ^{12}C for different multipoles and their sum versus momentum transfer. The experimental data are taken from Goldemberg and Barber (1964) and Proca and Isabelle (1968).

D. Photonuclear Branching Ratios and Angular Distributions in ^{12}C

Barker and Mann (1957) deduced the following formula for isolated states with single exit channels

$$\sigma(\gamma, p)/\sigma(\gamma, n) \approx (P_p/P_n)\,|\,(1+\alpha_0)/(1-\alpha_0)\,|^2. \quad (4.5)$$

to relate the ratio of the (γ, p) and the (γ, n) cross section to the relative amplitude α_0 of the $T=0$ admixture in the 1^- wave function. Here P_p and P_n are the proton and neutron penetrabilities, respectively. In deriving Eq. (4.5) it is assumed that the transition probabilities may be expressed in terms of reduced widths and that the proton and neutron angular distributions are identical. This formula can also be derived with the eigenchannel formalism (Rabie, 1970). It has frequently been used in the analysis of experiments (Segal, 1966; Wu, *et al.*, 1968); Rabie, 1970). So, Segel estimates $\alpha_0 \approx 0.06$ for ^{12}C, while Wu, *et al.* give $\alpha_0 \approx 0.1$ except around 22.5 MeV where it reaches about 0.25.

As mentioned in Sec. IV.B a precise separation into internal and external mixing is not possible. This is of no importance in computing branching ratios in a continuum calculation. The results of the eigenchannel calculations are here reported.

In Figs. 16(a) and 16(b) the calculated (γ, p) and (γ, n) cross sections respectively are represented. The s-wave peak at 17.7 MeV lies below the neutron threshold and thus is seen only in the (γ, p) cross section. This s-wave resonance, however, seems to be responsible for the slightly irregular behavior of the (γ, n) cross section just above its threshold.

A comparison of Figs. 16(a) and 16(b) with Figs. 7(a) and 7(b) shows immediately that only gross structure appears in the calculated curves. This feature is the same as in the case of the total cross section. Also, the agreement between the corresponding experimental and theoretical curves is of the same kind as in the case of the total cross section.

Of particular interest is the ratio $\sigma(\gamma, p_0)/\sigma(\gamma, n_0)$. The experimental curve for this ratio of Wu, *et al.* (1968) is shown in Fig. 17(a). It is essentially flat from very close to the (γ, n) threshold on except for the region around the giant resonance. In the flat region, this ratio has the value ≈ 1.6. On the other hand, the theoretical ratio has a qualitatively different behavior [c.f. Fig. 17(b) from the calculation of Mshelia (1971).] First, the influence of the (γ, n) threshold is strong and extends to rather high energies. It even seems to delay the rise of the (γ, n) cross section on the low energy side of the giant resonance. Secondly, the theoretical ratio continues to drop and reaches a value

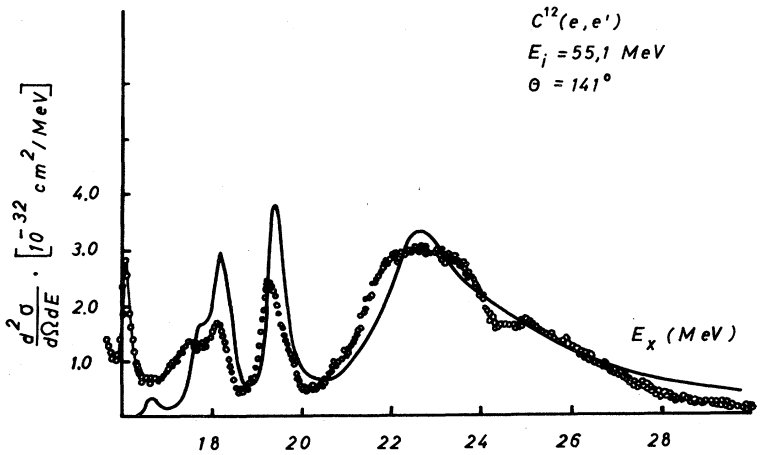

FIG. 15. Comparison of a calculated differential cross section for inelastic electron scattering on ^{12}C $(1^-+2^-+3^-)$ with data from a recent Darmstadt experiment (Antony-Spies, *et al.*, 1970). The experimental results clearly indicate the 2^- peaks which occur in the theoretical curve at 18.2 and at 19.4 MeV. The theoretical peaks have been folded with the energy width of the electron beams. (A Gaussian distribution has been assumed) No comparison can be done between the absolute heights since the experimental points only represent counting rates.

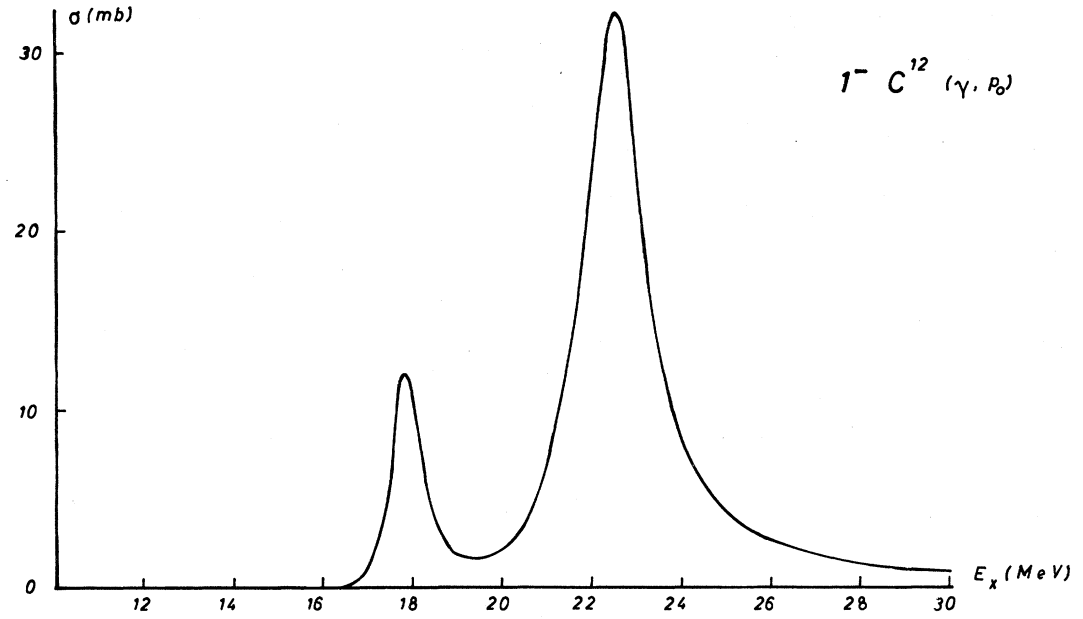

(a)

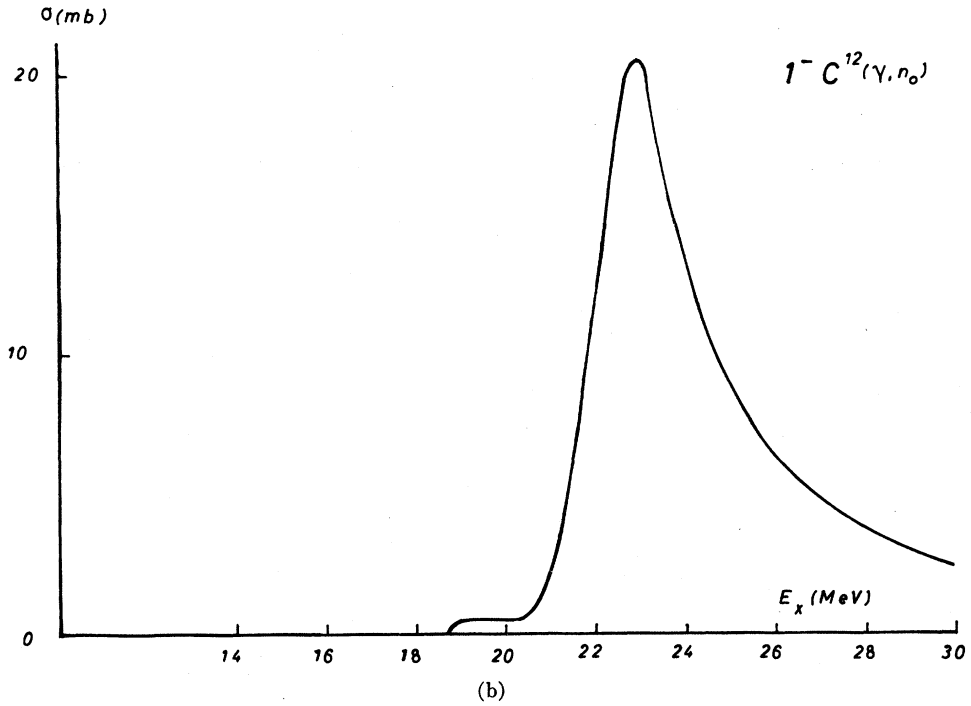

(b)

FIG. 16. Calculated partial 1^- photo cross sections of ^{12}C. Since it is assumed that single hole states can only be formed in the $1p_{3/2}$ subshell, only the following partial photoreactions are possible: (a) the photoproton process leading to the ground state of B^{11}; (b) the photoneutron process leading to the ground state of C^{11}.

$\approx$1.1. This failure of the theoretical curve to reproduce the experimental results is particularly surprising since these features represent gross effects and not fine structure. Therefore, this discrepancy must be considered to be a strong clue that the 1-particle–1-hole model is inadequate in more ways than one would have guessed, and that this deficiency has to be taken seriously. Its origin is definitely not understood at this time.

It should be mentioned that Fig. 15 actually

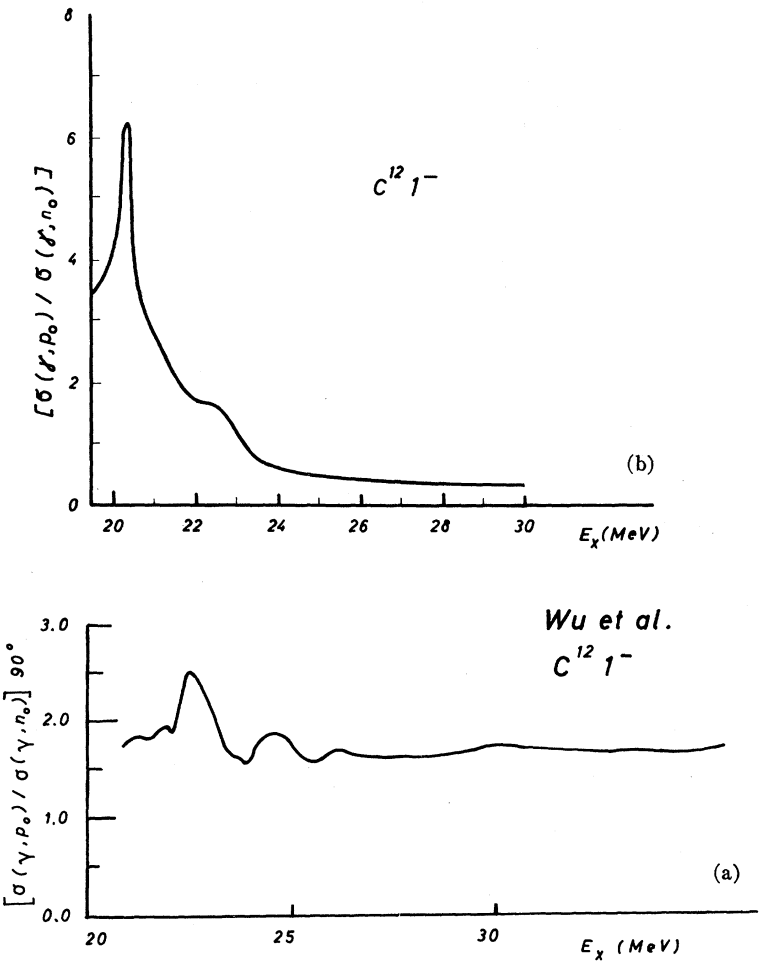

FIG. 17. (a) Ratio of the measured differential cross section (Wu, *et al*; 1968) (γ, p_0) and (γ, n_0) at 90°. (b) The corresponding theoretical result (see Fig. 16).

shows the ratio of the 90° differential cross sections. But since the angular distributions remain relatively constant above the giant resonance, as we will see below, this is not important.

As long as only $E1$ transitions are important, the angular distribution of the ejected nucleons is given by

$$d\sigma/d\Omega = A_0[1+a_2P_2(\cos\theta)]. \qquad (4.6)$$

If the giant resonance were due to a single $(d_{5/2}p_{3/2}^{-1})$ 1^- configuration, then we would have $a_2=-0.4$. The amplitudes taken from the bound-state $1p$–$1h$ calculations would yield $a_2\approx-0.6$. This is the value to which the experimental data from the (γ, p_0) reaction decrease between 19.2 MeV, where $a_2\approx0$, and 22.4 MeV [see Fig. 18(a)]. Between 22.4 MeV and 29 MeV the experimental a_2 values remain in the range between -0.5 and -0.6, except in the vicinity of the 25-MeV peak where a_2 increases to -0.4. Within a $1p$–$1h$ approximation, this would have to be explained by a relative enhancement of the $(d_{3/2}p_{3/2}^{-1})$ 1^- contribution (Frederick and Sherik, 1968). For a pure $d_{3/2}p_{3/2}^{-1}$ configuration, one obtains $a_2=+0.4$. Actually the interference terms of this configuration in the general expression for a_2 are relatively small. It is the incoherent contribution which counts.

The energy behavior of the coefficient a_3 [omitted in Eq. (4.6)] indicates that $E2$ transitions occur throughout the region considered in Fig. 18(a), but contribute only about one percent (Frederick and Sherik, 1968). In principle $M1$ excitations could also occur. Restricting ourselves to the $p_{1/2}p_{3/2}^{-1}$ configuration, $M1$ transition strength is expected only at about 16 MeV (Vinh-Mau and Brown, 1962). Experimentally a sharp 1^+ state is observed at 15.1 MeV. Thus it seems most reasonable to presume that the asymmetry ($a_1\approx+0.2$, $a_3\approx-0.2$) observed in the experimental angular distributions is due to $E1$–$E2$ interference.

The result of the $1p$–$1h$ continuum calculation for the a_2 values in the (γ, p_0) reaction is represented in Fig. 18(b). In a fashion similar to the $(\gamma, n)/(\gamma, p)$ ratio, the angular distribution shows a behavior which is qualitatively different from that of the experimental curve in that it has clear trends with changing energy;

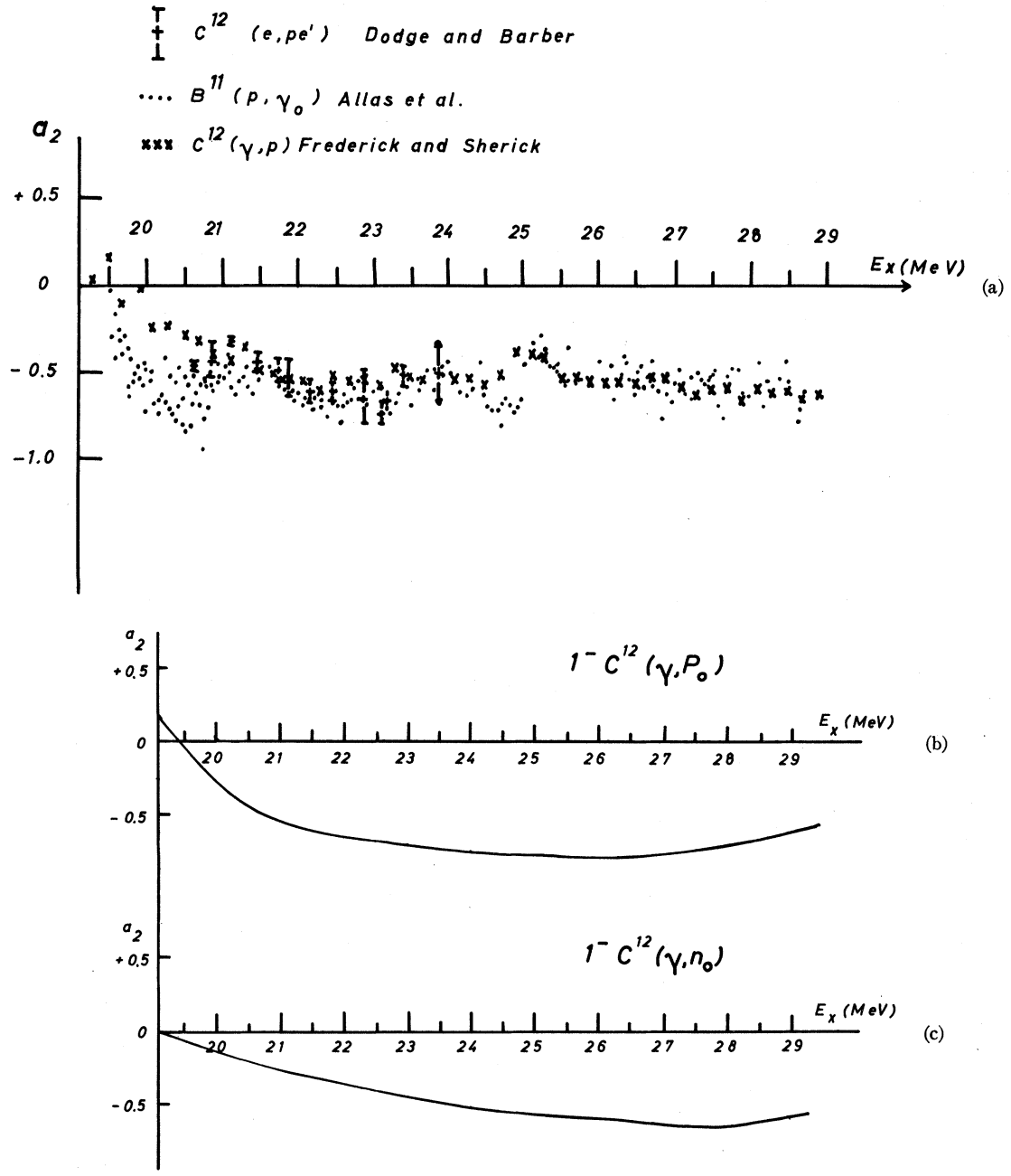

FIG. 18. (a) Comparison of different experimental results (Dodge and Barber, 1962; Allas, *et al.*, 1964; Frederick and Sherick, 1968) for the a_2 coefficients of the angular distributions of photoprotons from ^{12}C. (b) The corresponding theoretical a_2 coefficients assuming pure $E1$ transitions from the calculations of Mshelia (1971) including the $s_{1/2}^{-1}p_{1/2}$ configurations. (c) The analogous theoretical coefficents for the photoneutron process.

a_2 changes by a factor $\sim$2 between 22 and 29 MeV. In the same way, this discrepancy must be taken seriously since the relative energy independence of a_2 even over regions where the absorption cross section shows appreciable structure seems to be characteristic for light nuclei (Allas, *et al.*, 1964). This is not reproduced by the calculations.

E. Reaction Cross Section of ^{12}C

We turn now to the nucleon–nucleus reactions. Since ^{11}C is radioactive, only the proton induced reactions have been studied experimentally. Furthermore, we restrict ourselves to the charge-exchange reactions ^{11}B$(p, n_0)^{11}$C, since the Rutherford contribution to the

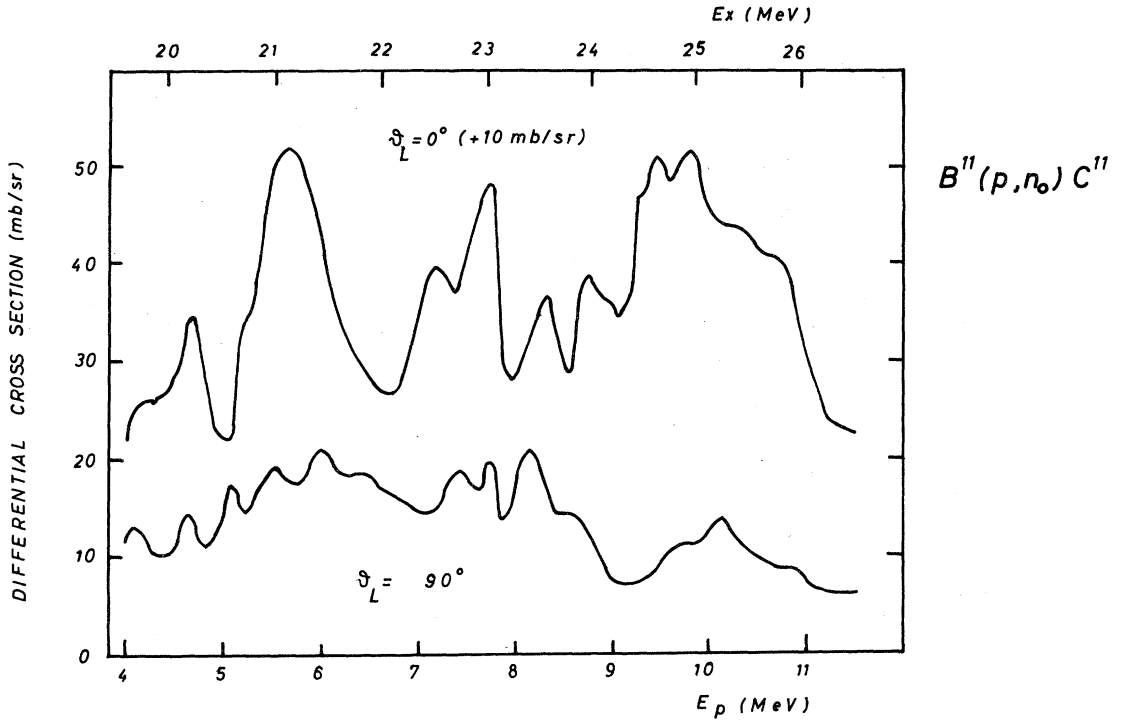

FIG. 19. Measured differential cross sections as a function of proton energy for the ^{11}B (p, n) ^{11}C reaction with ^{11}C formed in its ground state (Overley and Borches, 1965). The 0° curve is displaced from its origin by 10 mb/sr. The upper scale indicates the excitation energy in ^{12}C.

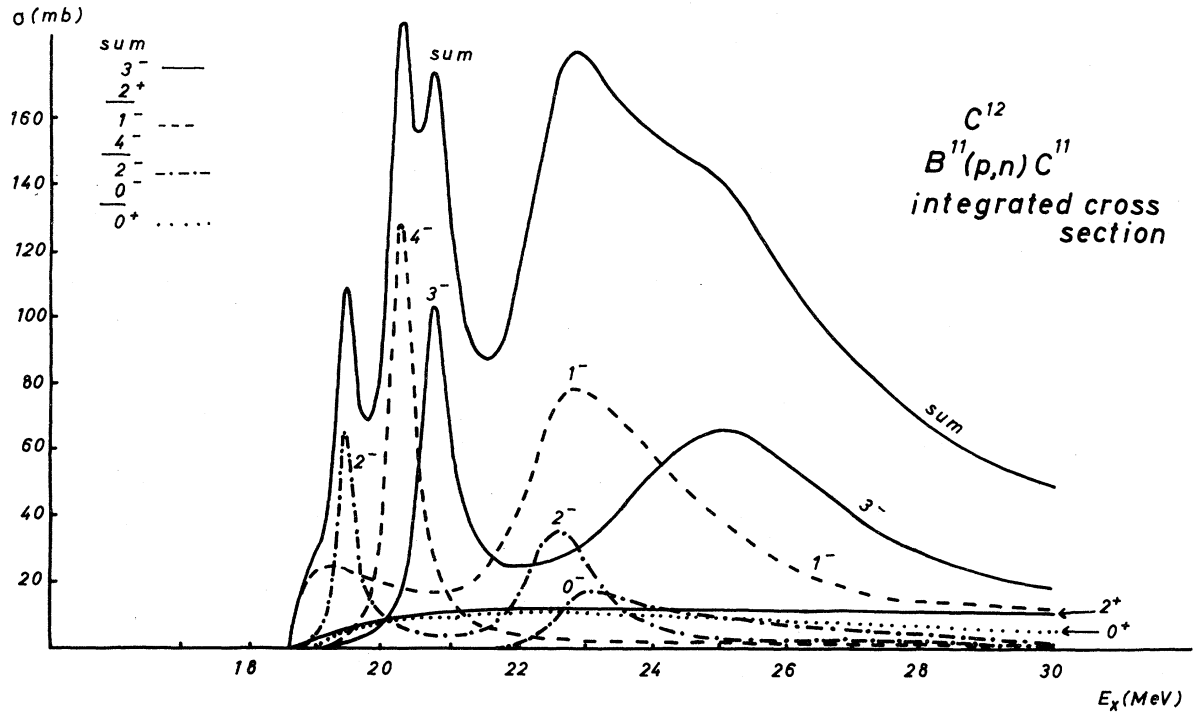

FIG. 20. Theoretical integrated-over-angle ^{11}B (p, n) ^{11}C cross sections corresponding to the multipoles 0^- 1^- 2^- 3^- 4^- 0^+ 1^+ 2^+ and their sum; the 1^+ cross section is too small to be seen in the scale used.

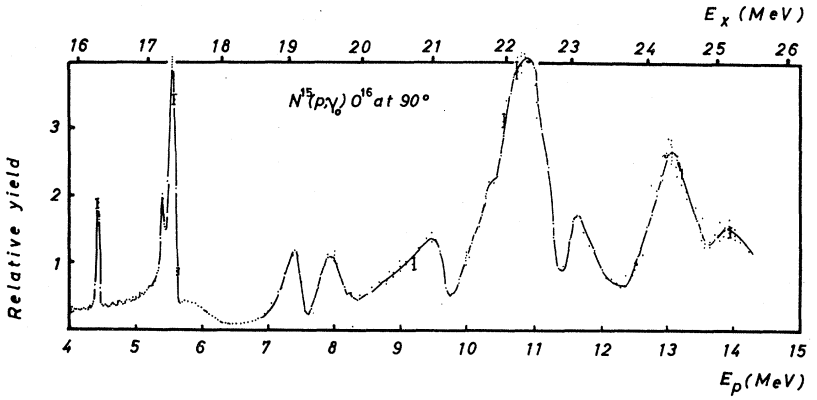

FIG. 21. The experimental excitation for the $N^{15}(p, \gamma_0)$ O^{16} reaction at 90° (from Tanner, *et al.*, 1964).

scattering cross section is included in the calculation of the S-matrices and thus a very large number of $S^{J\pi}$-matrices would be necessary for the description of the Rutherford scattering.

Overley and Borches (1965) performed time-of-flight experiments for the (p, n_0) reaction which cover the energy range 19.6 MeV$\leq E_x \leq$26.5 MeV, i.e., they start 0.9 MeV above the neutron threshold. The experimental excitation function is characterized by peaks with roughly equal widths and fairly uniform spacings. The positions of the peaks correlate with the structure in the $^{11}B(p, \gamma)^{12}C$ reaction and with some of the (γ, nucleon) structure. However, there occur 14 resonances in the (p, n_0) experiment between 19.6 and 26.5 MeV, and their widths are in general only about 200 keV. Thus they cannot be associated with the $1p$–$1h$ states, and the result of the continuum calculation essentially can account for only the background underlying the observed structure.

Moreover, no convergence is found in the theoretical result for negative parities up to $J=4$. This indicates that fairly large (probably up $\sim$7–8) nuclear spins contribute to that background. Indeed, the resonance at $E_x=21.49$ MeV (Overley and Borches, 1965) seems to result from $J>4$, which confirms the statement on the convergence. The J values of the numerous experimental peaks could not be identified for any of these levels.

TABLE VI. Levels (E) and widths (Γ) in the range 16 MeV$\leq E_x \leq$30 MeV from the $1p$–$1h$ continuum calculation.

	$T=0$		$T=1$	
J^π	E (MeV)	Γ (MeV)	(MeV)	Γ (MeV)
0^-	23.8[a]	$\simeq$3	$\simeq$24.3[a]	$\simeq$3
1^-	...		17.8	0.9
	...		22.6	2.1
	19.2[a]	$\simeq$2	24.5	$\simeq$4
2^-	16.6	0.3	18.2	0.3
	17.8	0.2	19.4	0.4
	22.6[a]	1.2	23.0	$\simeq$3
3^-	...		18.8	0.25
	20.7	0.8	24.7	$\simeq$4
4^-	...		20.3[a]	0.4
2^+	...		17.2	0.3

[a] From the ^{11}B (p, n_0) reaction.

In Fig. 19 we show the differential cross sections for 0° and 90° (laboratory angle) of the $^{11}B(p, n_0)$ experiment of Overley and Borches (1965). Contributions from non-ground state neutrons should only be important above 21.5 MeV.

The computed integrated over angle cross section is shown in Fig. 20. Both the contributions of the different angular momenta and their sum are given. The 1^+ cross section is too small to be seen in this scale. Clearly, a detailed comparison with the experimental cross section is not meaningful. Nevertheless, these various theoretical cross sections are useful in the respect that they supply us with information on levels which do not show up in the photoabsorption or the (e, e') reactions. In the 0^- case, the distorted Breit–Wigner shape seems to indicate two overlapping resonances centered roughly at 23.8 and 24.3 MeV. One would expect the lower one to be $T=0$ and the upper one to be $T=1$. The over-all width is 3.8 MeV.

For $J^\pi=1^-$, a $T=0$ level occurs at 19.2 MeV. Its width is about 2 MeV. The peak associated with the main giant resonance is shifted upward by 300 keV and broadened by 1 MeV.

In the 2^- case, there occurs a resonance at 22.6 MeV whose width is only 1.2 MeV. It can hardly be identified with the broad $T=1$ resonance at 23 MeV occurring in bound-state calculations. Therefore we infer that it results from the missing $T=0$ state.

For $J^\pi=3^-$, no new level occurs. However, the 24.7 MeV $T=1$ state is shifted upward by 0.5 MeV and is slightly broadened.

In the 4^- case, one observes just one narrow resonance ($\Gamma=0.4$ MeV) at 20.3 MeV, which is due to the bound $d_{5/2}p_{3/2}^{-1}$ $T=1$ state.

For positive parity ($J^\pi=0^+$, 1^+, 2^+), only a smooth direct reaction structure arises.

Summarizing our results for the (p, n) process we state that the $1p$–$1h$ calculation yields only two resonances in the 19.6–26.5 MeV range whose widths are

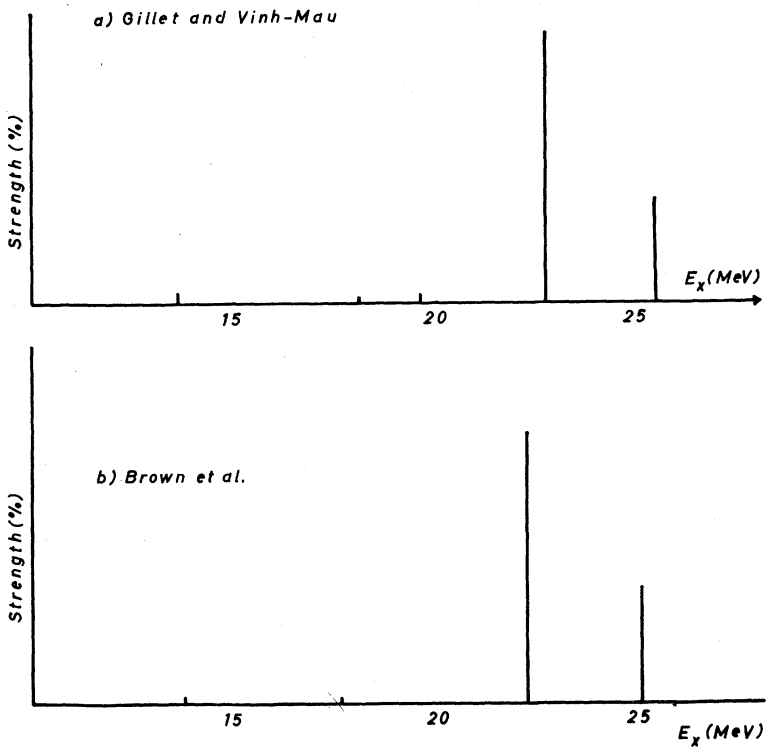

FIG. 22. Theoretical distribution of the dipole oscillator strengths in a bound state $1p$–$1h$ calculation (Brown, *et al.*, 1964; Gillet and Vinh-Mau, 1964) for ^{16}O.

less than 1 MeV. These are the 3^- state at 20.7 MeV, and the 4^- resonance at 20.3 MeV. Thus this $1p$–$1h$ continuum calculation can certainly not explain the full experimental structure (Fig. 19).

We collect the results of the $1p$–$1h$ continuum calculation for the level positions and the single-particle widths in Table VI.

F. The Giant Dipole Resonance in ^{16}O, Experiment and Bound-State Calculations

Some of the most important thresholds in ^{16}O are:

(i) single nucleon thresholds: 12.21 MeV ($p_{1/2}^{-1}$ proton), 15.67 MeV ($p_{1/2}^{-1}$ neutron), 18.35 MeV ($p_{3/2}^{-1}$ proton), 21.81 MeV ($p_{3/2}^{-1}$ neutron);

(ii) thresholds for composite particles: 7.16 MeV (α particle, $^{12}C_{g.s.}$), 20.74 (deuteron $^{14}N_{g.s.}$) 22.79 MeV (^{3}He, $^{13}C_{g.s.}$);

(iii) two-particle threshold: i.e., beginning of the double continuum: 22.95 MeV (p, n; $^{14}N_{g.s.}$).

A perusal of this list shows that a $1p$–$1h$ treatment is clearly very far removed from reality. On the other hand, the ground state of ^{16}O is presumably better represented by a simple shell model than is that of any other nucleus, except the $1s$ shell nuclei, and, perhaps, in a certain sense, ^{208}Pb. One therefore should view the $1p$–$1h$ calculation as a source of information concerning the deficiencies of the $1p$–$1h$ model, and, perhaps, look at agreements with experiment with a certain surprise.

A very large amount of experimental information on ^{16}O has been accumulated. We shall give only a cursory review of it here.

Figure 21 shows the measured excitation function of Tanner, *et al.* (1964) for the ^{15}N(p, γ_0) reaction at 90°. This cross section is well established with 200 keV resolution and, taking this into consideration, the agreement with the high-resolution (γ, p_0) results of Thompson and Baglin (1969) is perfect. Their net resolution is about 50 keV.

Wu, Firk, and Phillips (1968) performed time-of-flight (γ, n_0) measurements at 90° and compared their result with a combination of the (p, γ_0) data of Tanner, *et al.* (1964) and of the (γ, p) data of Morrison, *et al.* (1965). In contrast to the situation in ^{12}C, the agreement of (γ, p_0) and (γ, n_0) is excellent, except for the limited energy range between 19 and 21 MeV. Therefore Wu, *et al.* (1968) and Hayward 1964 concluded that in ^{16}O the major dipole states have a high degree of isospin purity. As is to be expected, more fine structure appears in the cross sections of ^{16}O than in those of ^{12}C. One observes a triple peak on top of the 22-MeV resonance (Morrison, *et al.*, 1965; Baglin, 1967; Black, *et al.*, 1967; Baglin and Thompson, 1969). The 23-MeV peak shows duality. In this case the components have a width of about 200 keV. Some of the fine structure peaks have a width of only 40 keV or less. This seems to indicate the influence of highly complex configurations. It is questionable whether ^{16}O already has a sufficient

level density at that energy, in order for this observed structure to be classified as statistical.

The a_3 coefficients turn out to be in general different from zero (Earle and Tanner, 1967; Baglin and Thompson, 1969) in the energy range between 20 and 25 MeV. Thus there must be a sizable contribution of $E2$ excitations throughout this interval. From the $(1p$–$1h)$ calculations of the even parity states in ^{16}O by Spicer and Eisenberg (1965) it follows that there are about twelve 2^+-levels per MeV near the 22 MeV excitation. This could account for some of the observed structure. Finally, we present the results obtained by Caldwell, *et al.* (1967) concerning the photon cross sections leading to the $p_{3/2}$ hole states in the daughter nucleus; i.e., to the state at 6.18 MeV in ^{15}O and to that at 6.33 MeV in ^{15}N (Fig. 24).

The experimental (γ, p_3) cross section shows no pronounced structure at 19.5 MeV, but there is again the not completely understood resonance at 21 MeV as in Fig. 21. Between 22 and 24.5 MeV, the experimental (γ, p_3) and (γ, p_0) results show similar structure, except for the fact that the 23-MeV peak has grown considerably in the (γ, p_3) case.

Since the inelastic neutron threshold lies in the center of the main dipole resonance there is little to be said about the (γ, n_3) cross section.

The structure seen in the less resolved result of Fig. 21 is richer than one would expect from the $1p$–$1h$ calculations. Such calculations predict the existence of two main peaks at 22.3 MeV and at 24.3 MeV (Fig. 22). The first state is predicted to be mainly $(d_{5/2}p_{3/2}^{-1})$ and should carry about two-thirds of the total dipole strength and the second state should be mainly $(d_{3/2}p_{3/2}^{-1})$ and carry about 1/3 of the dipole strength. Indeed, Earle and Tanner (1967) confirmed from

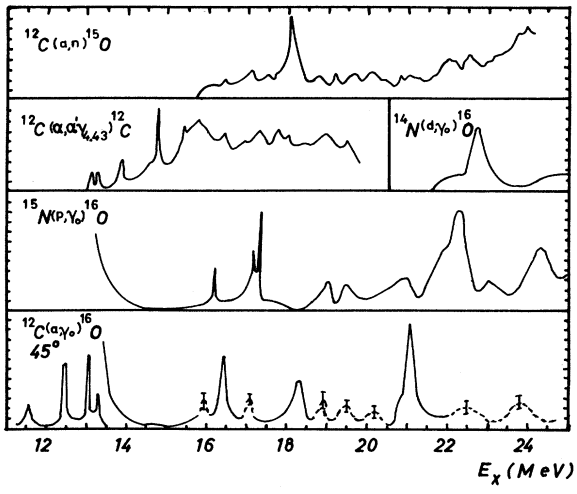

FIG. 23. Comparison of results for ^{15}N (p, γ_0) ^{16}O (Tanner, *et al.*, 1964). ^{12}C (α, γ_0) ^{16}O (Larson and Spear, 1964; Suffert and Feldman, 1967). ^{14}N (d, γ_0) ^{16}O (Suffert, 1965). ^{12}C $(\alpha, \alpha'\gamma_{4.43})$ ^{12}C (Mitchell, *et al.*, 1964), and ^{12}C (α, n) ^{15}O (Suffert and Feldman, 1967). [From Suffert and Feldman (1967)].

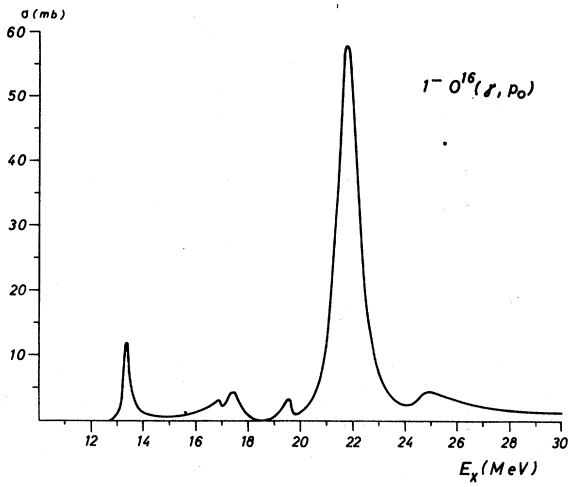

FIG. 24. Theoretical integrated-over-angle cross section obtained in the $1p$–$1h$ continuum calculation for the ^{16}O photoproton process leading to the ground state of ^{15}N.

angular distributions of the photoprotons that in accordance with the shell-model predictions the protons of both levels are emitted predominantly as d waves. In addition, the $1p$–$1h$ shell-model calculation yields $T=1$ levels at about 14 MeV, 18 MeV, and 20 MeV, which should be predominantly $(s_{1/2}p_{1/2}^{-1})$, $(d_{3/2}p_{1/2}^{-1})$ and $(s_{1/2}p_{3/2}^{-1})$, respectively. From its angular distribution, the first state can be identified with the experimental level at 13.1 MeV, and the second state can be identified with the broad resonance at 17 MeV ($\Gamma=1.5$ MeV). The 19-MeV $T=1$ dipole state cannot be uniquely identified (Spicer, 1966) with one of the experimental peaks in this region. Here $E2$ and $M1$ excitations seem to play an important role as is concluded from (e, e') experiments (Bishop and Isabelle, 1962; Barber, *et al.*, 1963). The level at 19.1 MeV is 2^+ (cf. also Earle and Tanner, 1967) and the level at 19.5 MeV is probably 1^+.

There is no certain assignment for the asymmetric peak at 21 MeV. From the rapid variation of the a_2 coefficient, Greiner (1963) concluded that this peak is not due to one simple state.

Since the $1p$–$1h$ model is clearly inadequate, several attempts have been made to enlarge the considered function space, i.e., to include $2p$–$2h$ configurations. Since even in ^{16}O there exists an unmanageably large number of such states, a certain selection is unavoidable. Recently the model of coupling of surface vibrations to the giant resonance has been used as a guide. One of the earliest calculations of this kind for ^{16}O was performed by Boeker (1966). As a microscopic model for the surface vibrations he used $1p$–$1h$ states which in LS coupling have $T=0$ and $S=0$, and adjusted the corresponding excitation energies to mimic the core polarization effects; i.e., the effects of many-particle–many-hole excitations. Other attempts (Boeker, *et al.*,

TABLE VII. Single-particle energies and well parameters in ^{16}O.

State	Protons			Neutrons		
	ϵ_b (MeV)	V_c (MeV)	V_{so} (MeV)	ϵ_b (MeV)	V_c (MeV)	V_{so} (MeV)
$1d_{3/2}$	4.50	54.36	5.27	0.94	54.94	5.27
$2s_{1/2}$	−0.10	55.91	...	−3.27	56.82	...
$1d_{5/2}$	−0.60	54.36	5.27	−4.14	54.94	5.27
$1p_{1/2}$	−12.11	57.95	9.89	−15.65	57.39	9.64
$1p_{3/2}$	−18.44	57.95	9.89	−21.81	57.39	9.64

1964; Seaborn, 1969) have used a phenomenological collective model for the surface vibrations, which were allowed to interact with the $1p$–$1h$ states. The spectrum obtained in this way is richer than the $1p$–$1h$ spectrum, and the collective treatment of Seaborn seems to be better correlated with the experimental structure than Boeker's microscopic treatment. A recent attempt at an explanation of the ^{16}O intermediate structure has been made by Wang and Shakin (1971) involving the coupling of $3p$–$3h$ configurations to the $1p$–$1h$ doorway states.

A fruitful approach to the problem of collective intermediate structure is to look at various experiments such as $^{14}N(d, \gamma_0)$, $^{12}C(\alpha, \gamma_0)$ (see Fig. 23), or $^{16}O(\gamma, \alpha)$, $^{16}O(\gamma, ^3He)$, etc. and try to detect a connection with the structure in the ^{16}O photoabsorption cross section. In this way, one can try to guess whether any peak in the absorption cross section is due to interference of $1p$–$1h$ configurations with a certain cluster state (or with more particle–more-hole states).

An experiment of this kind was performed by Suffert and Feldman (1967). They found a peak in the $^{14}N(d, \gamma_0)$ reaction (see Fig. 21). An explanation of this effect was given by Gillet, *et al.* (1967) which we have discussed in Sec. III.I. The $(\gamma, ^3He)$ process shows resonances at 24.1 and 25.1 MeV, where the latter peak should correspond to a ^3He cluster state. Thus it seems plausible that the 23-MeV peak is due to a $(2p$–$2h)$ state.

With respect to the structure at 21.7 MeV indicated by the asymmetry in the (p, γ_0) excitation curve, it should be noticed that the $^{12}C(\alpha, \gamma)^{16}O$ reaction (Suffert and Feldman, 1967) (Fig. 23) has a strong and narrow 1^- resonance at 21.05 MeV. Therefore it seems suggestive to assume that quartet states (Danos and Gillet, 1971) are responsible for the structure at 21.7 MeV. The $^{16}O(\gamma, \alpha)$ measurements indicate that quartet structure may also be evident near 25.3 MeV.

Another type of information comes from experiments which measure the reactions leading to other than the ground state of the daughter nucleus. Of particular interest here is an experiment performed by Caldwell, *et al.* (1967; Caldwell, 1967) with monoenergetic photons produced by annihilation in flight of

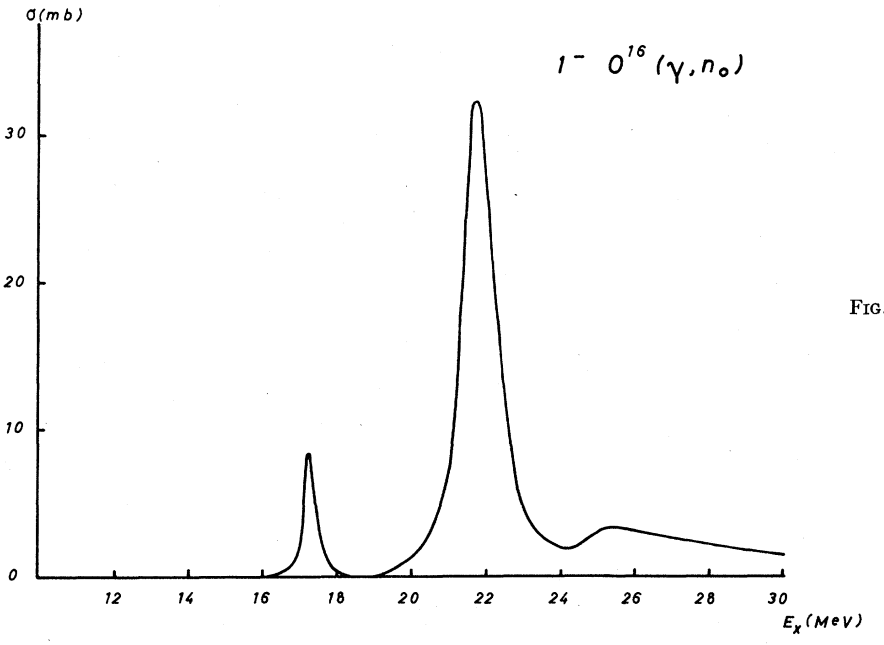

FIG. 25. The same as in Fig. 24, but for the photoneutron process.

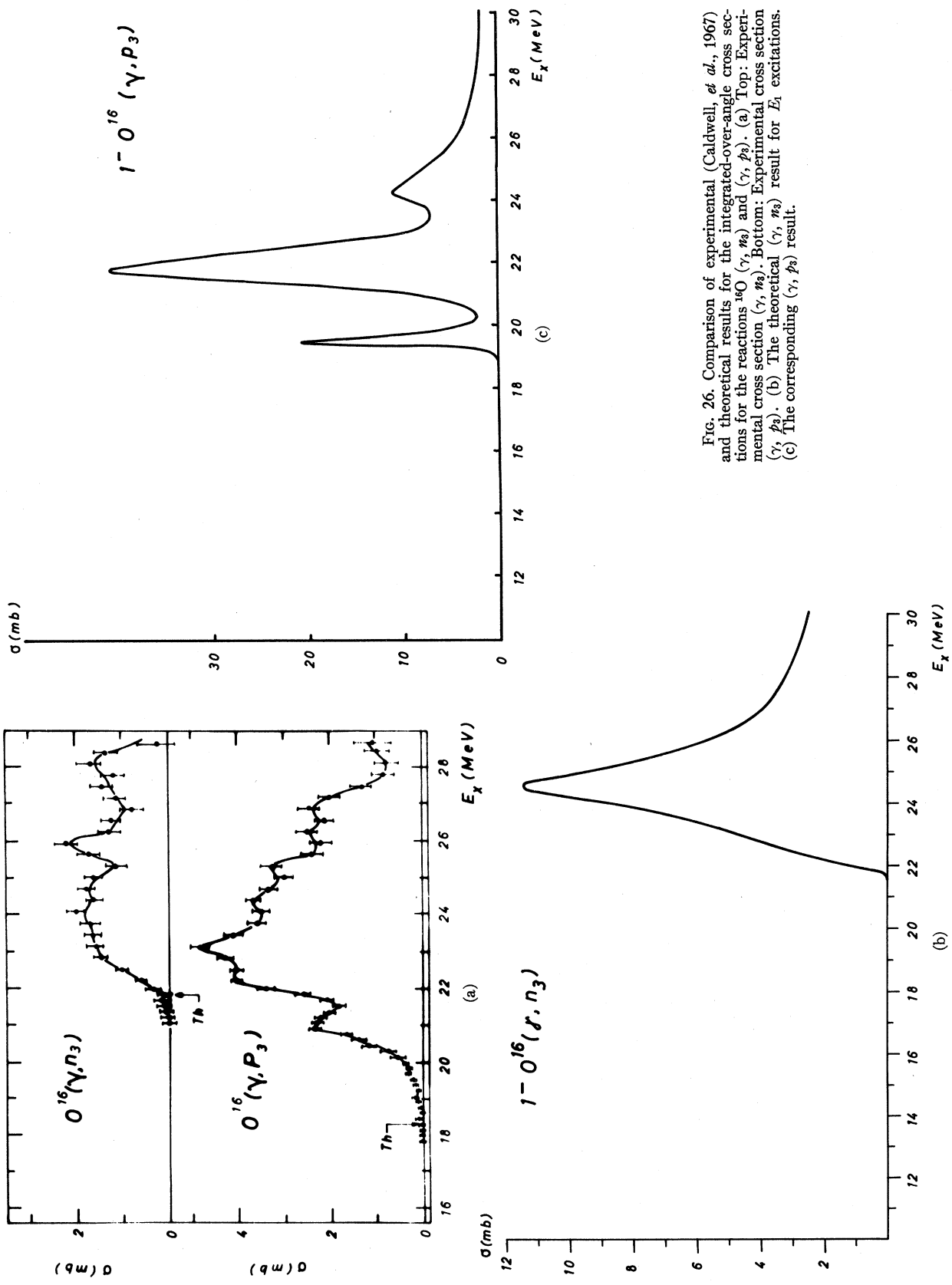

FIG. 26. Comparison of experimental (Caldwell, *et al.*, 1967) and theoretical results for the integrated-over-angle cross sections for the reactions ^{16}O (γ, n_3) and (γ, p_3). (a) Top: Experimental cross section (γ, n_3). Bottom: Experimental cross section (γ, p_3). (b) The theoretical (γ, n_3) result for E_1 excitations. (c) The corresponding (γ, p_3) result.

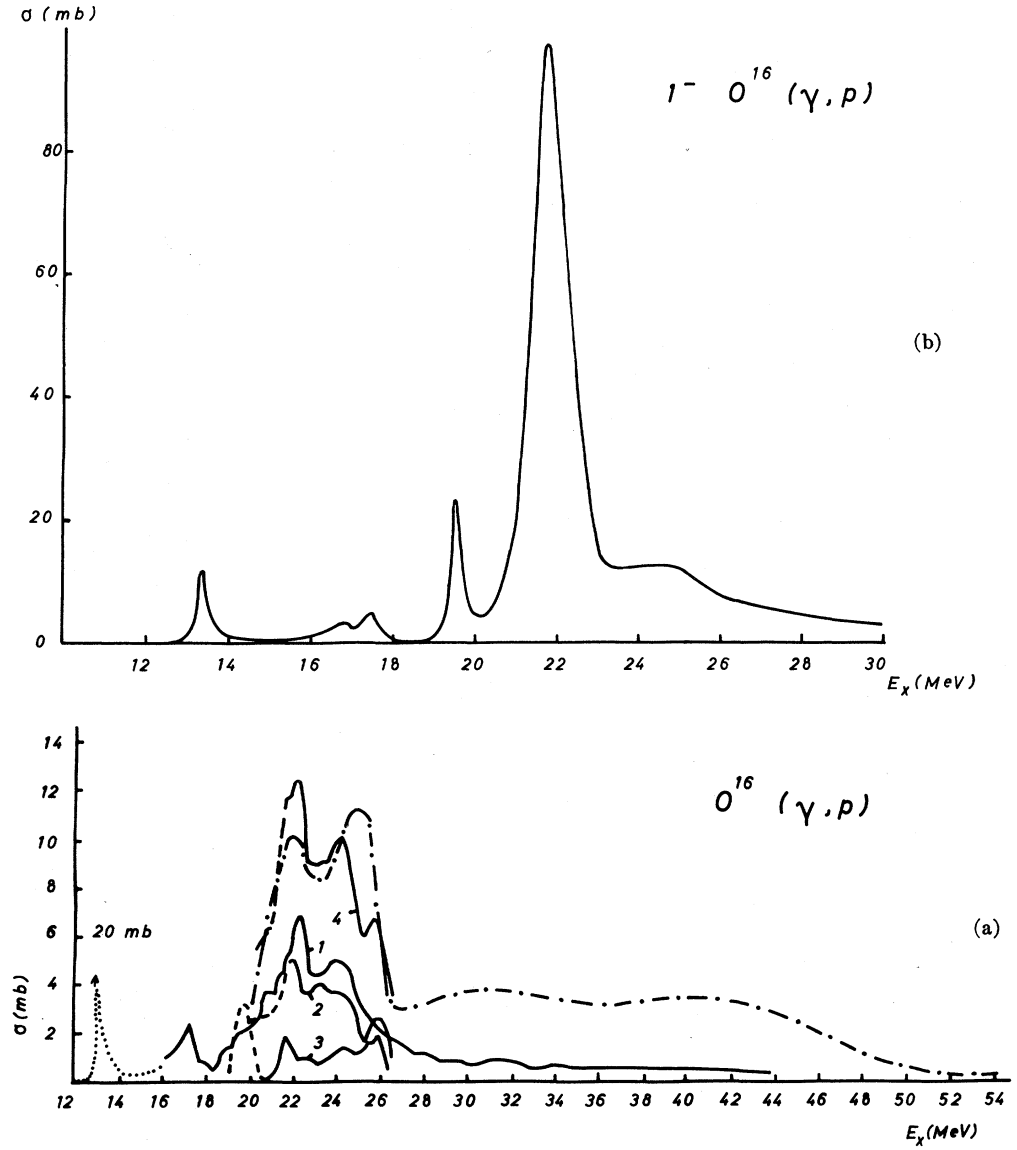

FIG. 27. Experimental and theoretical total photoproton cross section of ^{16}O. (a) Experiment (Denisovi *et al.*, 1968); 1, cross section (γ, p_0); 2, cross section (γ, p_3); 3, cross section $(\gamma, p_{1,2})$ for formation of ^{15}N in the first and second excited states; 4, the sum of cross sections 1+2=3; the dot-and-dash curve gives the cross section σ_p for emission of protons with energy 3.4–30 MeV. (b) Result of the $1p$–$1h$ continuum calculation.

fast positrons. They observed the deexcitation γ rays from the residual nuclei and separated the $(\gamma, p\gamma')$ and $(\gamma, n\gamma')$ events. By combining the $(\gamma, n\gamma')$ relative cross section with information from earlier experiments (Caldwell, *et al.*, 1965), an absolute scale for the partial cross sections integrated up to 28.7 MeV has been obtained. The data of Finckh and Hegel (1961), Dodge Barber (1962), Tanner, *et al.* (1965) furnished information on the $^{16}O(\gamma, p_0)^{15}N$ reaction. In this way Caldwell *et al.* (1965) found that the sum of the $\frac{1}{2}^-$ (ground state) and the $\frac{3}{2}^-$ (third excited state) ^{15}O and ^{15}N final state cross sections is 78±8% of the total decay cross section integrated up to 28.7 MeV. The greatest part of the remaining 22% of the total decay strength is split between the ^{15}O and $^{15}N(\frac{1}{2}^+, \frac{5}{2}^+)$ doublet and the $(\frac{3}{2}^+)$ final states. Under this aspect the omission of the $(2p$–$2h)$ configurations which would enable transitions to the positive parity states of the mass-15 system seems not to be dangerous.

G. The Giant Dipole Resonance of ^{16}O in a Continuum $1p$–$1h$ Calculation

A large number of $(1p$–$1h)$ continuum calculations for ^{16}O have been performed (Eichler, 1964; Buck and Hill, 1967; Raynal, *et al.*, 1967; Wahsweiler *et al.*, 1968; Weiss, 1968; Saruis and Marangoni, 1969). The results

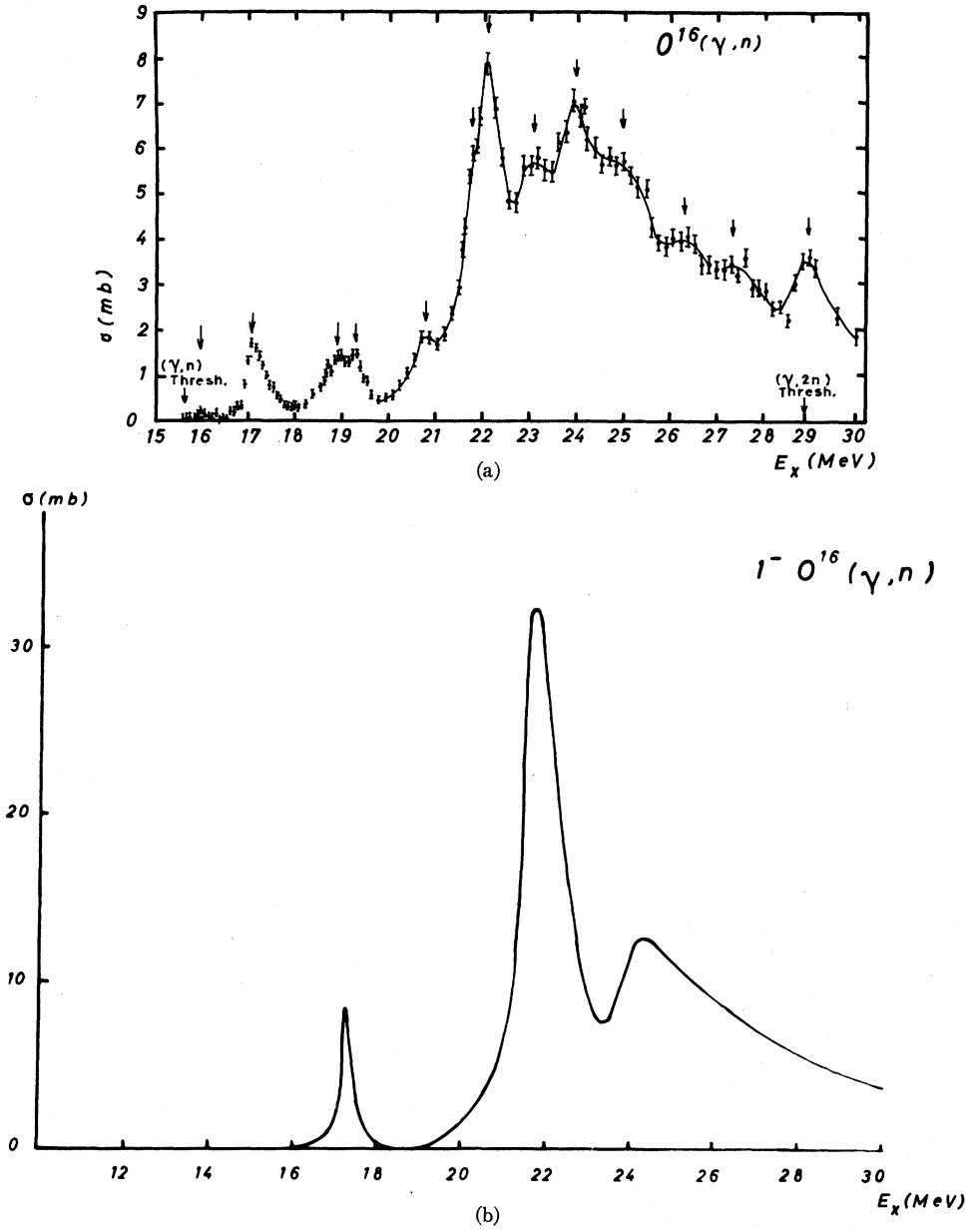

FIG. 28. Experimental and theoretical total photoneutron cross sections of ^{16}O. (a) Experiment (Caldwell, *et al.*, 1965) (b) $1p$–$1h$ continuum calculations.

of the various calculations are very similar. In the following we discuss an eigenchannel calculation (Delsanto, *et al.*, 1970) in which the same potential parameters were used as in the coupled-channel calculation of Buck and Hill (1967) (but without an imaginary part in the average nuclear potential). As usual, the following ($1p$–$1h$) neutron and proton configurations are taken into account in calculating the ^{16}O 1^- states:

$$1^-: \quad d_{5/2}p_{3/2}^{-1};\ d_{3/2}p_{3/2}^{-1};\ s_{1/2}p_{3/2}^{-1};\ d_{3/2}p_{1/2}^{-1};\ s_{1/2}p_{1/2}^{-1}.$$

The analytical form of the self-consistent potential is given by Eq. (4.1). The potential radius is relatively large (Elton, 1961), namely $R_0=3.09$ F, i.e., $R_0=1.25(15)^{1/3}$, and the diffuseness $d=0.53$ F (Buck and Hill, 1967). This value for d was obtained from an attempt to fit the position and width (90 keV) of the $d_{3/2}$ neutron resonance simultaneously with the position of the bound $1d_{5/2}$ neutron level by varying the central and spin–orbit depths and the diffuseness parameter. For the proton levels the same spin–orbit force was used as for the d-shell neutron states. Then the remaining d- and s-wave central potentials were deter-

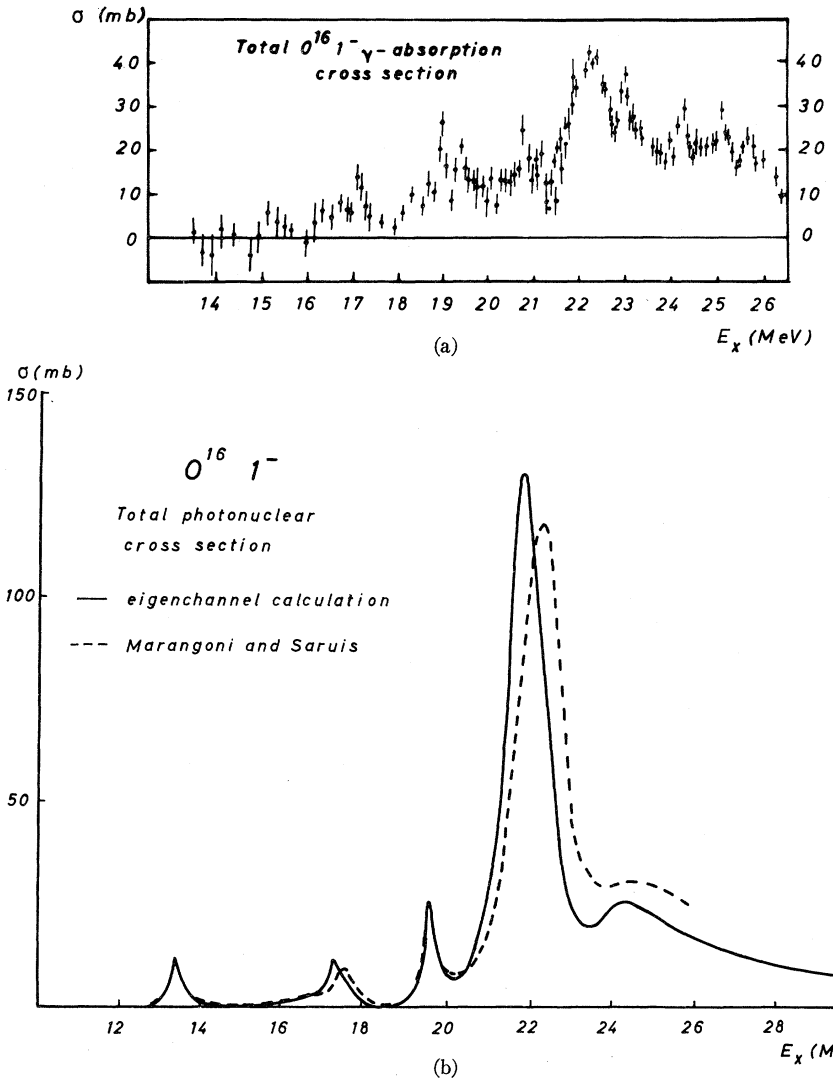

FIG. 29. Comparison of experimental and theoretical total photodisintegration cross sections of ^{16}O. (a) Measured data of Burgov, *et al.* (1963). (b) 1^- result of the $1p$-$1h$ continuum calculation.

mined. For the p shell, a simultaneous fit for the central and spin–orbit potential was made separately for neutrons and protons. The various well depths and the fitted single particle energies are listed in Table VII. In the case of protons, a Coulomb potential V_{Coul} for a homogeneously charged sphere of radius R_0 was added to the expression (4.1).

The two-body force was taken to be of the form (4.2);

TABLE VIII. Comparison of the 1^- $T=1$ levels of ^{16}O with bound-state and continuum calculations.

Brown (1961)		Gillet (1964)	Continuum calc		Main	Experiment	
(MeV)	%	(MeV)	(MeV)	Γ (MeV)	configuration	(MeV)	Γ (MeV)
13.7	1	13.6	13.3	0.2	$\bar{p}_{1/2}s_{1/2}$	13.1	0.15[a]
17.6	1	18.1	17.4	0.4	$\bar{p}_{1/2}d_{3/2}$	17.0	1.5[b]
20.0	1	19.6	19.5	0.3	$\bar{p}_{3/2}s_{1/2}$	21.0, perhaps[c]	
22.2	68	22.7	21.9	1.1	$\bar{p}_{3/2}d_{5/2}$	22.3	0.8[a]
25.0	29	25.4	24.3	broad	$\bar{p}_{3/2}d_{3/2}$	24.3	0.8[a]

[a] Tanner, *et al.* (1964).
[b] Earle and Tanner (1967).
[c] Hayward (1964).

i.e., the same as that used for ^{12}C. Its exchange character differs somewhat from that used by Buck and Hill (1967). However, the same strength was used as by Buck and Hill, with $V_0 = -650$ MeV fm^3. This value is about 10% larger than the value that corresponds to (4.3) which was employed by Brown, *et al.* (1961). The result of the $1p$–$1h$ continuum calculation for the integrated-over-angle cross section of the photoproton reaction leading to the ground state of ^{15}N is presented in Fig. 24. The analogous cross section of the photoneutron reaction leading to the ground state of ^{15}O is exhibited in Fig. 25.

Comparing Fig. 24 and Fig. 21 one realizes that the general shape of the curves does not agree well. Not only are the effects of the higher order configurations missing, but there is also the overpronounciation of the 22-MeV peak relative to the 24.3-MeV peak in the continuum calculation, which is disappointing. Buck and Hill (1967) improved this ratio by introducing an energy dependent absorptive surface potential whose strength at the nuclear edge is about 1-MeV in the main giant-resonance region. This was a device for approximately taking account of the reaction channels which were not explicitly included in the $1p$–$1h$ continuum calculation. Continuum calculations including such composite particle channels are very much called for.

In Fig. 26 we present the theoretical (γ, n_3) cross section leading to the third excited state in ^{15}O, i.e. the $\frac{3}{2}^-$ level at 6.18 MeV, and the corresponding (γ, p_3)

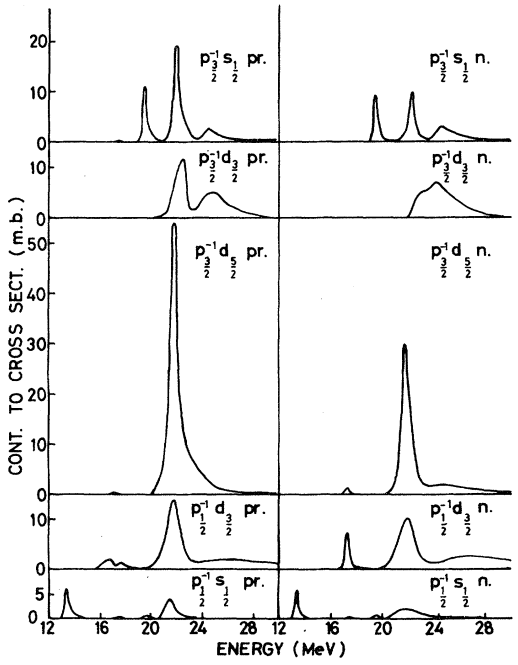

FIG. 30. Contribution of the different $1p$–$1h$ configurations to the dipole state in ^{16}O.

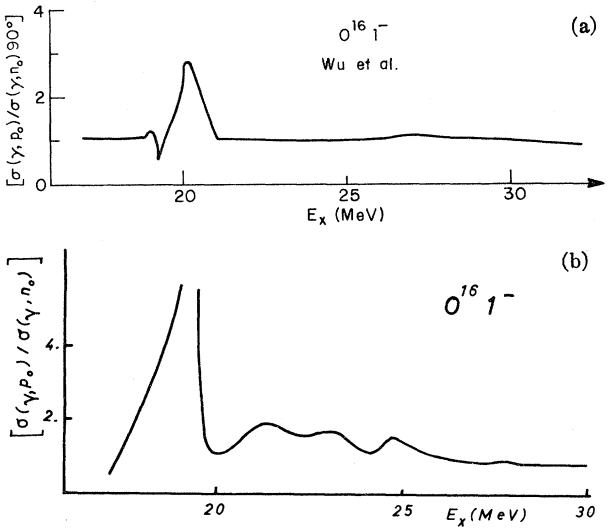

FIG. 31. (a) Ratio of the measured differential cross sections Wu, *et al.*, 1968 $\sigma(\gamma, p_0)$ and $\sigma(\gamma, n_0)$ at 90°. (b) The corresponding theoretical result from Figs. 20 and 21.

result; i.e., the $^{15}N(\frac{3}{2}^-)$ 6.33-MeV final-state cross section. The total (γ, p) and (γ, n) cross sections are shown in Figs. 27 and 28, respectively. The total photon absorption cross section is shown in Fig. 29, together with the results of the coupled channel calculation of Saruis and Marangoni (1969). We collect the information concerning the main peaks in Table VIII.

The level positions and widths of the present continuum calculation agree with the results of Saruis and Marangoni (1969), except for the positions of the peaks at 22 MeV and 24.3 MeV. These resonances are shifted upward in Saruis and Marangoni's results by about 400 keV due to the partial omission of the exclusion principle in that calculation. This effect can already be observed in Fig. 12 from the theoretical study of Raynal, *et al.* (1967). The results of Saruis and Marangoni and of Buck and Hill (1967) differ from each other practically only by the peak-height-reducing effect of the absorptive potential.

The difference between the level positions of the bound-state calculation of Brown, *et al.* (1961) and the continuum calculation (Table VIII) amounts to (0.4 ± 0.2) MeV only.

With respect to the s-wave resonance at 13.3 MeV, it should be mentioned that its position and height depend quite sensitively on the model parameters, as it is very close to the proton threshold. Its width agrees well with the experimental value. The corresponding peak in the total proton-induced reaction cross section is almost completely accounted for by the (p, α_0) process (Schardt, *et al.*, 1952; Hebbard, 1960) which indicates isospin mixing.

In the same way as for ^{12}C, the individual contributions of the different configurations to the photon absorption cross section (Fig. 30) reveal much more

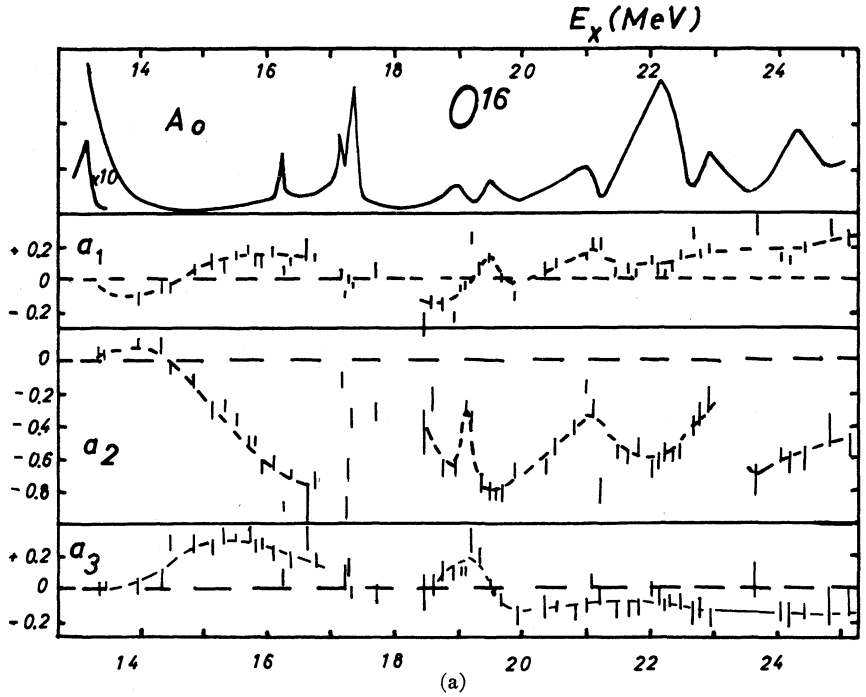

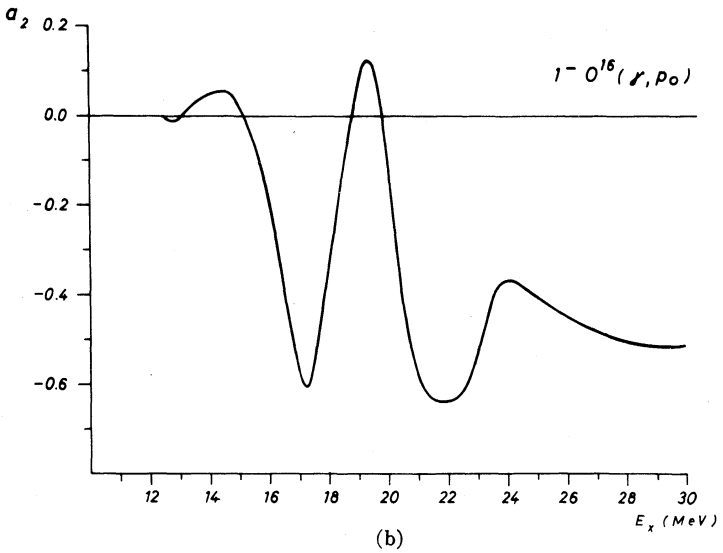

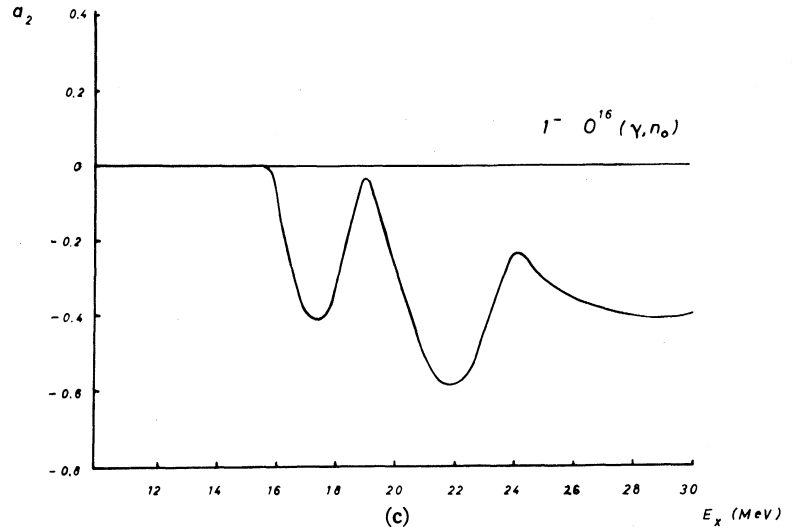

FIG. 32. (a) Experimental results (Earle and Tanner, 1967) for the total cross section A_0 of ^{15}N (p, γ_0) and the coefficients a_l from the multipole expansion of the angular distributions. The dashed durves are drawn smoothly through the experimental points. (b) The corresponding theoretical a_2 coefficients assuming pure $E1$ transitions. (c) The analogous theoretical coefficients for the photoneutron process.

structure than is evident from both the summed curves and the partial cross sections. The behavior of the inside wave function is much more complex than one notices in the asymptotic region. Perhaps the most striking result is the extreme isospin impurity above about 21 MeV. Thus, the isospin partners of the principal configuration, $d_{5/2}p_{3/2}^{-1}$, have, in addition to different behavior of the high-energy tails, very different peak heights. The threshold in the neutron channel seems to have no noticeable effect. On the other hand, the same threshold has a very pronounced effect on the $d_{3/2}p_{3/2}^{-1}$ neutron channel, and it seems also to have a strong indirect influence on the isospin partner, the proton $d_{3/2}p_{3/2}^{-1}$ channel. Similar striking differences exist in the $s_{1/2}p_{3/2}^{-1}$ configuration. A very narrow non-Lorentzian peak lies in the neutron channel at 22.4 MeV. The corresponding peak in the proton channel is much stronger and shifted down by 0.4 MeV, and has a rather more Lorentzian shape. Strong differences are also evident between the isospin partners in the $d_{3/2}p_{1/2}^{-1}$ configuration.

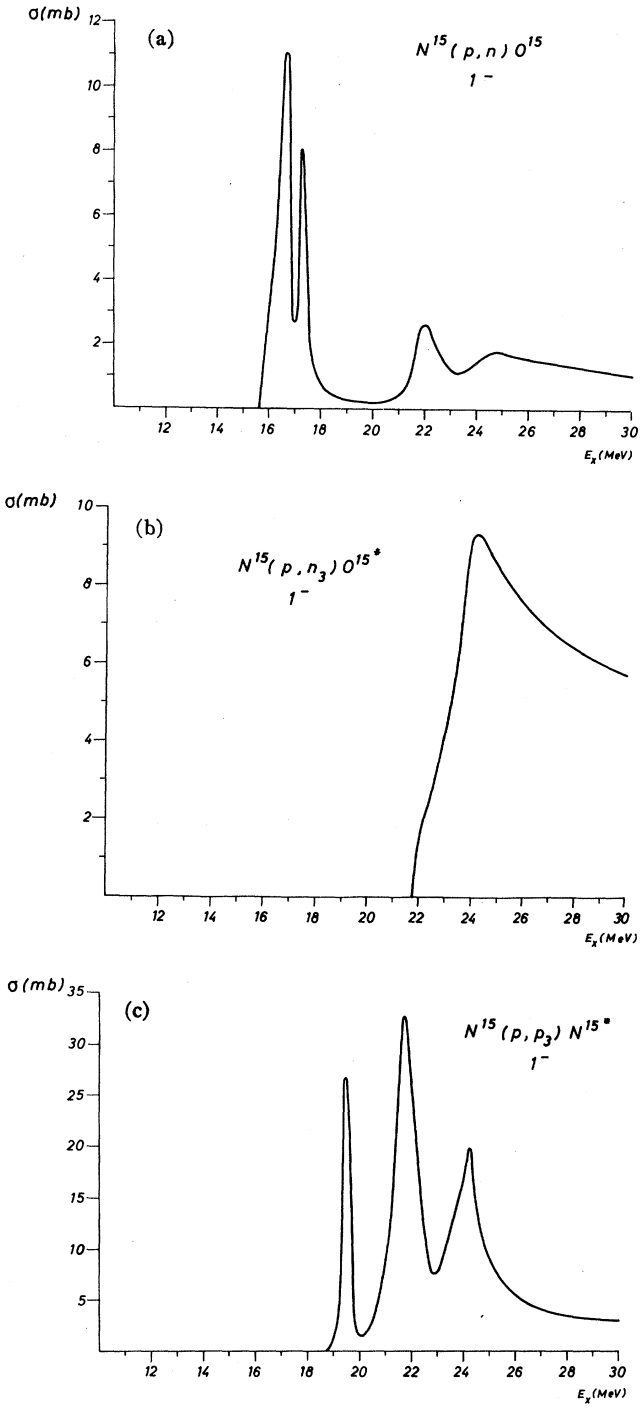

FIG. 33. Calculated 1^- contribution to (integrated-over-angle) particle reaction cross sections in ^{16}O. (a) The ^{15}N $(p, n)^{15}O$ process. (b) Contribution of the third excited state in ^{15}O to the (p, n) cross section. (c) The inelastic proton scattering process.

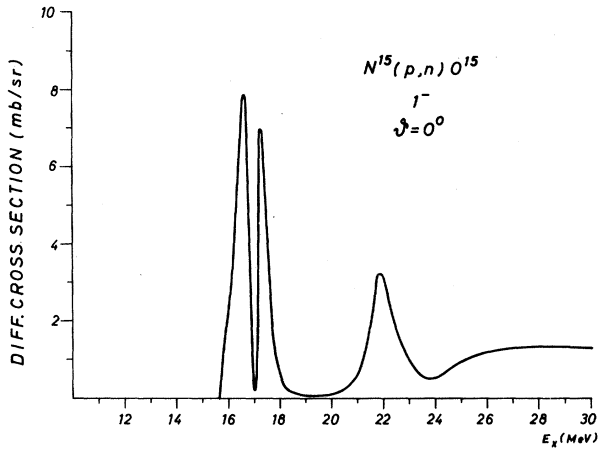

FIG. 34. Theoretical prediction for the differential 0° cross section of the ^{15}N (p, n) reaction.

At lower energies, the situation does not look as dramatic. Except for the striking difference between the partners of the $d_{3/2}p_{1/2}^{-1}$ configuration at the 17.3-MeV peak the behavior of the states is rather symmetric.

Finally, the mixing of the states is more pronounced in the continuum calculation than in the corresponding states of the bound-state calculation.

It is instructive to compare the configuration mixing curves in Fig. 30, which describe the wave function in the inside region, with the (γ, p_0), (γ, n_0) and (γ, p_3), (γ, n_3) curves of Figs. 24, 25, and 26(b, c) which are associated with the wave function at asymptotically large distances from the nucleus. For example, the ground-state transitions; i.e., (γ, p_0) and (γ, n_0), are associated with the $p_{1/2}$ hole. As one can see, the $p_{1/2}^{-1}$ configurations play only a secondary role in the inside region for the giant-resonance peak at 22 MeV, while the decay goes mainly through the ground-state channels. Nevertheless, the ratio of the proton and neutron contributions survives this transfer from one to the other channel essentially without suffering a

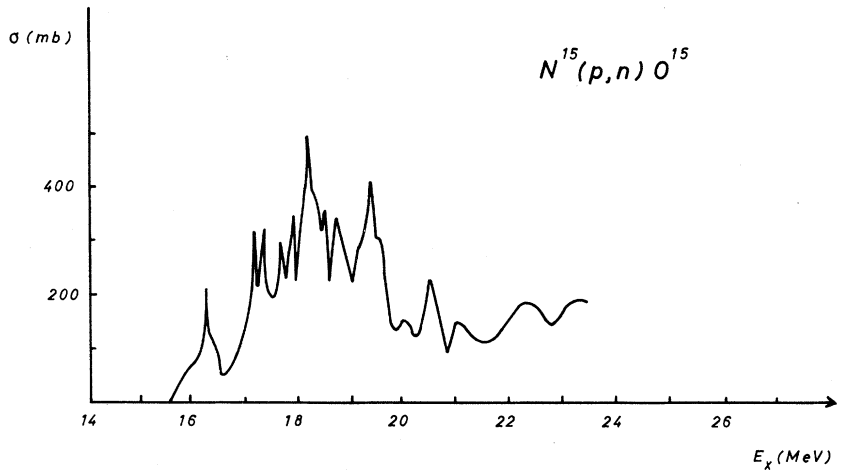

FIG. 35. The experimental integrated-over-angle (p, n) cross section of Barnett and Thomas (1964).

change. The opening of the inelastic neutron channel does not seem to have a noticeable effect on the open channels in the asymptotic region. On the other hand, there exist features which are not transferred from one configuration to another. Thus, the peak at 19.5 MeV in the $s_{1/2}p_{3/2}^{-1}$ configuration is most prominently seen in the (γ, p_3) channel, and the peak at 17.3 MeV of the $d_{3/2}p_{1/2}^{-1}$ neutron configuration shows up almost exclusively in the (γ, n_0) channel. The origin of this differing behavior clearly is rooted in the different boundary conditions for the different states, and in the continuum–continuum interaction; the mechanisms of the individual cases have, however, not been investigated in detail. The area under the γ-absorption cross section of the present continuum calculation [Fig. 29(b)] (from 12.2 MeV to 28.7 MeV) amounts to 286 MeV·mb. This value has to be compared with the experimental value of Wyckoff, *et al.* (1965) of 136±16 MeV·mb for the total photoabsorption cross section integrated to 28.7 MeV.

The reasons for this discrepancy are presumably the same as those in ^{12}C: the quasideuteron absorption process shifts some of the strength to higher energies, and the short-range correlations responsible for this process are not included in the $1p$–$1h$ model.

H. Photonucleon Branching Ratios and Angular Distributions in ^{16}O

We now discuss the branching ratio $(\gamma, p_0)/(\gamma, n_0)$, which has been studied experimentally by Wu, Firk, and Phillips (1968). Their ratio of the 90° cross sections is shown in Fig. 31(a). It is remarkably constant at a value of unity for energies above 21 MeV. Again, as in the case of ^{12}C, this value is achieved about 1 MeV above the neutron threshold, and undergoes variations only over a very limited region of the giant resonance, viz. about 19–22 MeV. This is so in spite of the pronounced structure in the absorption cross section. In contrast to this, the theoretical integrated-over-angle $\sigma(\gamma, p_0)/\sigma(\gamma, n_0)$ ratio has both more pronounced fluctuations, and a long term trend [Fig. 31(b)]. This kind of behavior one would, in fact, expect. It definitely is not understood which mechanism is responsible for the surprising features of the experimental results. Or, in different words, it is not at all evident how to improve the nuclear model so as to reproduce the experimental data.

The continuum calculations yield a second sensitive tool for investigating details of the nuclear model, namely, the photonucleon angular distributions. The (p, γ_0) measurements of Earle and Tanner (1967) showed sizable a_1 values, as well as a_3 values of comparable size about 18 MeV, suggesting that there is $E1$–$E2$ interference (rather than $E1$–$M1$ interference).

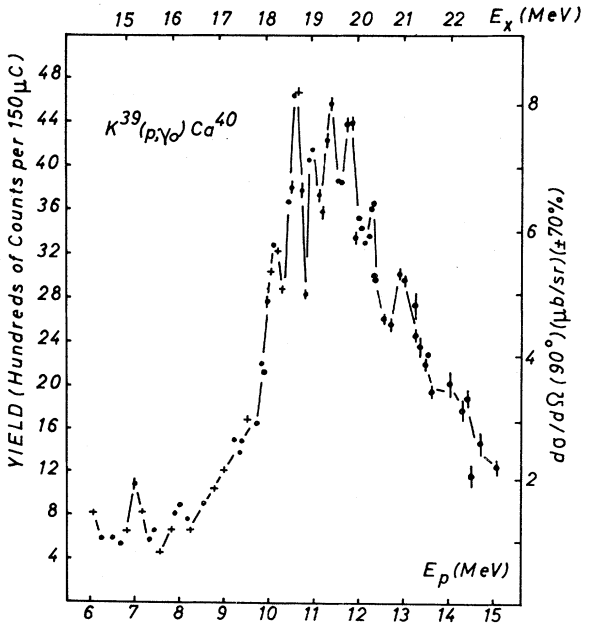

FIG. 36. Differential cross section at 90° for the ^{39}K (p, γ) ^{40}Ca reaction measured by Häfele, *et al.* (1964). The ordinate on the left gives the relative cross section, and the ordinate on the right gives the estimated absolute cross section.

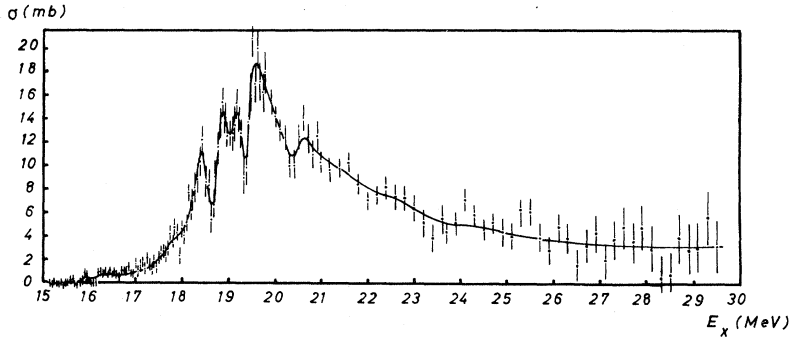

FIG. 37. Photoneutron cross section for ^{40}Ca measured by Baglin and Spicer (1964).

However, the $E2$ strength is only of the order of 1% of the $E1$ strength.

Tanner has pointed out that if one assumes 100% d-state $E1$ excitation, then the a_3/a_1 ratio will be -6 if the interfering $E2$ absorption involves p-wave nucleon emission, but only -0.4 for f-state emission. The experimental data favor the assumption of interfering 2^+ nuclear states involving f-state nucleons. Since, however, no detailed continuum calculations for the ^{16}O 2^+ states have been performed, we restrict ourselves to formula (4.6) with a_2 coefficients for pure $E1$ excitations. The effect of the $E2$ admixture on the a_2 values will be small, and therefore one finds approximate agreement with the a_2 coefficients of Buck and Hill (1967) who allowed for nonresonant direct quadrupole emission in their calculation of angular distribution At 15.25 and 19.1 MeV, Earle and Tanner observed narrow 2^+ states. Also, there exist other narrow 1^- and 1^+ states (cf. Bishop and Isabelle, 1962; Barber, *et al.*, 1963; Tanner, *et al.*, 1964b; Earle and Tanner, 1967).

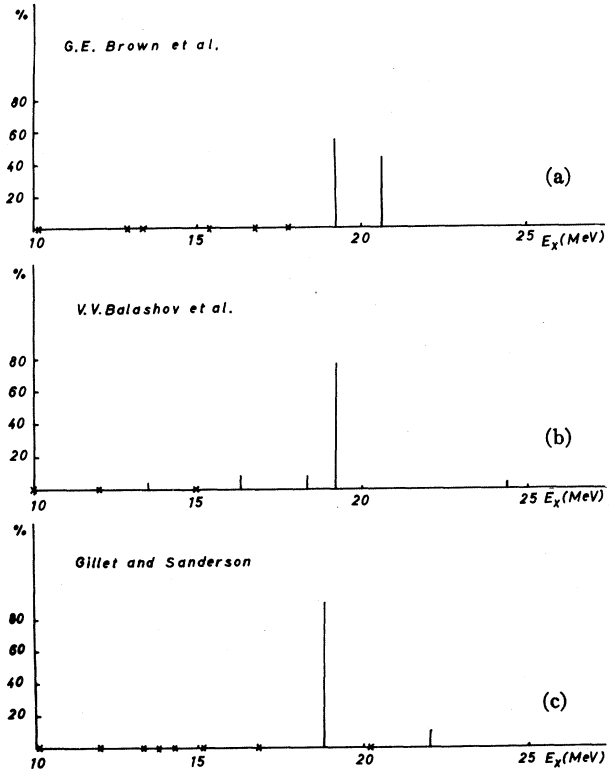

FIG. 38. Theoretical distributions of dipole oscillator strengths in ^{40}Ca from different j–j coupling $1p$–$1h$ bound state calculations: (a) Brown, *et al.* (1961), (b) Balashov, *et al.* (1961), (c) Gillet and Sanderson (1967).

The experimental a_2 values of Earle and Tanner are presented in Fig. 32(a). Figures 32(b) and 32(c) give the theoretical a_2 coefficients of the (γ, p_0) and (γ, n_0) reactions, respectively. These calculated coefficients for (γ, p_0) and (γ, n_0) look very similar. Evidently, their structure is correlated with the $(1p$–$1h)$ resonances listed in Table VIII. There is a minimum at the position of the 22-MeV giant-resonance peak, and a local maximum at 24.3 MeV. Above 20 MeV, the a_2 coefficients oscillate about -0.5; i.e., about the a_2 value for pure d-wave nucleon emission. This occurs in the theoretical as well as in the experimental results. The experimental structure, however, is more concentrated than the theoretical one.

The calculated s-wave resonance at 19.5 MeV has no counterpart in the a_2 coefficient obtained from experiment. Indeed, there is a large discrepancy between theory and experiment in the range between 16 and 20 MeV. One striking disagreement occurs at 17 MeV, where the experimental data indicate a steep positive slope. From the large negative a_2 values below 17 MeV it can, however, be concluded that the broad 17 MeV state contains predominantly d-wave configurations.

At the 13-MeV peak one again observes good agreement. Both angular distributions are almost isotropic in that region. A careful investigation, however, shows that this peak actually is not purely s wave but contains substantial d-wave contributions (Earle and Spicer, 1967). Nevertheless, the theoretical angular distributions seem to reproduce the experimental data much better than is the case for the branching ratios. The reasons for this are not clear.

I. Reaction Cross Sections of ^{16}O

The theoretical contributions of the $J^\pi = 1^-$ channels to the total ^{15}N(p, n), the ^{15}N(p, n_3) and the ^{15}N(p, p_3)

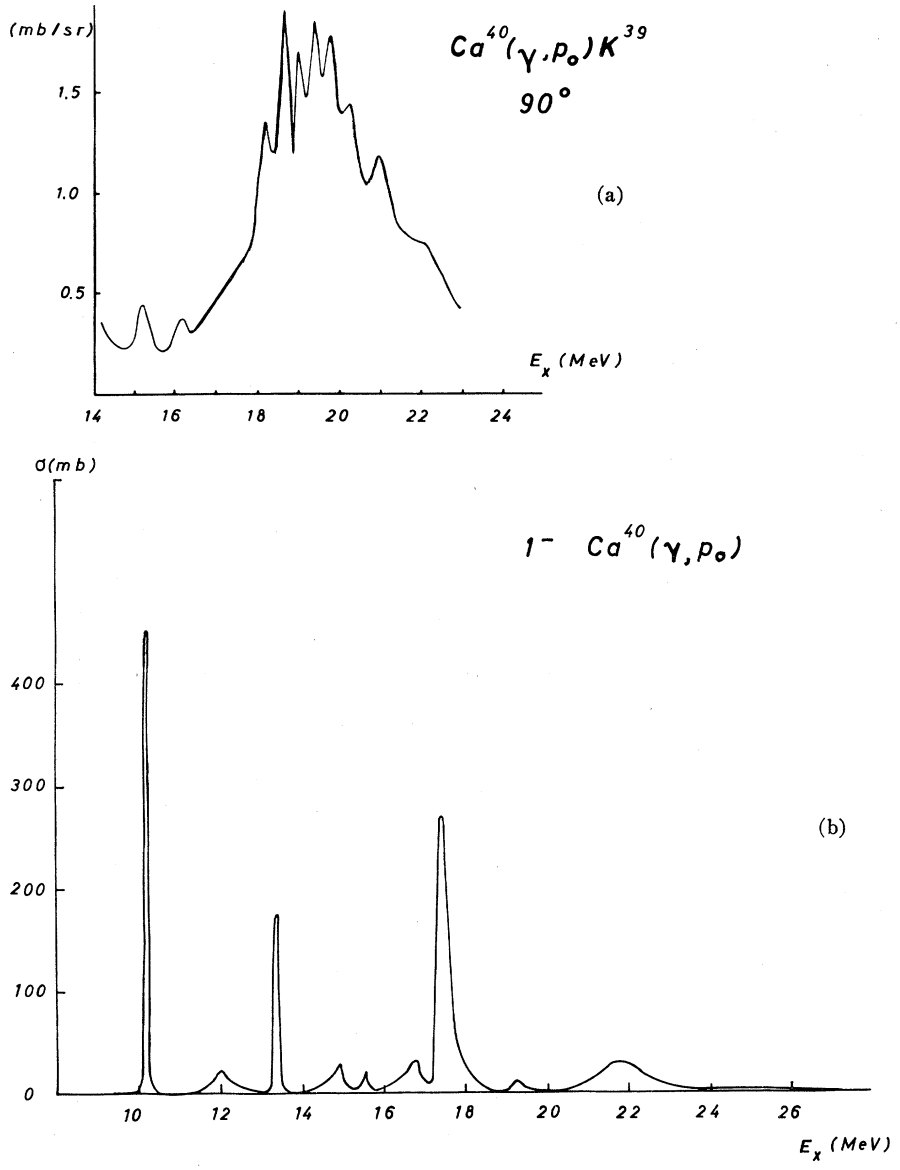

FIG. 39. Comparison of experimental and theoretical results for the ^{40}Ca photoproton process leading to the ground state of ^{39}K .(a) The experimental cross section obtained by Häfele, *et al.* (1964) by detailed balance from their data of the inverse reaction. (b) Result of the $1p$–$1h$ eigenchannel calculation.

cross sections are exhibited in Figs. 33(a), (b), (c). The total (p, n) cross section is the sum of $\sigma(p, n_0)$ and $\sigma(p, n_3)$.

There is a remarkably close correspondence between the shape of Fig. 33(b) and the theoretical (γ, n_3) cross section of Fig. 26(b), and also between Fig. 33(c) and the (γ, p_3) result of Fig. 26(c). In the (p, n_3) case only a single broad peak at 24.3 MeV appears with a very steep slope on the low-energy side. This shape does not cause any additional structure with respect to the total (p, n) cross section, but manifests itself as a smooth contribution above 24 MeV.

The inelastic proton scattering cross section $\sigma(p, p_3)$ consists of three peaks. Besides the particularly pronounced s-wave resonance at 19.5 MeV there are 21.9- and 24.3-MeV levels. All these states are very little shifted. In the (p, p_3) reaction the 24.3 MeV resonance is clearly separated from the background and has a width of only 1.7 MeV. The widths of the two other peaks agree with the entries of Table VIII.

In the total (p, n) cross section [Fig. 33(a)], the resonances are shifted by 200 to 300 keV from the positions given in Table VIII. Since, in this reaction, a strong resonance occurs at 16.6 MeV, it is confirmed that the small peak seen in the photoabsorption process at 16.9 MeV is due to a $T=0$ state. From Fig. 33(a) one sees that the width of this state is 0.6 MeV. In the (p, n) process it is again found that the 19.5-MeV resonance does not show up for outgoing neutron channels. However, all the other $1^- T=1$ levels are seen.

In Fig. 34 we present the calculated differential $1^-(p, n)$ cross section at 0°. This $1^-(p, n)$ result of the

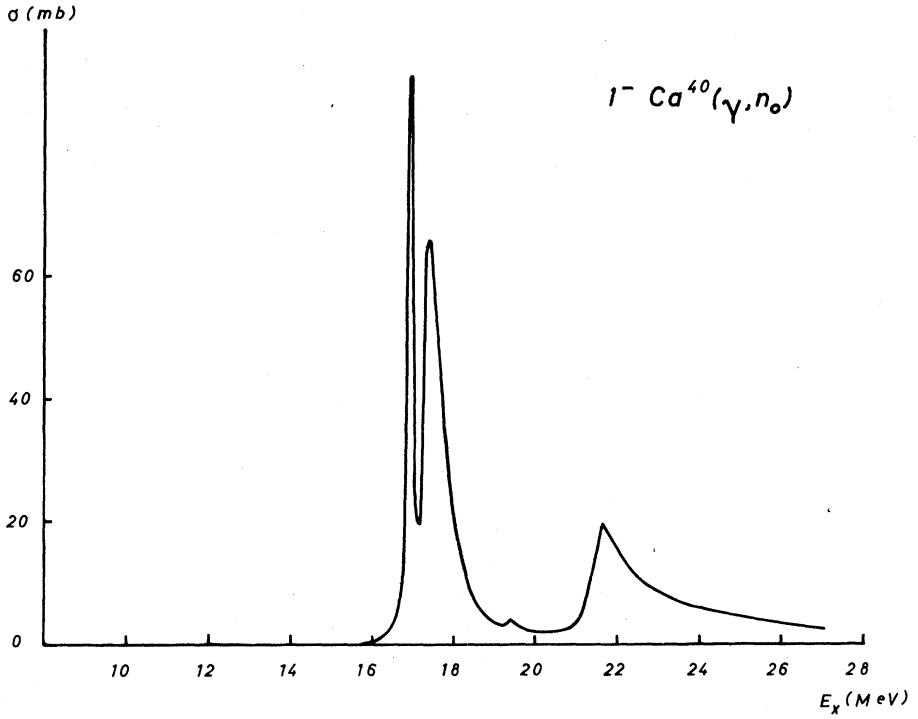

FIG. 40. Prediction of the $1p$–$1h$ eigenchannel calculation for the ground-state photoneutron emission process in ^{40}Ca.

continuum calculation may be compared with the experimental integrated-over-angle result of Barnett and Thomas (1964) (Fig. 35) or with the 0° cross section of Jones, *et al.* (1958). The latter authors extended their measurements only up to about 18 MeV. They found eight levels per megaelectronvolt. Most of the spins of these levels could not be identified (cf. Ajzenberg–Selove and Lauritsen, 1959). Since all these resonances have a width which is smaller than 250 keV, they can hardly be associated with the structure obtained in a $1p$–$1h$ continuum calculation.

J. The Giant Dipole Resonance in ^{40}Ca, Experiment and Bound-State Calculation

The giant resonance in ^{40}Ca essentially consists of several peaks concentrated between 18 and 21 MeV. The total width of the gross structure amounts to about 3 MeV. In Fig. 36 we show the 90° differential cross section for radiative proton capture with ground-state γ emission that has been measured by Häfele, *et al.* (1964). The general shape of the fine structure is in excellent agreement with the experimental results of Feldman, *et al.* (1967) and of Tanner, *et al.* (1964a) for the same process. In the range between 18 and 21 MeV, six fine structure peaks are observed (Feldman, *et al.*, 1967). In their recent high-resolution (p, γ) experiment, Bartko and Thwaites (1968) find 18(p, γ_0) peaks in the range between 12 and 14 MeV. These resonances can only be due to 1^-, 1^+, and 2^+ excitations. The widths of these resonances are 20 keV or less. The explanation of this result is clearly far beyond the capabilities of a $(1p$–$1h)$ calculation.

TABLE IX. Single-particle energies and well parameters in ^{40}Ca.

State	Protons		Neutrons	
	ϵ_b	V_c	ϵ_b	V_c
$1f_{5/2}$	>0.	49.83	−2.86	49.83
$2p_{1/2}$	>0.	53.07	−4.23	53.07
$2p_{3/2}$	−0.04	55.00	−6.29	53.86
$1f_{7/2}$	−1.63	50.93	−8.36	50.34
$1d_{3/2}$	−8.34	49.62	−15.73	59.72
$2s_{1/2}$	−10.84	54.38	−18.20	54.38
$1d_{5/2}$	−14.25	53.00	−21.86	53.43

Similar fine structure is also seen in the photoneutron reaction (Min, *et al.*, 1963; Baglin and Spicer, 1964; Firk and Rae, 1972). In Fig. 37, we show the (γ, n) data of Baglin and Spicer (1964). In this context it is noteworthy that the photoneutron emission is limited to (γ, n_0) transitions below the inelastic neutron threshold at 18 MeV. Therefore, photoneutron emission to the ground state of ^{39}Ca probably predominates throughout the giant resonance, since its center lies only slightly above that threshold.

In Fig. 38, we exhibit the relative dipole strengths from $1p$–$1h$ bound-state calculations of Balashov, *et al.* (1961), Brown, *et al.* (1961), and Gillet and Sanderson (1967). All these calculations predict a concentration of dipole strength in the vicinity of 19 MeV; however, they give no indication of the rich

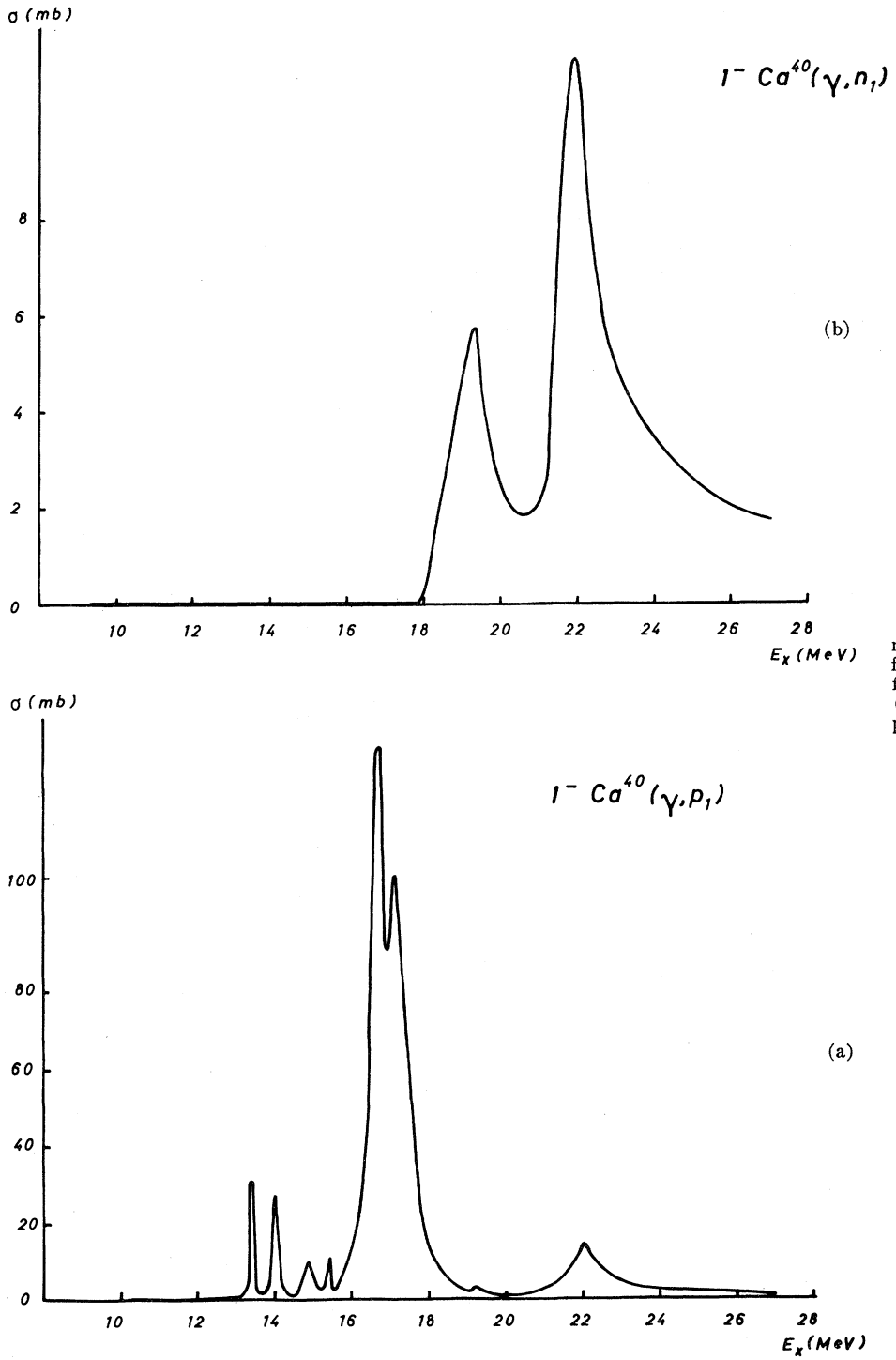

FIG. 41. Theoretical photonucleon cross sections for formation of ^{39}K or ^{39}Ca in its first excited ($2s_{1/2}$-hole) state: (a) photo-proton process, (b) photoneutron process.

pronounced fine structure observed in that region. Gillet and Sanderson allowed in their bound-state calculations for isospin mixing. They obtained nearly the total $T=1$ strength at the 18 MeV level. In their more recent work the precise position of this level is 18.76 MeV. Its predominant components are: $f_{7/2}d_{5/2}^{-1}$ (51%), $f_{5/2}d_{3/2}^{-1}$ (24%) and $p_{3/2}d_{5/2}^{-1}$ (12%). These three configurations are $T=1$. There is only a very small $T=0$ admixture at this energy. Most of the $T=0$ strength is in the spurious center-of-mass state at about 3 MeV. Finally, they predict only four states between 12 and 14 MeV, in contrast to the 18 peaks found experimentally by Bartko and Thwaites (1968).

The effect of enlarging the configurational space by

TABLE X. Comparison of bound-state and continuum calculations of the 1^- states of ^{40}Ca.

Brown (1961)		Gillet (1967)	Continuum calc			$1p$–$1h$ Components	
(MeV)	%	(MeV)	(MeV)	(MeV)		$T=1$	$T=0$
10.2	0	10.1	10.2	0.15		$p_{3/2}d_{3/2}^{-1}$	
12.9	0	12.0	12.1	0.3		$p_{1/2}d_{3/2}^{-1}$; $p_{3/2}s_{1/2}^{-1}$	
13.4	0	13.3	13.4	0.2		$p_{3/2}s_{1/2}^{-1}$	$f_{5/2}d_{3/2}^{-1}$; $f_{7/2}d_{5/2}^{-1}$
		13.8	14.0	0.2	p_1		$p_{3/2}d_{5/2}^{-1}$
15.4	0	14.3	15.0	0.3		$f_{5/2}d_{3/2}^{-1}$; $p_{1/2}s_{1/2}^{-1}$; $f_{7/2}d_{5/2}^{-1}$	small components
16.8	1	15.1	15.6	0.2		$f_{7/2}d_{5/2}^{-1}$; $f_{5/2}d_{3/2}^{-1}$; $p_{1/2}s_{1/2}^{-1}$	small components
17.8	0	16.8	16.8	0.4	n_0	$p_{3/2}d_{5/2}^{-1}$	
19.2	55	18.8	17.5	0.5	p_1	$f_{7/2}d_{5/2}^{-1}$; $f_{7/2}d_{3/2}^{-1}$	
		22.2	19.2	0.3			$f_{5/2}d_{5/2}^{-1}$
20.6	4	22.0	21.8	1.3		$f_{5/2}d_{5/2}^{-1}$; $f_{5/2}d_{3/2}^{-1}$	

surface quadrupole phonon excitations can be found in a recent paper by Seaborn (1969). The concept of collective intermediate structure (Drechsel *et al.*, 1967) seems to be one of the most promising concepts for the explanation of the main substructure of the giant resonances. Also it is known from pick-up experiments (Bock, *et al.*, 1965; Cline, *et al.*, 1965; Glashausser, *et al.*, 1965; Hinds and Middleton, 1966; Hiebert, *et al.*, 1967; Seth, 1967) that the ^{40}Ca ground state exhibits large deviations from a simple doubly closed shell nucleus. Calculating the ground state wave function for ^{40}Ca within the hypothesis of the quasiboson approximation (RPA) Gillet and Sanderson (1967) found that it was only 30% a pure shell-model state. Because of all these reasons, the agreement between a $1p$–$1h$ treatment and experiment certainly must be expected to be worse for ^{40}Ca than for ^{12}C and ^{16}O. Nevertheless there should be some interest in comparing the structure of a $1p$–$1h$ calculation with less resolved experimental data to find out up to what extent the experimental structure can be understood within a $1p$–$1h$ description.

The various single-particle thresholds are located as follows: $1d_{3/2}^{-1}$: 8.3 and 15.6 MeV for protons and neutrons, respectively (Hiebert, *et al.*, 1967; Lewis, *et al.*, 1968); $2s_{1/2}^{-1}$: 10.8 and 18.1 MeV, respectively. The $d_{5/2}^{-1}$-state, however, is spread over a range of about 3 MeV. The values 14.3 and 21.8 MeV seem to be in reasonable agreement with the centers of gravity (Hiebert, *et al.*, 1967). The uncertainty of the accurate

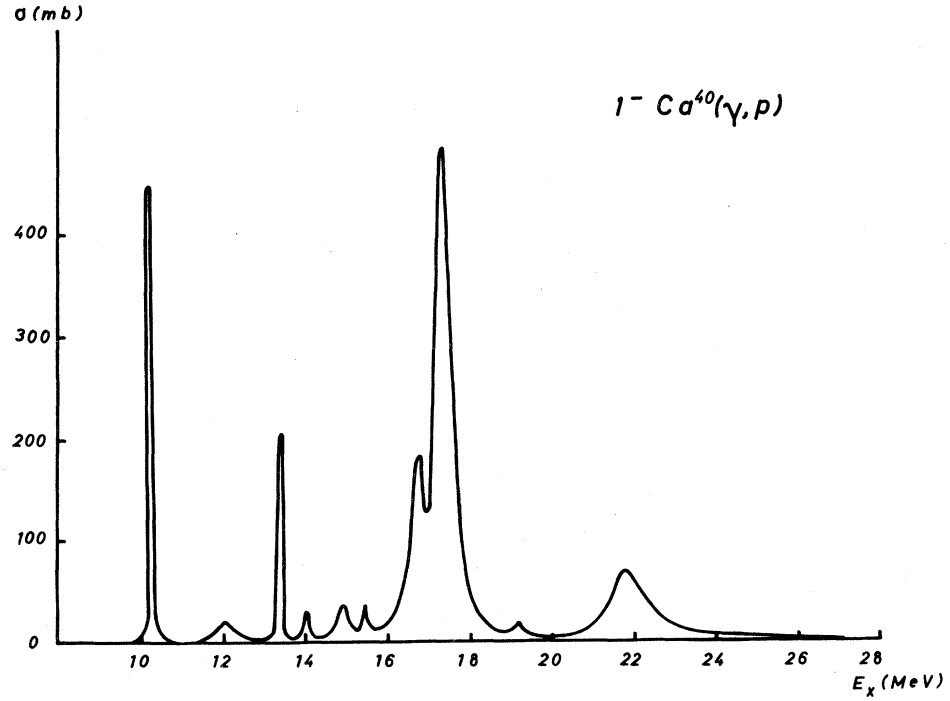

FIG. 42. Theoretical result for the total 1^- photoproton cross section of ^{40}Ca.

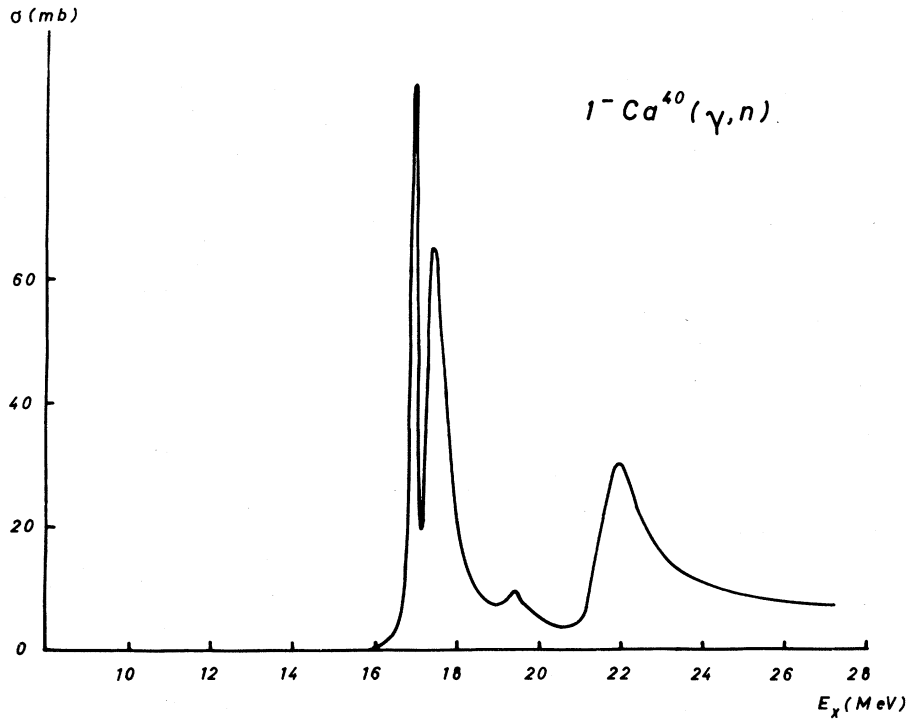

FIG. 43. Theoretical result for the total 1^- photoneutron cross section of ^{40}Ca.

position of this level is rather unpleasant, since the various $(1p$–$1h)$ 1^- basis configurations are mixed more strongly in ^{40}Ca than in ^{16}O or ^{12}C. Therefore the 1^- wave functions and the relative dipole strengths are more dependent on the model parameters.

K. The Giant Dipole Resonance of ^{40}Ca in a Continuum $1p$–$1h$ Calculation

In $1p$–$1h$ calculations for the 1^- state of ^{40}Ca, the following configurations for neutrons and protons are taken into account:

$$1^-: \; f_{7/2}(1d_{5/2})^{-1};\; p_{3/2}(1d_{5/2})^{-1};\; f_{5/2}(1d_{5/2})^{-1};$$
$$p_{3/2}(2s_{1/2})^{-1};\; p_{1/2}(2s_{1/2})^{-1};$$
$$p_{3/2}(1d_{3/2})^{-1};\; p_{1/2}(1d_{3/2})^{-1};\; f_{5/2}(1d_{3/2})^{-1}.$$

For the continuum treatment presented here (Delsanto and Wahsweiler, 1970), the parameters of the Woods–Saxon potential have been taken from an analysis by Divadeenam (1969). The spin–orbit force, the diffuseness parameter, and the potential radius were chosen in accordance with ^{16}O fits and then a search for well depths was performed to fit the experimental single-particle levels. The various parameters are: $R_0 = 1.281(39)^{1/3} = 4.35$ F, $d = 0.5$ F, and $V_{so} = 5.4$ MeV. The last value corresponds to the d-shell values quoted in Table VII. As for ^{16}O, the nuclear potential radius is larger than one would expect from electron scattering (Frosch, *et al.*, 1968). For ^{40}Ca, however, the radius of the nuclear potential and the radius of the homogeneous charge distribution were not set equal, but the latter radius was assumed five per cent larger. This is in accordance with the fact that the neutrons are more tightly bound than the protons in ^{40}Ca.

The well depths and the corresponding single particle energies are listed in Table IX. Some of these single-particle energies deviate from the values obtained by Gillet and Sanderson (1967) in their analysis of experimental data. In particular, it may be noticed that the $p_{3/2}$-proton resonance is replaced by a weakly bound state and that the mass difference between ^{41}Sc and ^{39}K has not been reduced by 0.5 MeV as was done by Gillet and Sanderson to account for the diagonal Coulomb effect. The two-body force is of the Soper-type as in Eq. (3.2). The strength was chosen to be -1000 MeV fm^3. This value is about 10% less than the strength of the zero-range force employed by Brown, *et al.* (1961), but about 20% more than the force used by Marangoni and Sarius (1969) in their recent coupled-channel treatment of the photodisintegration process in ^{40}Ca. The latter authors have also partly used an absorptive optical potential W to account for the effect of those configurations which are not included in a $1p$–$1h$ description. W was assumed to be linear in E_x. As far as their calculations were done for $W = 0$, they obtain essentially the same result as the one which we are going to discuss here.

We show the theoretical cross section of the photoproton ground-state reaction in Fig. 39(b). The corresponding 90° differential cross section derived by Häfele, *et al.* (1964) from their experimental (p, γ_0) data by detailed balance is depicted in Fig. 39(a). The theoretical (γ, n_0) result is presented in Fig. 40. It may be compared with the experimental cross section

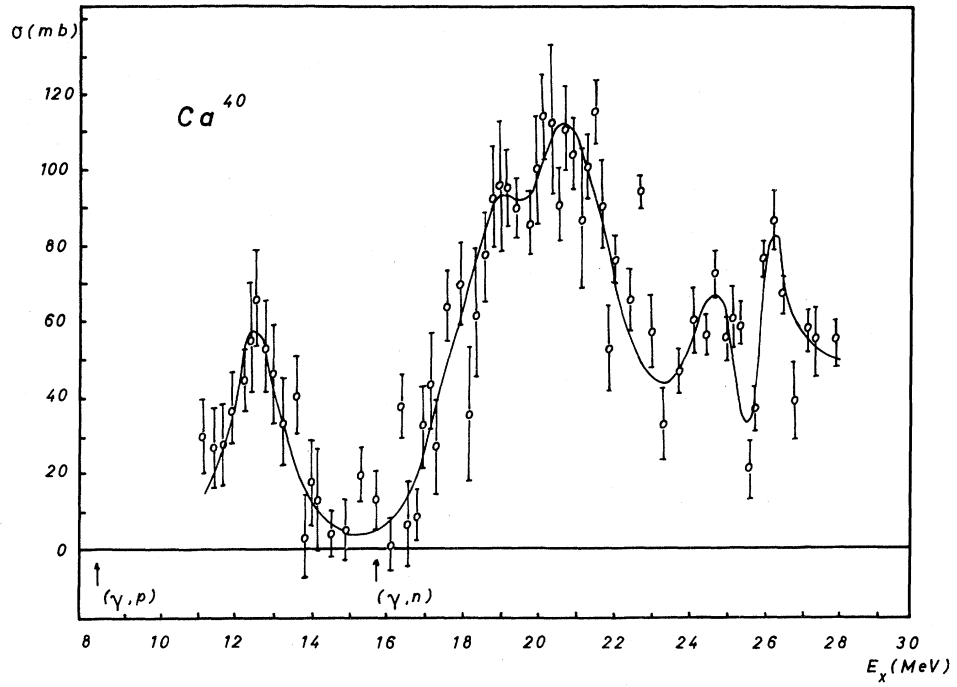

(a)

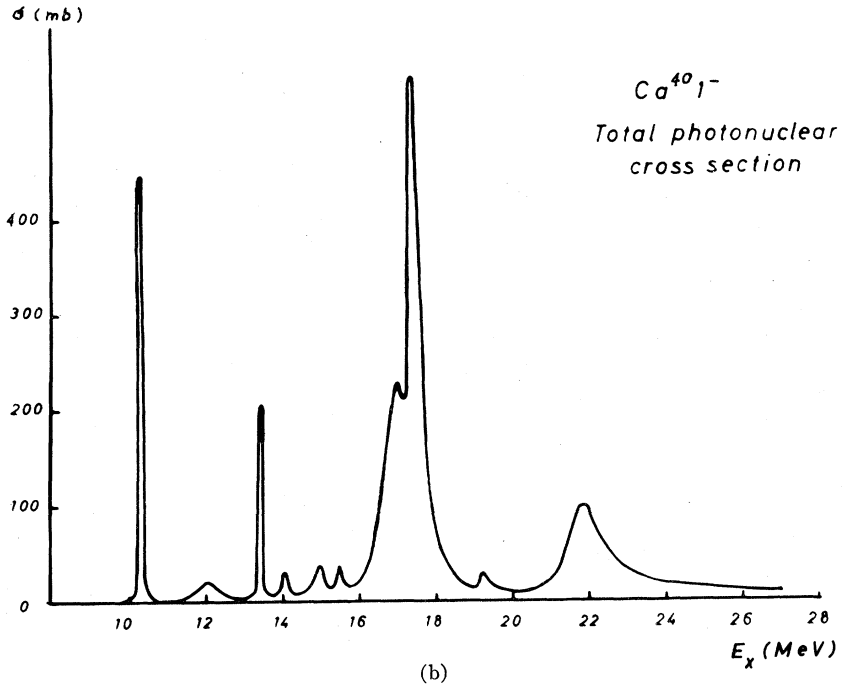

(b)

FIG. 44. Comparison of experimental and theoretical total photodisintegration cross sections of ^{40}Ca. (a) photoabsorption cross section measured data of Dolbilkin, *et al.* (1965). (b) 1^- result of the $1p$–$1n$ continuum calculation.

shown in Fig. 37. The continuum calculations give a height of the main dipole resonance which is about five times too large when no absorptive potential is employed.

From a comparison of Figs. 39(b) and 40, it is seen that the (γ, p_0) process contains considerably more dipole strength than the (γ, n_0) reaction. This is confirmed by experiment (Segal, 1966). In a recent paper Wu, *et al.* (1969) calculate the ratio $[\sigma(\gamma, p_0)/\sigma(\gamma, n_0)]_{90°}$ to have an almost constant value of 2.2.

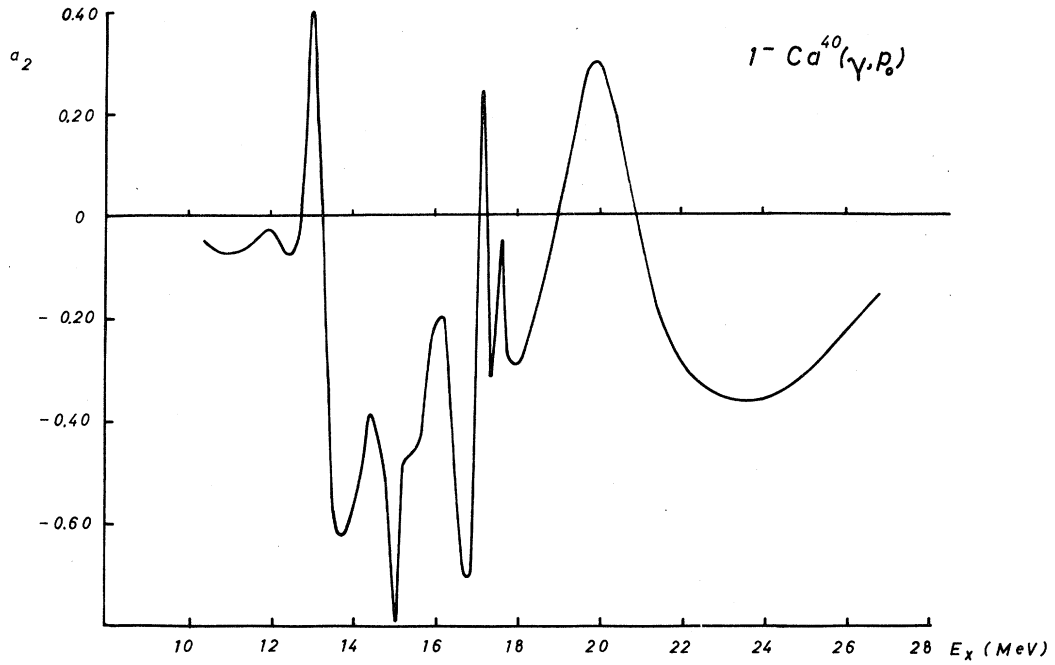

FIG. 45. Theoretical prediction for a_2-coefficients in the angular distributions of ground state photoprotons from ^{40}Ca assuming pure $E1$ transitions.

Consequently, using the Barker and Mann (1957) formula they infer a ratio of the $T=0$ to $T=1$ amplitudes of 0.2.

In Table X the level positions from the bound state and the eigenchannel–continuum calculations are compared.

In addition, we give the predominant $1p$–$1h$ $T=1$ and $T=0$ configurations at the resonance peaks which were determined by Marangoni and Saruis (1969) by looking at the components of their dipole transition matrix elements. The main configuration we have quoted for the 10.2-MeV state was taken from Gillet and Sanderson (1967). One should keep in mind, however, that these results are quite sensitive in respect to the model parameters.

The levels found by Gillet and Sanderson (1967) at 12.4 and at 14.0 MeV are not included in Table X. Actually, it is surprising that the 12.4-MeV state does not show up in a continuum calculation in spite of the fact that it is essentially $T=1$.

The main dipole resonance of the continuum calculation occurs at 17.5 MeV. That is rather low. This is partly due to the fact that in the present calculation the $f_{7/2}$–$d_{5/2}$ proton level spacing is 1 MeV less than that found by Gillet and Sanderson (1967) and Marangoni and Saruis (1967). Also there might be an additional upward shift in the coupled-channel result caused by the omission of the occupied $1p$-shell (partial neglect of antisymmetry—See Sec. III.C). Thus, in the present calculation, the 16.8-MeV level and the main resonance have moved together, while the spacing between the main resonance and the subsequent $T=0$ level has increased. This change in the relative spacings leads to an obvious difference in shape between the present (γ, n_0) result and the (γ, n) curve of Marangoni and Saruis (1967). Nevertheless, the main configuration of the 16.8-MeV state is the configuration given in Table X, since this level turns out to be relatively more pronounced in the (γ, p_1) than in the (γ, p_0) reaction, which indicates that it results to a large degree from a resonance in the inelastic $s_{1/2}^{-1}$ proton channel. A similar statement holds for the 14-MeV state which only shows up in the (γ, p_1) reaction. The cross section of this process which leads to the $(2s_{1/2})^{-1}$ ^{39}K state is exhibited in Fig. 41(a). The corresponding (γ, n_1) result is shown in Fig. 41(b).

Figure 42 represents the total theoretical (γ, p), and Fig. 43 the total (γ, n) cross section. These cross sections have been obtained by summing up the contributions for the final $d_{3/2}^{-1}$, $s_{1/2}^{-1}$ and $d_{5/2}^{-1}$ channels.

Finally, Fig. 44(b) represents the sum of $\sigma(\gamma, p)$ and $\sigma(\gamma, n)$; i.e., the total theoretical photodisintegration cross section of ^{40}Ca. The experimental data of Dolbilkin, *et al.* (1965) are depicted in Fig. 44(a). The area under the theoretical curve [Fig. 44(b)] below 28 MeV amounts to 725 MeV·mb. This must be compared with the experimental value of 920±100 MeV·mb. The unmodified classical sum rule gives 600 MeV·mb.

The discrepancy in the calculated and measured

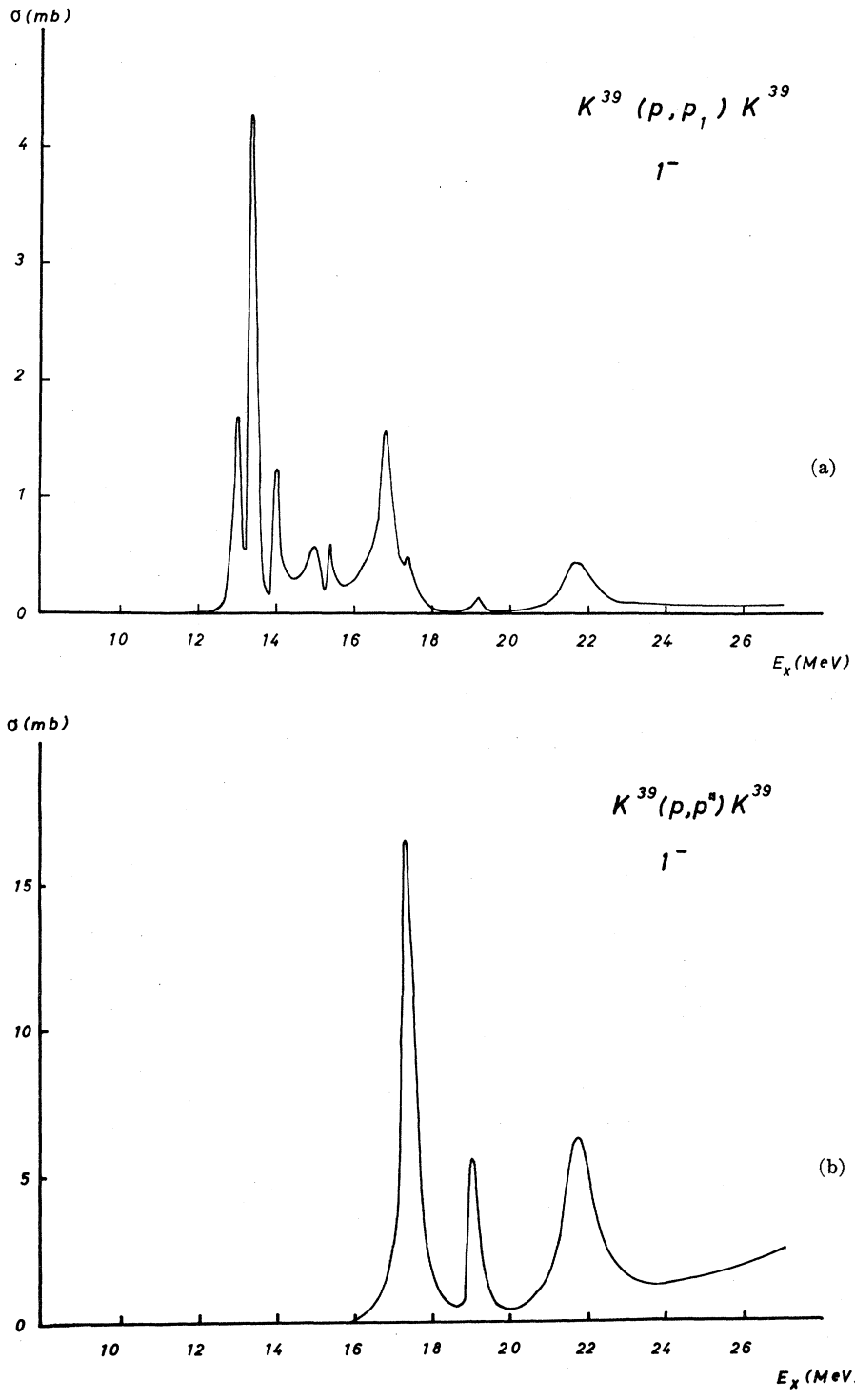

FIG. 46. Calculated 1^- contribution to proton-induced particle reaction cross sections in ^{40}Ca. (a) Formation of ^{39}K in the $2s_{1/2}$-hole state, (b) formation of ^{39}K in the smeared-out $1d_{5/2}$-hole state.

height of the main giant resonance peak exceeds a factor of five in ^{40}Ca. The analogous factor for ^{16}O was three, and for ^{12}C two. This is consistent with the fact that the number of open channels not taken into account in the $1p$–$1h$ approximation increases with mass number.

L. Photonucleon Angular Distribution in ^{40}Ca

The a_2 coefficient of the (γ, p_0) angular distribution near 20 MeV has been determined from bremsstrahlung experiments (Johansson and Forkman, 1962) to be about -0.38. Tanner (1965) quotes a value -0.3

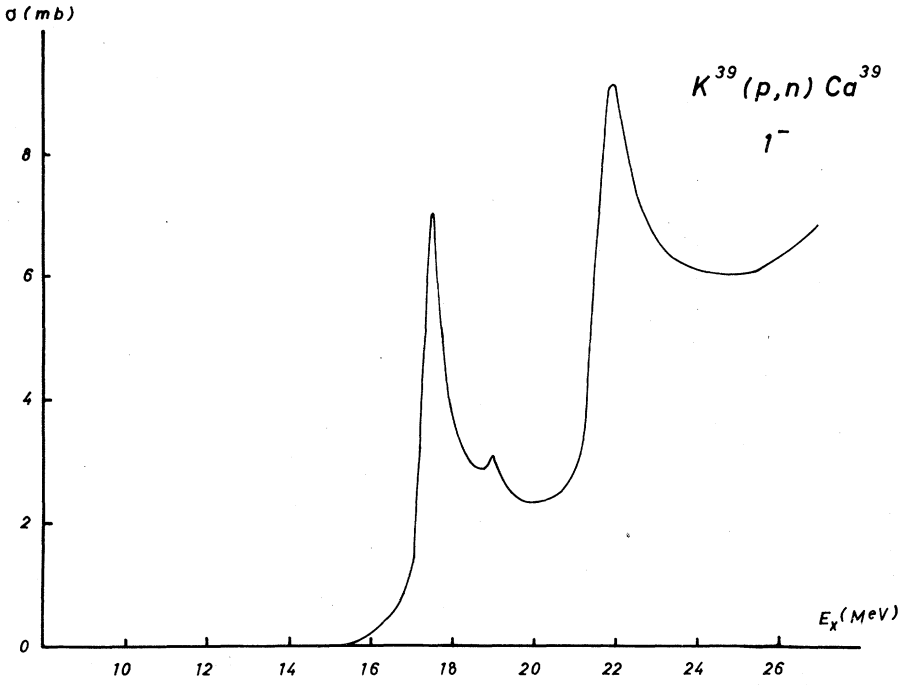

FIG. 47. Calculated 1^- contribution to the total cross section of the ^{39}K (p, n) ^{39}Ca reaction.

for ^{40}Ca in his survey on average a_2 coefficients in the giant resonances of various nuclei.

The theoretical prediction (Fig. 45) for the energy dependence of the a_2 coefficients does not contradict these experimental values. Figure 45 resembles closely the corresponding result of Marangoni and Saruis (1967).

M. Reaction Cross Sections of ^{40}Ca

We conclude the discussion of the giant resonance in ^{40}Ca by presenting some proton-induced reaction cross sections which proceed through the $J^\pi = 1^-$ channels.

Figures 46a, b show the integrated-over-angle 1^- cross sections of inelastic proton scattering which populate the $(2s_{1/2})^{-1}$ and the smeared-out $(1d_{5/2})^{-1}$ state of ^{39}K, respectively. The latter channel is denoted by a double prime. The level positions and widths which can be obtained from these curves are in accordance with the entries of Table X. Actually, there is even no contradiction to the configurations listed in Table X. The relative importance of the 13.4- and 16.8-MeV level in Fig. 46(a) supports the expectation that the predominant configurations of these states contain a $2s_{1/2}$–hole. The equal importance of the three upper states in Fig. 46(b) seems to confirm that they mainly contain $1d_{5/2}$–hole configurations. Inelastic proton scattering experiments on ^{39}K were performed by Sperduto and Buechner (1958). However, these measurements yield information only on the excited states of the final ^{39}K nucleus. Finally, we present the 1^- (p, n) cross section in Fig. 47. Almost no (p, n) experiments on ^{39}K have been performed (cf. Endt and van der Leun, 1967; Tai, *et al.*, 1958).

V. CONCLUSIONS AND OUTLOOK

From the material presented in this review, one may draw the conclusions that there exist several methods for the treatment of one-particle continua, which have been used successfully in actual numerical calculations. They yield the same results when applied to the same model and when they are done in the same approximation (the coupled-channel calculations tend to treat incompletely the antisymmetrization). In other words, the mathematical and numerical techniques have indeed been tested and proven out, and this seems to be in satisfactory condition, at least for situations which are not too involved. In fact, Barrett and Delsanto (1971) very recently applied the eigenchannel method to the calculation of the giant dipole resonance in ^{208}Pb. This case corresponds to 31 coupled channels. In Fig. 48, we present the results of the E.C. calculation for the 1^- photoabsorption cross section for ^{208}Pb in the $1p$–$1h$ model. For comparison, the experimental (γ, n) cross section (Beil, *et al.*, 1969) is shown, together with the results of a bound-state calculation by Kuo, *et al.* (1970). The results of the E.C. calculation for ^{208}Pb have been discussed in detail by Barrett and Delsanto.

As far as the practicability of the eigenchannel method is concerned, the computed time needed to calculate the complete S-matrix at one energy requires, on a Univac 1108 computer, for a system of the com-

plexity of ^{16}O about 3–5 min, and for ^{208}Pb about 25–30 min. In the simpler case, the coupled-channel method is faster; for ^{208}Pb no comparison is possible as no calculations of equivalent complexity employing any other method have been reported.

On the other hand, the calculations have revealed that in light nuclei, the $1p$–$1h$ model is disappointingly inadequate, even as far as the reproduction of the gross features of the experimental results is concerned. We refer to the intermediate structure in the photon absorption process, to the angular distributions of certain partial cross sections, and to the proton to neutron branching ratio. The surprising aspect here is evident from the result that in the experimental absorption cross section there is more structure than in the theoretical, while, at the same time, in the experimental angular distributions there is less structure than in the theoretical. Even more surprising is the uncanny constancy in the $(\gamma, p_0)/(\gamma, n_0)$ branching ratio. What would have been expected would be more structure in the experimental values than in the theoretical for all these quantities. This evidence suggests that the "dipole state" is a very strong structure indeed. In contrast to the theoretical result in which in, ^{16}O say, there are two dipole states within the $1p$–$1h$ states, which thus have different configuration mixtures and consequently different angular distributions, it seems that there exists essentially only one dipole state in the $1p$–$1h$ hierarchy, and that the orthogonal $1p$–$1h$ states have very small absorption strength. The splitting into two major parts, and the fragmentation into fine structure, seems to leave this dipole state intact. The separation of this dipole state from the orthogonal $1p$–$1h$ states (which are also continuum states and which have different angular distributions) seems to remain weak even though the interaction with the fragmentation states is evidently strong. These effects seem to require for their explanation the assumption that the cross links between the different $1p$–$1h$ states are located in the $4p$–$4h$ and higher members of the hierarchy, and that they are damped by the α-particle channels. At any rate, this is only a speculation, and is intended to indicate the extent to which the $1p$–$1h$ model seems to be inadequate to explain the seemingly contradictory experimental findings. To re-emphasize, these findings include so-called gross structure which supposedly should be explicable within the $1p$–$1h$ model.

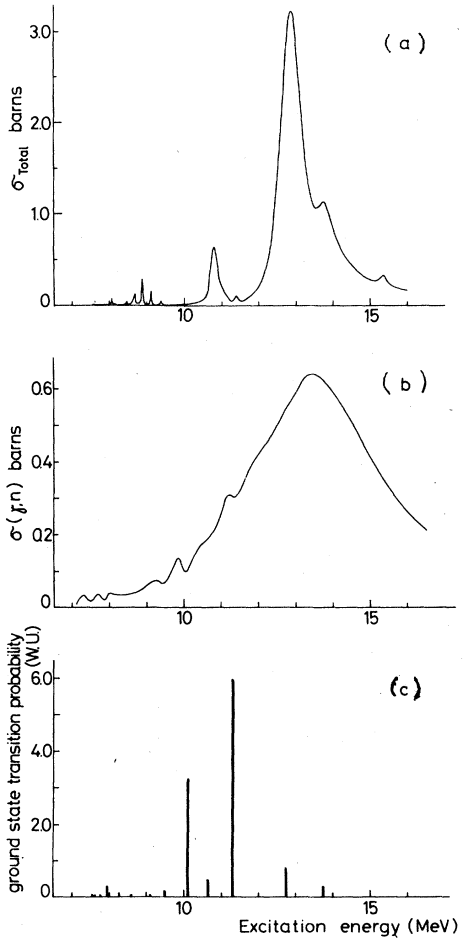

FIG. 48. (a) Total photo-absorption cross section of ^{208}Pb calculated from the eigenchannel reaction theory (Barrett and Delsanto, 1971). (b) Experimental photoneutron cross section of ^{208}Pb due to Beil, *et al.* (1969). (c) Results of a bound-state calculation (including RPA) for ^{208}Pb photo-absorption cross section by Kuo, *et al.* (1970).

As for future development, one should consider two directions separately. The first concerns the development of practical methods to treat two-particle and many-particle channels. There exist proposals for it in the frame work of the eigenchannel theory (Grauel, 1971), and naturally, there exist the Fadeev equations. However, no reasonably realistic nuclear (as contrasted with three-body) problem has been treated as yet.

The other direction is the development of more realistic nuclear models. This is meant in the sense of adding more closed channels; i.e., quasi-bound states, to the nuclear model. As we tried to indicate, the addition of some $2p$–$2h$ configurations must be only a very first step. In fact, we believe that some invention will have to take place before progress in the understanding of the physics becomes possible. From the point of view of nuclear physics this second direction seems to be the more pressing of the two.

ACKNOWLEDGMENTS

We acknowledge many stimulating discussions and help by Dr. A. Rabie and Dr. P. Antony-Spies. A number of discussions with Professor B. M. Spicer (Melbourne) and Dr. E. Fuller (NBS) illuminated many points on the structure of giant resonances for us. Furthermore we thank Mrs. M. Knolle and Mrs. B.

Utschig (at Frankfurt/M), and Mrs. C. A. Gentzler (at Duke University) for their help in preparing the final manuscript.

We wish to acknowledge also computational help from the Triangle Universities Computing Center (Research Triangle Park, N. C.) and partial support, during these computations, (for P.-P. D. and H. G. W.) from the National Science Foundation and the Army Research Office (Durham). R. F. B. acknowledges the support of the Alexander von Humboldt-Stiftung in the form of a post-doctoral fellowship. The Bundesministerium für Bildung und Wissenschaft also supported this work.

REFERENCES

Ajzenberg-Selove, F., and T. Lauritsen, 1959, Nucl. Phys. **11,** 1.
Allas, R. G., S. S. Hanna, L. Meyer-Schützmeister, and R. E. Segal, 1964, Nucl. Phys. **58,** 122.
Arenhövel, H., and W. Greiner, 1969, Prog. in Nucl. Phys. **10,** 167.
P. Antony-Spies, P. P. Delsanto, E. Spamer, A. Goldmann, and O. Titze (1970). Phys. Letters **31B,** 632.
——, 1972, Nucl. Phys. **A188,** 641.
Baglin, J. E. E., and B. M. Spicer, 1964, Nucl. Phys. **54,** 549.
——, and M. N. Thompson, 1969, Nucl. Phys. **A138,** 73.
Balashov, V. V., P. Doleshal, V. L. Korotkih, and V. N. Fetisov, 1965a, Sov. J. Nucl. Phys. **2,** 461.
——, D. Pal, and V. N. Fetisov, 1965b, Phys. Letters **17,** 290.
——, V. G. Shevchenko, and N. P. Yudin, 1961, Nucl. Phys. **27,** 323.
Barber, W. C., J. Goldemberg, G. A. Peterson, and Y. Torizuka, 1963, Nucl. Phys. **41,** 461.
Bardsley, J. N., and F. Mandl, 1968, Rep. Prog. Phys. XXXI, Part 2.
Barker, F. C., and A. K. Mann, 1957, Phil. Mag. **2,** 5.
Barett, A. R., and G. C. Thomas, 1964, *Comptes Rendus Congres International de Physique Nucleaire,* II, edited by P. Gungenberger (Centre National de Recherche Scientifique, Paris), 387.
Barrett, R. F., and P. P. Delsanto, 1971, Nucl. Phys. **A173,** 641.
Bartko, J., and T. T. Thwaites, 1968, Phys. Letters **27B,** 212.
Beil, H. R. Bergère, P. Carlos, and A. Veyssière, 1969, *Compt. Rend.* **269,** 216.
Bishop, G. R., and D. B. Isabelle, 1962, Phys. Letters **1,** 323.
Biedenharn, L. C., E. Baumgartner, P. Huber, and H. B. Willard, 1963, in *Fast Neutron Physics,* edited by J. B. Marion and J. L. Fowler, (Wiley-Interscience, New York), Chap. V.E.
Black, J. L., W. J. O'Connell, S. S. Hanna, and G. L. Latshaw, 1967, Phys. Letters **25B,** 405.
Blatt, J., and L. C. Beidenharn, 1952, Rev. Mod. Phys. **24,** 258.
Bloch, C., 1957, Nucl. Phys. **4,** 503.
——, 1966, "An Introduction to the Many-Body Theory of Nuclear Reactions", in *Proc. of the International School of Physics,* Enrico Fermi, Course XXXVI, (Academic, New York).
——, and V. Gillet, 1965, Phys. Letters **16,** 62.
Bock, R., H. H. Duhm, and R. Stock, 1965, Phys. Letters **18,** 61.
Boeker, E., 1966, Physica **32,** 669.
——, W. M. DeMuiguck, and C. C. Jouher, 1964, Congres International de Physique Nucleaire, Paris, II, 405.
Bohr, A., J. Damgaard, and B. R. Mottelson, 1967, in *Nuclear Structure* edited by A. Hossian (North-Holland Publ. Co., Amsterdam).
Brenig, W., and R. Haag, 1959, Fortschritte der Physik **7,** No. 4/5, 183, cf. Sec. 4; translation in *Quantum Scattering Theory,* edited by Marc Ross (Indiana U. P., Bloomington, 1963).
Brink, D. M., 1957, Nucl. Phys. **4,** 214.
Brown, G. E., 1966, *The Unified Theory of Nuclear Models,* (North-Holland Publ. Co., Amsterdam), 2nd ed.
——, L. Castillejo, and J. A. Evans, 1961, Nucl. Phys. **22,** 1.
Buck, B., and A. D. Hill, 1967, Nucl. Phys. **A95,** 271.
Bur, G. A., T. E. Drake, R. M. Hutcheon, V. W. Stobie, and H. S. Caplan, 1968, Nuovo Cimento **53B,** 7.
Burgov, N. A., G. V. Danilyau, B. S. Dolbilkin, L. E. Lazareva, and F. A. Nikolaev, 1963, Zh. Eksp. Teor. Fiz. [Sov. Phys.—JETP] **16,** 50.
Buttle, J. P. A., 1967, Phys. Rev. **160,** 719.
Caldwell, J. T., 1967, Ph.D. Thesis, University of California, Livermore, unpublished.
——, R. L. Bramblett, B. L. Berman, R. R. Harvey, and S. C. Fultz, 1965, Phys. Rev. Letters **15,** 976.
——, S. C. Fultz, and R. L. Bramblett, 1967, Phys. Rev. Letters **19,** 447.
Cline, D., W. P. Alford, and L. M. Blau, 1965, Nucl. Phys. **73,** 33.
Cook, B. C., J. E. E. Baglin, J. N. Bredford, and J. E. Griffln, 1966, Phys. Rev. **143,** 724.
Crannel, H., H. A. Dahl, and F. H. Lewis, Jr., 1967, Phys. Rev. **155,** 1062.
Danos, M., 1958, Nucl. Phys. **5,** 23.
——, 1961, Photonuclear Physics Lectures, University of Maryland, unpublished.
——, 1967, Lectures delivered at Les Houches during the 1968 session of the Summer School of Theoretical Physics; edited by C. DeWitt and V. Gillet (Gordon and Breach, New York).
——, and E. G. Fuller, 1965, Ann. Rev. Nucl. Sci. **15,** 29.
——, and V. Gillet, 1971, Phys. Letters **34B,** 24.
——, and W. Greiner, 1964, Phys. Rev. **134,** B284.
——, and W. Greiner, 1965, Phys. Rev. **138,** B93.
——, and W. Greiner, 1966, Phys. Rev. **146,** 708.
——, and W. Greiner, 1967, Z. Phys. **202,** 125.
de Alfaro, V., and T. Regge, 1965, *Potential Scattering* (North-Holland Publ. Co., Amsterdam).
de Forest, T., Jr., 1965, Phys. Rev. **139,** B1217.
——, and J. D. Walecka, 1966, Advan. Phys. **15,** 1.
Delsanto, P., M. F. Roetter, and H. G. Wahsweiler, 1969, Z. Physik **222,** 67.
——, and H. G. Wahsweiler, University of Frankfurt, 1970, unpublished results.
——, H. G. Wahsweiler, and R. F. Barrett, 1970, University of Frankfurt, unpublished results.
——, H. Wahsweiler and W. Greiner, 1967, Phys. Rev. Letters **19,** 706.
Denisov, V. P., A. P. Komar, and L. A. Kulchilsky, 1968, Nucl. Phys. **A113,** 289.
Dietrich, K., 1967, "Shell-Model Description of Nuclear Reactions", in *Fundamentals in Nuclear Theory, Lectures presented at Trieste, 1966* (International Atomic Energy Agency, Vienna).
——, and K. Hara, 1968, Nucl. Phys. **A111,** 392.
Dirac, P. A. M., 1927, Z. Physik **44,** 585.
Divadeenam, M., 1969, unpublished results.
Dodge, W. R., and W. C. Barber, 1962a, Phys. Rev. **127,** 1146.
——, and W. C. Barber, 1962b, Phys. Rev. **127,** 1745.
Dolbilkin, B. S., V. I. Korin, L. E. Lazareva, and F. A. Nikolaev, 1968, Phys. Letters **17,** 49.
Donnelly, T. W., J. D. Walecka, I. Sick, and E. B. Hughes, 1968, Phys. Rev. Letters **21,** 1196.
Drechsel, D., J. B. Seaborn, and W. Greiner, 1967, Phys. Rev. **162,** 983.
Earle, E. D., and N. W. Tanner, 1967, Nucl. Phys. **A95,** 241.
Ebenhöh, W., W. Glöckle, and J. Hüfner, 1967a, Phys. Letters **24,** 361.
——, W. Glöckle, J. Hüfner, and H. A. Weidenmüller, 1967b, Z. Phys. **202,** 302.
Eichler, J., 1964, Nucl. Phys. **56,** 577.
Elliott, J. P., and B. H. Flowers, 1957, Proc. Royal Soc. **A242,** 57.
Elton, L. R. B., 1961, *Nuclear Sizes,* Oxford Library of the Physical Sciences (Oxford U.P., London).
Endt, P. M., and C. van der Leun, 1967, Nucl. Phys. **A105,** 1.
Fallerios, S., Thesis, Univ. of Maryland, Tech. Rept. No. 195.
Fano, U., 1935, Nuovo Cimento **12,** 156.
——, 1961, Phys. Rev. **124,** 1866–1878.
Feldman, L., B. B. Baliga, and M. Nessin, 1967, Phys. Rev. **157,** 921.
——, M. Suffert, and S. S. Hanna,1968, Bull. Am. Phys. Soc. **13,** 822.
Feshbach, H., 1958, Ann. Phys. (New York), **5,** 357.
——, 1960, in *Nuclear Spectroscopy* edited by F. Ajzenberg-Selove, (Academic, New York), Chap. 5, Part B.
——, 1962, Ann. Phys. (New York), **19,** 287 (1962).
——, A. Kerman, and R. H. Lemmer, 1967, Ann. Phys. (New York) **41,** 230.

Finckh, E., and U. Hegel, 1961, Z. Physik **162,** 154.
Firk, F. W. K., 1970, Ann. Rev. Nucl. Sci. **20,** 39.
——, K. H. Lokan, and E. M. Bowey, 1962, in "Proceedings of the Conference on Direct Interactions and Nuclear Reaction Mechanism, Padua," edited by E. Clementel and C. Villi (Gordon and Breach, New York).
——, and E. R. Rae, private communication (see Feldman, *et al.*, 1967).
Frederick, D. E., and A. D. Sherik, 1968, Phys. Rev. **176,** 1177.
Friar, J. L., 1966, Nucl. Phys. **84,** 150.
Friedman, W. A., and H. Feshbach, 1968, in *Spectroscopic and Group Theoretical Methods in Physics* (North-Holland Publ. Co., Amsterdam).
Friedrichs, K. O., 1948, Comm. Pure and Appl. Math. **1,** 361–406.
Frosch, R. F., R. Hofstadter, J. S. McCarthy, G. K. Nöldecke, K. J. van Oostrum, M. R. Yearian, B. C. Clark, R. Herman, and D. G. Ravenhall, 1968, Phys. Rev. **174,** 1380.
Fultz, S. C., J. T. Caldwell, B. L. Berman, R. L. Bramblett, and R. R. Harvey, 1966, Phys. Rev. **143,** 790.
Gallagher, D. F., and L. Wilets, 1968, Phys. Rev. **169,** 139.
Garside, L., and W. Tobocman, 1968, Phys. Rev. **173,** 1047.
Gillet, V., and C. Bloch, 1965, Phys. Letters **18,** 58.
——, M. A. Melkanoff, and J. Raynal, 1967, Nucl. Phys. **A97,** 631.
——, and E. A. Sanderson, 1967, Nucl. Phys. **A91,** 292.
——, and N. Vinh-Mau, 1964, Nucl. Phys. **54,** 321.
Glashausser, C., M. Kondo, M. E. Rickey, and E. Rost, 1965, Phys. Letters **14,** 113.
Glöckle, W., J. Hüfner, and H. A. Weidenmüller, 1967, Nucl. Phys. **A90,** 481.
Goldemberg, J., and W. C. Barber, 1964, Phys. Rev. **134,** B963.
Goldhaber, M. and E. Teller, 1948, Phys. Rev. **74,** 1046.
Goldmann, A., and E. Spamer, 1970, unpublished results.
Grauel, A., 1971, Ph.D. Thesis, University of Frankfurt.
Greiner, W., 1963, Nucl. Phys. **49,** 522.
Hafele, J. C., F. W. Bingham, and J. S. Allen, 1964, Phys. Rev. **135,** B365.
Hahne, F. J. W., and C. B. Dover, 1969, Nucl. Phys. **135A,** 65.
Hayward, E., 1964, "Nuclear Structure and Electromagnetic Interactions," edited by N. MacDonald (Oliver and Boyd, London) (Scottish University Summer School, Edinburgh, London, 1964); and E. Hayward Proc. International School of Physics, Varenna, Course 36, page 559.
Hebbard, D. F., 1960, Nucl. Phys. **15,** 289.
Herzenberg, A., K. L. Kwok, and F. Mandl, 1964, Proc. Phys. Soc. **84,** 477.
——, and F. Mandl, 1963, Proc. Roy. Soc. A274, 253; Phys. Letters **6,** 288.
Hiebert, J. C., E. Newman, and R. H. Bassel, 1967, Phys. Rev. **154,** 898.
Hinds, S., and R. Middleton, 1966, Nucl. Phys. **84,** 651.
Hüfner, J., C. Mahaux, and H. A. Weidenmüller, 1967, Nucl. Phys. **A105,** 489.
Ince, E. L., 1927, "Ordinary Differential Equations" (Longmans–Green, London), Chap. 10.
Jensen, J. H. D., and P. Jensen, 1950, Z. Naturforsch **5a,** 343.
Johansson, S. A. E., and B. Forkman, 1962, Nucl. Phys. **36,** 141.
Johns, K. W., L. J. Lidofsky, and J. L. Weil, 1958, Phys. Rev. **112,** 1252.
Kabachnik, N. M., V. L. Korotkih, and H. J. Unger, 1967, Nucl. Phys. **A103,** 450.
Kamimura, M., K. Ikeda, and A. Arima, 1967, Nucl. Phys. **A95,** 129.
Kapur, P. L., and R. E. Peierls, 1938, Proc. Roy. Soc. (London) **A166,** 277.
Kerman, A. K., 1965, in "Lectures in Theoretical Physics" (Univ. of Colorado Press, Boulder, Colorado).
——, and L. Kisslinger, 1969, Phys. Rev. **180,** 1483.
Kuo, T. T. S., J. Blomqvist, and G. E. Brown, 1970, Phys. Letters **31B,** 93.
Lane, A. M., and D. Robson, 1966, Phys. Rev. **151,** 774.
——, and D. Robson, 1967, Phys. Rev. **151,** 774.
——, and D. Robson, 1969, Phys. Rev. **178,** 1715.
——, and R. G. Thomas, 1958, Rev. Mod. Phys. **30,** 257.
Larson, J. D., and R. H. Spear, 1964, Nucl. Phys. **56,** 497.
Lemmer, R. H., and C. M. Shakin, 1964, Ann. Phys. (New York) **27,** 13.
——, and M. Veneroni, 1968, Phys. Rev. **170,** 883.
Le Tourneux, J., 1965, Kgl. Danske Videnskap. Selskap. Mat. Fys. Medd. **34,** 11.
Lewis, M. B., N. R. Roberson, and D. R. Tilley, 1968, Phys. Rev. **168,** 1205.
Lewis, F. H., Jr., and J. D. Walecka, 1964, Phys. Rev. **133,** B849.
Lochstet, W. A., and E. Stephens, 1966, Phys. Rev. **141,** 1002.
MacDonald, W. M., 1964, Nucl. Phys. **54,** 393; **56,** 636.
Mahaux, C., and H. A. Weidenmüller, 1965, Ann. Phys. (New York) **32,** 259.
——, and H. A. Weidenmuller, 1967, Nucl. Phys. **A91,** 241; **A94,** 1; **A97,** 378.
——, and H. A. Weidenmüller, 1968, Phys. Rev. **170,** 847.
——, and H. A. Weidenmüller, 1969, *Shell Model Approach to Nuclear Reactions* (North-Holland Publ. Co., Amsterdam).
Marangoni, M., and A. M. Saruis, 1967, Phys. Letters **24B,** 218.
——, and A. M. Saruis, 1969, Nucl. Phys. **A132,** 649.
McVoy, K. W., 1965, Phys. Letters **17,** 42.
Migdal, A., 1945, Zh. Eksp. Teor. Fiz. [Sov. Phys. JETP] **15,** 81.
Min, K., L. N. Bolen, and W. D. Whitehead, 1963, Bull. Am. Phys. Soc. **8,** 358.
Mitchell, G. E., E. B. Carter, and R. H. Davis, 1964, Phys. Rev. **133,** B1434.
Mohan, R., M. Danos, and L. C. Biedenharn, 1971, Phys. Rev. **3C,** 468.
Morrison, R. C., J. R. Stewart, and J. S. O'Connell, 1965, Phys. Rev. Letters **15,** 509.
Mshelia, 1971, University of Frankfurt, unpublished results.
Nilsson, S. G., J. Sawicki, and N. K. Glendenning, 1961, Nucl. Phys. **33,** 239.
Overly, J. C., and R. R. Borches, 1965, Nucl. Phys. **65,** 156.
Philips, C. C., T. A. Griffy, and L. C. Biedenharn, 1960, Nucl. Phys. **21,** 327.
Proca, G. A., and D. B. Isabelle, 1968, Nucl. Phys. **A109,** 177.
Puttaswamy, N. G. and D. Kohler, 1966, Phys. Letters, **20,** 288.
Rabie, A., 1970, University of Frankfurt, unpublished results.
Raynal, J., M. A. Melkanoff, and T. Sawada, 1967, Nucl. Phys. **A101,** 369.
Reay, N. W., N. M. Hintz, and L. L. Lee, 1963, Nucl. Phys. **44,** 338.
Rice, O. K., 1933, J. Chem. Phys. **1,** 375.
Robson, B. A., and D. Robson, 1967, Phys. Letters, **25B,** 504.
Robson, D., 1965, Phys. Rev. **137,** B535.
Rosenfeld, L., 1967, in Proc. International Conference on Nuclear Structure, Tokyo, pps. 9–13.
——, 1968, *Spectroscopic and Group Theoretical Methods in Physics* (North-Holland Publ. Co., Amsterdam).
Rotenberg, M., 1962, Ann. Phys. (New York) **19,** 262.
——, 1963, Ann. Phys. (New York) **21,** 579.
Saruis, A. M., and M. Marangoni, 1969, Nucl. Phys. **A132,** 433.
Schardt, A. W. A. Fowler, and C. C. Lauritsen, 1952, Phys. Rev. **86,** 527.
Seaborn, J. B., 1969, Phys. Rev. **179,** 958.
Segel, R. E., 1966, in *Isobaric Spin in Nuclear Physics*, edited by J. D. Fox and D. Robson (Academic, New York).
Seth, K. K., 1967, Phys. Rev. **164,** 1450.
Shakin, C. M., and W. L. Wang, 1971, Phys. Rev. Letters, **26,** 902.
Shevchenko, V., and N. Yudin, 1965, At. Energy **3,** 3.
Sperduto, A., and W. W. Buechner, 1958, Phys. Rev. **109,** 462.
Spicer, B. M., 1969, Advan. in Nucl. Phys. **2,** 1.
——, and J. M. Eisenberg, 1965, Nucl. Phys. **63,** 520.
Steinwedel, H., and J. H. D. Jensen, 1950, Z. Naturforsch. **5a,** 413.
Suffert, M., 1965, Nucl. Phys. **75,** 226.
——, and W. Feldman, 1967, Phys. Letters **24B,** 579.
Tai, Y., G. P. Millburn, S. N. Kaplan, and B. J. Moyer, 1958, Phys. Rev. **109,** 2086.
Tanner, N. W., 1965, Nucl. Phys. **63,** 383.
——, G. C. Thomas, and E. D. Earle, 1964a, Nucl. Phys. **52,** 29.
——, G. C. Thomas, and E. D. Earle, 1964b, Nucl. Phys. **52,** 45.
Teichman, T., and E. P. Wigner, 1952, Phys. Rev. **87,** 123.
Thomas, R. G., 1955, Phys. Rev. **97,** 224.
Thompson, M. N., and J. E. E. Baglin, 1967, Phys. Letters **25B,** 256.
Tobocman, W., and M. A. Nagarjan, 1967, Phys. Rev. **163,** 1011.
Villars, F., 1967, in "Fundamentals in Nuclear Theory", edited by A. de Shalit and C. Villi (International Atomic Energy Agency, Vienna).

Vinh-Mau, N., and G. E. Brown, 1962, Nucl. Phys. **29,** 89.
——, and G. E. Brown, 1966, Phys. Letters **23,** 257.
Wahsweiler, H., M. Danos, and W. Griner, 1966, Phys. Rev. Letters **17,** 395.
——, M. Danos, and W. Greiner, 1968, Phys. Rev. **170,** 893.
Warburton, E. K., 1966, in "Isobaric Spin in Nuclear Physics", edited by J. D. Fox and D. Robson, (Academic, New York).
Weber, H. J., M. G. Huber, and W. Greiner, 1966, Z. Physik **92,** 223.
Weidenmüller, H. A., 1966a, Nucl. Phys. **75,** 189.
——, 1966b, Nucl. Phys. **85,** 241.
——. 1967, Nucl. Phys. **A99,** 269, 289.
——, and K. Dietrich, 1966, Nucl. Phys. **83,** 332.
Weinberg, S., 1963, Phys. Rev. **130,** 776.
——, 1964, Phys. Rev. **131,** 440.
Weiss, M. S., 1965, Phys. Letters **19,** 393.
Weisskopf, V. F., 1961, Phys. Today **14,** 18.
Wild, W., 1955, Sitzungsbericht Bayr. Akad. München.
Wilkinson, D. H., 1956, Physica **22,** 1039.
Willard, H., and L. C. Biedenharn, 1958, Proc. Roy. Soc. **62,** 874.
Willis, J. E., Jr., 1958, Phys. Rev. **109,** 891.
Wu, C. P., J. E. E. Baglin, F. W. K. Firk, and T. W. Phillips, 1968, Phys. Rev. Letters **29B,** 359.
——, F. W. K. Firk, and T. W. Phillips, 1968, Phys. Rev. Letters **20,** 1182.
Wyckoff, J. M., B. Ziegler, H. W. Koch, and R. Uhlig, 1965, Phys. Rev. **137,** B576.